To the Graduate Council:

I am submitting herewith a dissertation written by John S. Neal entitled "Forecasting Dose-Time Profiles of Solar Particle Events Using a Dosimetry-Based Bayesian Forecasting Methodology." I have examined the final copy of this dissertation for form and content and recommend that it be accepted in partial fulfillment of the requirements for the degree of Doctor of Philosophy, with a major in Nuclear Engineering.

Dr. Lawrence W. Townsend, Major Professor

We have read this dissertation
and recommend its acceptance:

Dr. Peter G. Groer

Dr. J. Evans Lyne

Dr. Laurence F. Miller

Accepted for the Council:

Interim Vice Provost and
Dean of The Graduate School

FORECASTING DOSE-TIME PROFILES OF SOLAR PARTICLE EVENTS USING A DOSIMETRY-BASED BAYESIAN FORECASTING METHODOLOGY

A Dissertation

Presented for the

Doctor of Philosophy

Degree

The University of Tennessee, Knoxville

John S. Neal

May 2001

Copyright © John S. Neal, 2001

All rights reserved

DEDICATION

This dissertation is dedicated to my wife,

Valerie Lynn Neal,

my children,

Caroline Bisset Neal, Benjamin Stuart Neal, Madalyn Rose Neal,

my parents,

Richard Elwood Neal and Carroll Maida Neal,

and Valerie's parents,

Alfred Asbury and Leona Mae Asbury.

ACKNOWLEDGEMENTS

I am especially grateful to Dr. Lawrence W. Townsend, my major professor, for his advice and for the freedom to pursue this goal in a manner most beneficial for me and my family. I would also like to thank my graduate committee, Dr. Peter G. Groer, Dr. J. Evans Lyne, and Dr. Laurence F. Miller, for their suggestions which helped to make this a successful endeavor.

I would like to acknowledge the financial support for this research provided by the University of Tennessee's Department of Nuclear Engineering and the National Aeronautics and Space Administration through its Graduate Student Researchers Program.

Lastly, I am thankful for my family's support through these arduous times.

ABSTRACT

A dosimetery-based Bayesian methodology for forecasting astronaut radiation doses in deep space due to radiologically significant solar particle event proton fluences is developed. Three non-linear sigmoidal growth curves (Gompertz, Weibull, logistic) are used with hierarchical, non-linear, regression models to forecast solar particle event dose-time profiles from doses obtained early in the development of the event. Since there are no detailed measurements of dose versus time for actual events, surrogate dose data are provided by calculational methods. Proton fluence data are used as input to the deterministic, coupled neutron-proton space radiation computer code, BRYNTRN, for transporting protons and their reaction products (protons, neutrons, ^{2}H, ^{3}H, ^{3}He, and ^{4}He) through aluminum shielding material and water. Calculated doses and dose rates for ten historical solar particle events are used as the input data by grouping similar historical solar particle events, using asymptotic dose and maximum dose rate as the grouping criteria. These historical data are then used to lend strength to predictions of dose and dose rate-time profiles for new solar particle events. Bayesian inference techniques are used to make parameter estimates and predictive forecasts. Due to the difficulty in performing the numerical integrations necessary to calculate posterior parameter distributions and posterior predictive distributions, Markov Chain Monte Carlo (MCMC) methods are used to sample from the posterior distributions.

Hierarchical, non-linear regression models provide useful predictions of asymptotic dose and dose-time profiles for the November 8, 2000 and August 12, 1989 solar particle events. Predicted dose rate-time profiles are adequate for the November 8, 2000 solar particle event. Predicitions of dose rate-time profiles for the August 12, 1989 solar particle event suffer due to a more complex dose rate-time profile. Model assessment indicates adequate fits of the data. Model comparison results clearly indicate preference for the Weibull model for both events.

Forecasts provide a valuable tool to space operations planners when making recommendations concerning operations in which radiological exposure might jeopardize personal safety or mission completion. This work demonstrates that Bayesian inference methods can be used to make forecasts of dose and dose rate-time profiles early in the evolution of solar particle events. Bayesian inference methods provide a coherent methodology for quantifying uncertainty. Hierarchical models provide a natural framework for the prediction of new solar particle event dose and dose rate-time profiles.

TABLE OF CONTENTS

CHAPTER			PAGE
1.	INTRODUCTION		1
	1.1	General	1
	1.2	Objective of the Work	4
	1.3	Impact and Originality of the Work	5
	1.4	Outline of Dissertation	5
2.	SPACE RADIATION ENVIRONMENT		6
	2.1	General	6
	2.2	Galactic Cosmic Rays	6
	2.3	Solar Particle Events	7
3.	PARTICLE TRANSPORT AND DOSE CALCULATIONS		10
	3.1	Particle Transport	10
	3.2	GOES Data	14
	3.3	BRYNTRN Transport Code	15
4.	BAYESIAN STATISTICS		17
	4.1	Bayes' Theorem	17
	4.2	Prior Distributions	18
	4.3	Likelihood Function	19
	4.4	Hierarchical Models	20
	4.5	Bayesian Inference	20

4.5.1 Point Estimation 21

4.5.2 Prediction 21

4.6 Model Assessment and Comparison 22

4.6.1 Model Assessment 23

4.6.2 Model Comparison 25

5. MARKOV CHAIN MONTE CARLO TECHNIQUES 27

5.1 General 27

5.2 Markov Chains 28

5.3 Gibbs Sampler 29

5.3.1 General 29

5.3.2 Sampling from Full Conditional Densities 31

5.3.3 Rejection Sampling 33

5.3.4 Adaptive Rejection Sampling 33

5.4 Metropolis-Hastings Sampling 34

5.5 Slice Sampling 35

5.6 Convergence Diagnostics 36

5.7 Forming the Sample 38

6. METHODOLOGY AND RESULTS FOR INDIVIDUAL SPE 40

NON-LINEAR REGRESSION MODELS

6.1 Computational Techniques 40

6.2 Investigations Utilizing Individual SPE Non-Linear Regression Models 41

6.2.1 Fitting of Organ Doses Using Alternative Growth Curves 42

6.2.2 Calculation of Doses in Water 54

6.2.3 Prediction of Dose-Time Profiles 65

6.2.4 Conclusions on the Use of Individual Non-Linear Regression Models 74

7. METHODOLOGY AND RESULTS FOR HIERARCHICAL NON-LINEAR REGRESSION MODELS 75

7.1 Investigations Utilizing Hierarchical Non-Linear Regression Models 75

7.1.1 Categorization of SPE 75

7.1.2 Hierarchical Non-Linear Regression Models 77

7.2 November 2000 SPE 83

7.3 August 1989 SPE 100

7.4 Conclusions 109

8. CONCLUSIONS AND RECOMMENDATIONS FOR FUTURE WORK 118

WORKS CONSULTED 121

References 122

Bibliography 128

APPENDICES 129

Appendix A 130

Appendix B 135

Appendix C 141

Appendix D 146

VITA 167

LIST OF FIGURES

FIGURE		PAGE
6.1	Skin dose-time profile fits using posterior parameter means for the March 23, 1991 SPE.	48
6.2	Eye dose-time profile fits using posterior parameter means for the March 23, 1991 SPE.	49
6.3	Skin dose-time profile fits using posterior parameter means for the June 4, 1991 SPE.	50
6.4	Eye dose-time profile fits using posterior parameter means for the June 4, 1991 SPE.	51
6.5	Skin dose-time profile fits using posterior parameter means for the August 4, 1972 SPE.	52
6.6	Eye dose-time profile fits using posterior parameter means for the August 4, 1972 SPE.	53
6.7	Water dose-time profile fits using posterior parameter means for the May 6, 1989 SPE.	60
6.8	Water dose-time profile fits using posterior parameter means for the January 31, 1991 SPE.	61
6.9	Water dose-time profile fits using posterior parameter means for the March 23, 1991 SPE.	62
6.10	Water dose-time profile fits using posterior parameter means for the June 4, 1991 SPE.	64
6.11	Water dose-time profile fits using posterior parameter means for the August 26, 1991 SPE.	64
6.12	Water dose-time profile prediction using posterior predictive means for the November 8, 2000 SPE and Weibull growth curves.	66

6.13 Water dose-time profile prediction using posterior predictive means for the November 8, 2000 SPE and Gompertz growth curves. 67

6.14 Water dose-time profile prediction using posterior predictive means for the November 8, 2000 SPE and logistic growth curves. 68

6.15 Water dose-time profile prediction using posterior predictive means for the September 29, 1989 SPE and Weibull growth curves. 69

6.16 Water dose-time profile prediction using posterior predictive means for the September 29, 1989 SPE and Gompertz growth curves. 70

6.17 Water dose-time profile prediction using posterior predictive means for the September 29, 1989 SPE and logistic growth curves. 71

7.1 Water dose-time profile prediction using posterior predictive means for the November 8, 2000 SPE and Weibull growth curves. 86

7.2 Water dose-time profile prediction using posterior predictive medians for the November 8, 2000 SPE and Gompertz growth curves. 87

7.3 Water dose-time profile prediction using posterior predictive medians for the November 8, 2000 SPE and logistic growth curves. 88

7.4 Water dose rate-time profile prediction using posterior predictive means for the November 8, 2000 SPE and Weibull growth curves. 89

7.5 Water dose rate-time profile prediction using posterior predictive medians for the November 8, 2000 SPE and Gompertz growth curves. 90

7.6 Water dose rate-time profile prediction using posterior predictive medians for the November 8, 2000 SPE and logistic growth curves. 91

7.7 Weibull model 50% predictive interval widths for November 8, 2000 SPE. 94

7.8 Weibull model 95% predictive interval widths for November 8, 2000 SPE. 95

7.9 Gompertz model 50% predictive interval widths for November 8, 2000 SPE. 96

7.10	Gompertz model 95% predictive interval widths for November 8, 2000 SPE.	97
7.11	Logistic model 50% predictive interval widths for November 8, 2000 SPE.	98
7.12	Logistic model 95% predictive interval widths for November 8, 2000 SPE.	99
7.13	Water dose-time profile prediction using posterior predictive means for the August 12, 1989 SPE and Weibull growth curves.	103
7.14	Water dose-time profile prediction using posterior predictive means for the August 12, 1989 SPE and Gompertz growth curves.	104
7.15	Water dose-time profile prediction using posterior predictive means for the August 12, 1989 SPE and logistic growth curves.	105
7.16	Water dose rate-time profile prediction using posterior predictive means for the August 12, 1989 SPE and Weibull growth curves.	106
7.17	Water dose rate-time profile prediction using posterior predictive means for the August 12, 1989 SPE and Gompertz growth curves.	107
7.18	Water dose rate-time profile prediction using posterior predictive means for the August 12, 1989 SPE and logistic growth curves.	108
7.19	Weibull model 50% predictive interval widths for August 12, 1989 SPE.	111
7.20	Weibull model 95% predictive interval widths for August 12, 1989 SPE.	112
7.21	Gompertz model 50% predictive interval widths for August 12, 1989 SPE.	113
7.22	Gompertz model 95% predictive interval widths for August 12, 1989 SPE.	114

7.23 Logistic model 50% predictive interval widths for August 12, 1989 SPE. 115

7.24 Logistic model 95% predictive interval widths for August 12, 1989 SPE. 116

LIST OF TABLES

TABLES		PAGE
6.1	Weibull growth curve posterior parameter means and 95% confidence intervals for skin dose.	45
6.2	Weibull growth curve posterior parameter means and 95% confidence intervals for eye dose.	45
6.3	Gompertz growth curve posterior parameter means and 95% confidence intervals for skin dose.	46
6.4	Gompertz growth curve posterior parameter means and 95% confidence intervals for eye dose.	46
6.5	Logistic growth curve posterior parameter means and 95% confidence intervals for skin dose.	47
6.6	Logistic growth curve posterior parameter means and 95% confidence intervals for eye dose.	47
6.7	Calculated negative cross-validatory log-likelihood values of skin and eye dose-time profile fits.	54
6.8	Weibull growth curve posterior parameter means and 95% confidence intervals for water dose.	57
6.9	Gompertz growth curve posterior parameter means and 95% confidence intervals for water dose.	58
6.10	Logistic growth curve posterior parameter means and 95% confidence intervals for water dose.	59
6.11	Calculated product of conditional predictive ordinate values for November 8, 2000 SPE predictions.	72
6.12	Calculated product of conditional predictive ordinate values for September 29, 1989 SPE predictions.	73
7.1	Hierarchical model group characteristics and initial SPE members.	76

7.2	Criteria for categorization of new events.	76
7.3	Hyperpriors distribution for groups 1 through 4 Weibull growth curve hierarchical models.	78
7.4	Hyperpriors distribution for groups 1 through 4 Gompertz growth curve hierarchical models.	80
7.5	Hyperpriors distribution for groups 1 through 4 logistic growth curve hierarchical models.	82
7.6	Calculated product of conditional predictive ordinate values for November 8, 2000 SPE predictions.	93
7.7	Calculated product of conditional predictive ordinate values for August 12, 1989 SPE predictions.	110
A.1	Skin and eye dose data for the March 23, 1991 SPE, estimated using the BRYNTRN computer code.	131
A.2	Skin and eye dose data for the June 4, 1991 SPE, estimated using the BRYNTRN computer code.	132
A.3	Skin and eye dose data for the August 4, 1972 SPE, estimated using the BRYNTRN computer code.	133
A.4	Percentage of observations that fall within 50% and 95% predictive intervals of skin and eye dose-time profile fits.	134
B.1	Water dose data for the May 6, 1989 SPE, estimated using the BRYNTRN computer code.	136
B.2	Water dose data for the January 31, 1991 SPE, estimated using the BRYNTRN computer code.	137
B.3	Water dose data for the March 23, 1991 SPE, estimated using the BRYNTRN computer code.	138
B.4	Water dose data for the June 4, 1991 SPE, estimated using the BRYNTRN computer code.	139

B.5	Water dose data for the August 26, 1991 SPE, estimated using the BRYNTRN computer code.	140
C.1	Water dose data for the November 8, 2000 SPE, estimated using the BRYNTRN computer code.	142
C.2	Water dose data for the September 29, 1989 SPE, estimated using the BRYNTRN computer code.	143
C.3	Percentage of observations that fall within 50% and 95% predictive intervals for the November 8, 2000 SPE.	144
C.4	Percentage of observations that fall within 50% and 95% predictive intervals for the September 29, 1989 SPE.	145
D.1	Water dose data for the July 14, 2000 SPE, estimated using the BRYNTRN computer code.	147
D.2	Water dose data for the March 23, 1991 SPE, estimated using the BRYNTRN computer code.	148
D.3	Water dose data for the October 19, 1989 SPE, estimated using the BRYNTRN computer code.	149
D.4	Water dose data for the September 29, 1989 SPE, estimated using the BRYNTRN computer code.	150
D.5	Water dose data for the June 4, 1991, SPE, estimated using the BRYNTRN computer code.	151
D.6	Water dose data for the March 19, 1990 SPE, estimated using the BRYNTRN computer code.	152
D.7	Water dose data for the November 30, 1989 SPE, estimated using the BRYNTRN computer code.	153
D.8	Water dose data for the August 26, 1991 SPE estimated using the BRYNTRN computer code.	154
D.9	Water dose data for the January 31, 1991 SPE, estimated using the BRYNTRN computer code.	155

D.10 Water dose data for the November 8, 1987 SPE, estimated using the BRYNTRN computer code. 156

D.11 Water dose data for the November 8, 2000 SPE, estimated using the BRYNTRN computer code. 157

D.12 Water dose rate data for the November 8, 2000 SPE, estimated using the BRYNTRN computer code. 158

D.13 Percentage of observations that fall within 50% and 95% predictive intervals for the November 8, 2000 SPE using hierarchical models and Weibull growth curves. 159

D.14 Percentage of observations that fall within 50% and 95% predictive intervals for the November 8, 2000 SPE using hierarchical models and Gompertz growth curves. 160

D.15 Percentage of observations that fall within 50% and 95% predictive intervals for the November 8, 2000 SPE using hierarchical models and logistic growth curves. 161

D.16 Water dose data for the August 12, 1989 SPE, estimated using the BRYNTRN computer code. 162

D.17 Water dose rate data for the August 12, 1989 SPE, estimated using the BRYNTRN computer code. 163

D.18 Percentage of observations that fall within 50% and 95% predictive intervals for the August 12, 1989 SPE using hierarchical models and Weibull growth curves. 164

D.19 Percentage of observations that fall within 50% and 95% predictive intervals for the November 8, 2000 SPE using hierarchical models and Gompertz growth curves. 165

D.20 Percentage of observations that fall within 50% and 95% predictive intervals for the November 8, 2000 SPE using hierarchical models and logistic growth curves. 166

NOMENCLATURE

A	atomic mass
D	absorbed energy per unit mass, dose
e_i	error
E	energy
$f_{i,j}$	differential cross sections for elastic and inelastic collision processes
m	mass
N	number of target molecules per unit volume
Q	quality factor
r	radius
$R_j(E)$	range of particle type j with energy E
$S_j(E)$	stopping power of the medium for particle type j with energy E
v	velocity
x	distance
Z	atomic number
φ	flux or fluence
π	pi=3.141592...
σ	cross section
Ω	direction vector taken as being normal to the surface of a sphere
ψ	$S(E)*\varphi(X,E)$, characteristic function

LIST OF ABBREVIATIONS

BFO	Blood Forming Organs
BOA	Bayesian Output Analysis
BRYNTRN	Baryon Transport
BUGS	Bayesian Inference Using Gibbs Sampling
c	centi
CME	Coronal Mass Ejection
CPO	Conditional Predictive Ordinates
EPS	Energetic Particle Sensor
EVA	Extra-Vehicular Activity
g	gram
GCR	Galactic Cosmic Ray
GOES	Geosynchronous Operational Earth Satellite
Gy	Gray
m	meter
MCMC	Markov Chain Monte Carlo
NOAA	National Oceanic and Atmospheric Administration
PPS	Proton Prediction System
s	second
SEC	Space Environment Center
SPE	Solar Particle Event

sr	steradian
SRAG	Space Radiation Analysis Group
Sv	Sievert

CHAPTER 1

INTRODUCTION

1.1 General

As humans extend their presence in space, the need to understand the space radiation environment and the resultant radiological consequences grows more critical. Galactic Cosmic Radiation (GCR) may provide an annual chronic dose of up to 13.3 cGy (38.4 cSv) to an astronaut's bone marrow assuming a spacecraft aluminum shield thickness of 3.0 g/cm^2 (Townsend, Cucinotta and Wilson, 1992). Recent calculations of dose due to Solar Particle Event (SPE) protons include absorbed dose of 40 cGy to the bone marrow behind 5 g/cm^2 of aluminum shielding for the August 1972 SPE (Parsons and Townsend, 2000), up to 22 cGy to the blood forming organs (BFO) behind 2 g/cm^2 of aluminum shielding for four of the major SPEs that occurred between August 1989 and December 1989 (Zapp et al., 1998), and approximately 25 cGy to the BFO behind 5 g/cm^2 of aluminum shielding for the October 1989 SPE (Townsend and Zapp, 1999). As such, SPEs are the most important radiation hazard for short-duration missions of two to three months (Wilson, et al., 1991). The ability to provide forecasts of individual SPEs and to estimate event sizes and rise times is currently inadequate. Necessary predictions include dose-time profiles, asymptotic dose, and dose rate-time profiles. These predictions may allow better-

informed decisions concerning activities such as Extra-Vehicular Activity (EVA) and planet surface exploration.

In the context of space radiation protection and prediction, forecasting can be divided into two general categories: space weather forecasting and climatological forecasting (Turner, 1997). Space weather forecasts attempt to predict the probability that an SPE will occur within weeks, days, or hours. NASA's Space Radiation Analysis Group (SRAG) uses space weather forecast information to predict the magnitude and duration of an SPE as well as time to reach dose limits and time until dose rate returns to a safe level. Climatological forecasts are concerned with the statistical distribution of SPEs over years, decades, or longer. This forecast information is then used for radiation effects analysis, total dose estimates, and spacecraft shielding design.

There is no currently adequate capability to predict SPEs weeks in advance. One to three day forecasts prepared by the National Oceanic and Atmospheric Administration (NOAA) Space Environment Center (SEC) predict the probability that an SPE will occur. These forecasts are largely based on forecaster judgement from review of solar observables such as sunspots, and predictions consistently overestimate the likelihood of a large SPE (Turner, 1997). Near-term forecasts predict the probability that an SPE will occur as well as its peak particle flux. Near-term forecasts are based on real-time data such as soft x-ray fluence, solar radio burst data, and locations of solar flares. These forecasts

require forecaster judgement but also use computer programs to aid in development of the forecast: PROTONS and the Proton Prediction System. PROTONS model output includes the probability that there will be an SPE, start time and time of maximum flux, and magnitude of the peak flux. The Proton Prediction System (PPS) generates forecasts within 15 minutes after the occurrence of a significant solar flare or after observation of an increase in proton flux. PPS produces a 300 hour time-flux intensity profile for 20 proton energy channels. Currently, space weather forecasts correctly predict the occurrence or non-occurrence of an SPE, after observation of a significant x-ray event, eighty percent of the time. Approximately fifty percent of the predicted SPEs, however, failed to occur. An event occurs approximately five to ten percent of the times when non-occurrence is predicted. Predicted peak particle flux is generally within an order of magnitude, and longer term (one to three days) predictions consistently overestimate the likelihood of a large SPE (Heckman, et al., 1992).

Other prediction techniques have considered correlation of SPE fluence with solar observables, such as solar flare activity, radio and X-ray radiation characteristics, SPE fluxes of different energies, and characteristics of active regions of the sun (Kovtunenko, et al., 1994). One of the most recent developments is the recognition of S-shaped patterns (sigmoids) in X-ray images of the sun which may help forecast large coronal mass ejections (CME) (Canfield, 1999).

Recent efforts have included parameterization of dose-time profiles (Lamarche and Poston, 1996; Zapp et al., 1998) and the use of artificial neural networks (Tehrani, 1998) to predict asymptotic dose early in an SPE. To date, parameterizations of dose-time profiles have not considered the asymptotic dose as a parameter, but rather, as a known value. While these efforts do not enable one to make predictions about future doses within an ongoing SPE, Zapp's work has provided information regarding the range of the parameter space when considering a Weibull growth model. Initial investigations utilizing artificial neural networks have predicted asymptotic dose early in an SPE, but these investigations provide no dose-time profile information, no measure of the uncertainty in predictions, and have only considered a small portion of the available parameter space.

1.2 Objective of the Work

The purpose of this research is to develop statistical models which utilize Bayesian methods to predict future doses and dose rates. Doses calculated from SPE proton fluence data early in an event are used in the models to predict asymptotic dose and future dose and dose rates. This methodology utilizes model assessment techniques to determine how well the model fits the data and model comparison techniques in order to make judgements as to which is the "best" model.

1.3 Impact and Originality of the Work

Previous work has considered prediction of flux through correlation with related observables, parameterization of dose-time profiles given the asymptotic dose, and the prediction of asymptotic dose using artificial neural networks. This research is the first work to employ Bayesian inference techniques implemented by Markov Chain Monte Carlo methods for forecasting SPE dose-time profiles, asymptotic dose, and dose rate-time profiles. This work also considers long-term growth models not utilized in prior work.

1.4 Outline of Dissertation

Chapter two reviews the space radiation environment. Chapter three provides an overview of charged particle transport, the implementing transport computer code, and the sources of data for this investigation. Chapter four discusses Bayesian inference, prediction, and model assessment/comparison. Chapter five reviews Markov Chain Monte Carlo techniques. Chapter six describes the methodology and results associated with individual non-linear regression models. Chapter seven describes the methodology and results associated with hierarchical non-linear regression models. Chapter eight provides conclusions and recommendations for future work.

CHAPTER 2

SPACE RADIATION ENVIRONMENT

2.1 General

The radiation environment outside the Earth's geomagnetic field is dominated by two sources: GCR and SPEs. The GCR source flux is approximately constant (with factors of 2-3 variation at most) and comprised of particles ranging from protons to uranium nuclei of low flux but high energy. Particles heavier than iron are of little radiation protection concern because their fluxes are too small. The SPE source is comprised of protons and other heavy nuclei that can vary in intensity by several orders of magnitude over time. While these SPE particles are generally of lower energy than GCR particles, the flux is typically orders of magnitude greater with SPE occurring over periods of hours to days. Radiations with energies below 100 keV and SPE protons with energies below 10 MeV are considered biologically unimportant.

2.2 Galactic Cosmic Rays

The GCR flux varies over the approximate 11-year solar cycle due to the changing interplanetary plasma resulting from the changes in the solar corona. The GCR background is a relatively high energy, isotropic field composed of approximately 88 percent protons, 10 percent helium nuclei, and 2 percent heavy

ions. The most abundant elements include helium, carbon, oxygen, magnesium, silicon, and iron (Wilson et al., 1991). These seven ions and protons provide over 80 percent of the unshielded GCR dose. Abundances of elements heavier than iron are generally 2 to 4 orders of magnitude smaller than iron (Adams et al., 1981). These GCR particles may provide an annual chronic dose of up to 13.3 cGy (38.4 cSv) to an astronaut's bone marrow (Townsend et al., 1992) assuming a 3.0 g/cm^2 aluminum shield thickness.

The major concern associated with GCR is the potential for spallation or fragmentation reactions within the shielding material. Reaction products could provide a high energy radiation source within the shielding material. Additionally, the biological implications of relatively rare, high energy, heavy ions are not well understood. As such, GCR are assumed to provide a chronic dose to astronauts.

2.3 Solar Particle Events

The NOAA SEC defines an SPE as occurring when the number of particles with energy greater than 10 MeV exceeds 10 particles-s^{-1}-cm^{-2}-sr^{-1} for more than 15 minutes (SESC Users Guide, 1993). An idealized flux versus time profile (Turner, 1996) reveals the nominal characteristics of SPEs: a propagation delay between initial acceleration and onset of particle increase (20-90 minutes); a relatively rapid rise in intensity to a maximum value (1-3 hours); and a slow

decay to background level (roughly exponential decay, typically dropping to 1/e within 10-14 hours). A period of flux enhancement may occur as a fast, powerful interplanetary shock passes over the observer.

SPEs are classified as belonging to one of two categories: impulsive events and gradual events. Impulsive events are electron-rich, relatively short-lived (hours) and dominated by acceleration at the flaring site. Impulsive events have enhanced heavy isotopic abundances and a He-3/He-4 ratio which is orders of magnitude larger than for gradual events. Gradual events are proton-rich and long-lived (days) and are believed to be associated with the shock produced during CMEs (Kahler, 1994; Reames, 1996).

Large SPE are a concern to planners of crewed, deep space, exploratory missions. These SPE may present a significant health hazard to crews and could be mission-threatening unless adequate shielding is provided. The largest recorded SPE (in terms of particle fluence) occurred in August 1972. The spectrum was relatively soft (rapid decrease in fluence with increasing particle energy) and would have been easily shielded by a reasonably thick spacecraft. The February 1956 SPE probably had the hardest spectrum but approximately one tenth of the August 1972 SPE fluence and may not have been mission or life-threatening. Recent calculations of dose due to SPE protons include absorbed dose of 40 cGy to the bone marrow behind 5 g/cm^2 of aluminum shielding and maximum skin dose rates of 21 cGy/hr for the August 1972 SPE (Parsons and

Townsend, 2000), up to 22 cGy to the Blood Forming Organs (BFO) (Zapp et al., 1998) behind 2 g/cm^2 of aluminum shielding for four of the major SPE that occurred between August 1989 and December 1989, and approximately 25 cGy to the BFO (Townsend and Zapp, 1999) behind 5 g/cm^2 of aluminum shielding and 11 cGy/hr skin dose rate behind 2 g/cm^2 (Zapp et al., 1999) for the October 1989 SPE. Crew operations involving little shielding may result in acute effects which are known to be dose and dose rate dependent. These calculated doses and dose rates clearly indicate the necessity for development of models to forecast dose-time profiles, asymptotic dose, and dose rate-time profiles.

CHAPTER 3

PARTICLE TRANSPORT AND DOSE CALCULATIONS

3.1 Particle Transport

In order to calculate the doses and dose rates used for growth curve parameter inference, the incident particle fluxes and their secondaries must be transported through a spacecraft's aluminum shielding. For this work, the incident particles consist of protons produced during an SPE. The Boltzmann transport equation is derived by applying conservation principles to a particle flux. Vector quantities are indicated by bold font in the text and by arrows in equations. First, define a small, spherical region of space of radius r, filled with matter described by atomic and nuclear cross sections. The number of particles of type j leaving a surface element $r^2 d\Omega$ is given as $\varphi_j(\mathbf{x}+r\Omega,\Omega,E)\ r^2 d\Omega$ where $\varphi_j(\mathbf{x},\Omega,E)$ is the particle flux density, $\mathbf{x}$ is a vector to the center of the sphere, Ω is normal to the surface element, and E is the particle energy. The projection of the surface element through the sphere center to the opposite side of the sphere defines a flux tube through which pass a number of particles of type j given as $\varphi_j(\mathbf{x}-r\Omega,\Omega,E)\ r^2 d\Omega$, which would equal the number leaving the opposite face if the defined tube were a vacuum. Since the tube is filled with matter, the number of particles passing by the opposite faces differs by gains and losses created by atomic and nuclear collisions as follows:

$$\varphi_j(\vec{x}+r\vec{\Omega},\vec{\Omega},E)r^2d\vec{\Omega}=\varphi_j(\vec{x}-r\vec{\Omega},\vec{\Omega},E)r^2d\vec{\Omega} \tag{3.1}$$
$$+r^2d\vec{\Omega}\int_{-r}^{r}dl\sum_k\int\sigma_{jk}(\vec{\Omega},\vec{\Omega}',E,E')\varphi_k(\vec{x}+l\vec{\Omega},\vec{\Omega}',E')d\vec{\Omega}'dE$$
$$-r^2d\vec{\Omega}\int_{-r}^{r}dl\sigma_j(E)\varphi_j(\vec{x}+l\vec{\Omega},\vec{\Omega},E)$$

where $\sigma_j(E)$ and $\sigma_{jk}(\Omega,\Omega',E,E')$ are shielding material macroscopic cross sections. The $\sigma_{jk}(\Omega,\Omega',E,E')$ cross section describes all processes by which type k particles moving in direction Ω' with energy E′ produce a type j particle in direction Ω with energy E. Several reactions may produce this result, and the appropriate cross sections are the inclusive ones. The second term on the right hand side of this equation is the source of secondary particles integrated over the total volume, and the third term is the loss through nuclear reactions integrated over the total volume. After expanding the terms on both sides of equation (3.1) to order r^3 and dividing by the flux tube volume, the resulting equation may be written as

$$\vec{\Omega}\bullet\nabla\varphi_j(\vec{x},\vec{\Omega},E)=\sum_k\int\sigma_{jk}(\vec{\Omega},\vec{\Omega}',E,E')\varphi_k(\vec{x},\vec{\Omega}',E')d\vec{\Omega}'dE' \tag{3.2}$$
$$-\sigma_j(E)\varphi_j(\vec{x},\vec{\Omega},E)+O(r)$$

Equation (3.2) is a time independent form of the Boltzmann equation for a tenuous gas. Collisions with atomic electrons preserve the identity of the particle with both terms of the right-hand side contributing. Separation of σ_{jk} into atomic

and nuclear contributions allows writing equation (3.3) in the continuous slowing down approximation as

$$\bar{\Omega} \bullet \nabla \varphi_j(\bar{x},\bar{\Omega},E) - \frac{\partial}{\partial E}[S_j(E)\varphi_j(\bar{x},\bar{\Omega},E)] + \sigma_j(E)\varphi_j(\bar{x},\bar{\Omega},E) \qquad (3.3)$$
$$= \int \sum_k \sigma_{jk}(\bar{\Omega},\bar{\Omega}',E,E')\varphi_k(\bar{x},\bar{\Omega}',E')d\bar{\Omega}'dE'$$

where the cross sections contain only the nuclear contributions and $S_j(E)$, the stopping power, is written according to Bethe's theory (Bethe, 1930) as

$$S_j(E) = \frac{4\pi N Z_1^2 Z_2 e^4}{mv^2}[\ln(\frac{2mv^2}{(1-\beta^2)I_t}) - \beta^2] \qquad (3.4)$$

where N is the number of targets, Z_1 is the projectile charge, Z_2 is the number of electrons per target, m is the electron mass, v is the projectile velocity, c is the velocity of light, β=v/c, and I_t is the mean excitation energy.

Now, assuming that space radiations are approximately isotropic and that secondary ions are produced only in the direction of motion of the primary ions (the straight ahead approximation), the transport equation may be simplified in one dimension as

$$[\frac{\partial}{\partial x} - \frac{\partial}{\partial E} S_j(E) + \sigma_j(E)]\varphi_j(x,E) = \sum_k \int_E^{\infty} \sigma_{jk}(E,E')\varphi_k(x,E')dE' \qquad (3.5)$$

The assumption of isotropic space radiation allows reduction of the transport equation to one dimension. Particles which leave the sun move along the interplanetary magnetic field lines which stream away from the sun in an Archimedal spiral pattern (Smart and Shea, 1997). Charged particles follow spiral paths along these lines with varying radii due to a spread in particle energy. Due to a large number of magnetic field lines, some spiral paths will overlap. Particle paths are also perturbed because of interactions with other charged particles and irregularities in the interplanetary magnetic fields. Thus, incoming particles to a spacecraft outside the Earth's magnetosphere will appear to be isotropically distributed. The equivalence of calculations for dose in the center of a spherical shield with isotropic incident radiation and a one-dimensional slab shield with normally incident radiation allows reduction of the transport equation to one dimension.

Equation (3.5) is solved using the method of characteristics. After mapping solutions back to variables x and E, the differential fluence solution for light ions is:

$$\psi_j(x+h,r_j) \approx e^{-\sigma h}\psi_j(x,r_j+h) + e^{-\sigma h}\int_0^h dz \int_{r_j}^{\infty} dr' f_j(r_j+z,r'+z)\psi_j(x,r'+h) \quad (3.6)$$

where $\psi_j(x,r_j)=S_j(E)\varphi_j(x,E)$ and σ is σ_j, the macroscopic cross section for j type particles with energy greater than E to interact and produce particles of type j with energy E. The variable f_j is the nuclear contribution to the separated total cross section σ_{jk}. The range of a j-type particle with energy E is denoted by r_j and the numerical step size by h. Equation (3.6) is solved numerically by "marching" through the shield material. This methodology is implemented in the BRYNTRN computer code that is described in section 3.3.

3.2 GOES Data

The data used in this investigation are five minute proton flux averages (particles/cm^2-s-sr) and were measured by the Geosynchronous Operational Earth Satellites (GOES), in this case, GOES-7 and GOES-8. Data are taken from the >30, >50, >60, and >100 MeV channels of the Energetic Particle Sensor (EPS) instrument for GOES-7 and from the >10, >30, >50, and >100 MeV channels for GOES-8. The EPS consists of solid-state detectors with pulse-height discrimination. The look direction of the EPS is perpendicular to the GOES spin axis which is approximately aligned with the earth's rotation axis. The EPS provides a spin averaged estimate of the local high-pitch-angle particle fluxes (Wilkinson and Ushomirskiy, 1994).

Flux data are integrated over a spherical 4π area and a 300 second collection time yielding particle fluence data (number-cm^{-2}) for dose calculations.

Flux data are integrated over a spherical 4π area yielding particle flux data (number-cm^{-2}-sec^{-1}) for dose rate calculations. Fluence and flux data are fit to an exponential rigidity function, $J=J_0e^{-R/Ro}$, using least squares regression techniques, where J is the particle fluence and R is the particle rigidity. Particle rigidity is a measure of proton momentum per unit charge at energy, E, given by

$$R = \frac{(E^2 + 2mc^2E)^{.5}}{e} \qquad (3.7)$$

where m is particle mass, c is the speed of light, E is particle energy, and e is the electron charge. J_0 and R_0 are the fitting parameter inputs to the BRYNTRN transport code.

3.3 BRYNTRN Transport Code

For this investigation, SPE incident protons are transported through the shield material using the deterministic, coupled neutron-proton space radiation computer code, BRYNTRN, which was developed at the NASA Langley Research Center (Wilson et al., 1991). In addition to the incident primary protons, secondary protons and neutrons, deuterons, tritons, ^{3}He, and alpha particles are transported through the shield material. BRYNTRN uses a marching algorithm based on the integral solutions to a one-dimensional Boltzmann

transport equation incorporating the straight-ahead approximation. Details of the code are described elsewhere (Wilson et al., 1989; Wilson et al., 1991).

After inputting J_0 and R_0, the parameters for the fluence spectrum, the spectrum is differentiated in energy. This differential spectrum is used as the incident spectrum. After transport, the fluence of particles of type j at a point x with energy greater than or equal to E is

$$\varphi_j(x,>E) = \int_{R_j(E)}^{\infty} \psi_j[x,r]dr \tag{3.8}$$

where ψ_j corresponds to the Boltzmann equation solution (equation 3.6) above. The dose, energy absorbed per gram of water, is calculated as

$$D_j(x,>E) = \int_{E}^{\infty} A_j \psi_j[x, R_j(E')]dE' \tag{3.9}$$

where A_j is the mass of the projectile, $R_j(E')$ is the range of j-type particle with energy E', and ψ_j is the integral solution of equation (3.6).

It is important to note that the above-described calculations are necessary as there is little or no dosimetric data available for SPE protons. Particle flux data measured by GOES required extensive review and correction and are thus, not available in real-time. As such, a surrogate data set, as calculated by BRYNTRN, must be used in this work to demonstrate the potential use of real-time dosimetry for predicting SPE dose and dose rate early in an event.

CHAPTER 4

BAYESIAN STATISTICS

4.1 Bayes' Theorem

Probability is used as the fundamental measure of uncertainty in Bayesian statistics. Bayes' Theorem is attributed to the Reverend Thomas Bayes (1701-1760) and was communicated in 1763 to the Royal Society after Bayes' death (Price, 1763). If H represents a hypothesis and D represents data, Bayes' Theorem may be derived from consideration of the definition of conditional probability:

$$p(H \mid D) = \frac{p(H,D)}{p(D)} \tag{4.1}$$

Noting that p(H,D)=p(D,H), one may then set p(D|H)P(H)=p(H|D)p(D) and rearrange to yield:

$$p(H \mid D) = \frac{p(D \mid H)p(H)}{p(D)} \tag{4.2}$$

where p(H|D) is a probabilistic statement about H after observing data (posterior distribution), p(D|H) is the likelihood of the data given the hypothesis, p(H) is a probabilistic statement of belief about H before observing the data (prior distribution), and p(D) is the marginal distribution of the data. It is the

conditioning on the data and consideration of a prior distribution that distinguishes Bayesian statistics from other statistical methods.

If a hypothesis can be expressed as the parameters of a given model, Bayes' Theorem allows one to update the probabilistic beliefs about model parameters in a logical fashion as

$$p(\theta \mid y) = \frac{p(y \mid \theta)p(\theta)}{p(y)} \tag{4.3}$$

where θ represents the parameter(s) and y represents the data.

4.2 Prior Distributions

Specification of the prior distribution captures the investigator's beliefs about model parameters prior to observing the data. A large body of work exists describing the specification of prior distributions. Methods include specification based on information accumulated from past studies and from opinions of subject-matter experts; by restricting the prior distribution to a familiar distribution; or by using a non-informative distribution. Non-informative prior distributions are often described as vague or diffuse.

Alternatively, one might choose a prior distribution that is conjugate to the likelihood, that is, one that leads to a posterior distribution belonging to the same distributional family as the prior distribution. Choice of such a prior distribution leads to mathematically convenient solutions. It is important to note that as more

data become available, the effect of the prior distribution becomes less important allowing the likelihood function and thus, the data, to take a dominant role in determining the posterior distribution (Le Cam, 1953).

4.3 Likelihood Function

Using Bayes' Theorem with a given probability model means that the data affect posterior inferences only through the likelihood function. To model a time series and thus, construct the likelihood function, consider observations sampled at discrete times consisting of the sum of a growth model term, G_i, and an error term, ε_i:

$$y_i = G_i(\theta, t_i) + \varepsilon_i \tag{4.4}$$

The probability distribution of the error term, the difference between the model term and the data, is then used to construct the likelihood function. In the case of a normally distributed error term when the ε_i are assumed independent, the probability of obtaining a set of ε_i values is given as

$$p(\varepsilon_i \mid \theta) \propto \prod_{i=1}^{N} \frac{1}{(2\pi\sigma^2)^{.5}} \exp\left(\frac{-\varepsilon_i^2}{2\sigma^2}\right) \tag{4.5}$$

The likelihood function is then written as

$$L(\theta) \propto \sigma^{-N} \exp\left(\frac{-1}{2\sigma^2} \sum_{i=1}^{N} [y_i - G_i(\theta, t_i)]^2\right) \tag{4.6}$$

4.4 Hierarchical Models

Many statistical problems involve parameters that can be regarded as related by the structure of the problem. This relationship may be modeled by using a prior distribution in which the individual parameters are viewed as a sample from a population distribution. This idea of exchangeability expresses an unchanging distribution on parameters when the individual parameter suffixes are permutated (Lindley and Smith, 1972).

When considering growth curve analysis where observations are obtained at times for multiple individuals assumed to be drawn from a population, the problem may be modeled hierarchically where parameters describing individual growth are exchangeable under a common population parameter (Fearn, 1975). These models often assume independence between observations and allow inference concerning both individual and population parameters.

4.5 Bayesian Inference

In the case of multiple parameter models, posterior distributions are joint distributions in that they describe the probability distribution of a set of parameters rather than a single parameter. From this joint distribution, marginal distributions may be calculated through summation for discrete distributions or integration for continuous distributions. As an example, given the continuous joint distribution for parameters γ and θ, $p(\gamma,\theta)$, the marginal distribution for γ, $p(\gamma)$, is given as

$$p(\gamma) = \int p(\gamma,\theta)d\theta \tag{4.7}$$

In practice, the integrations required to calculate marginal distributions are often numerically challenging and seldom analytical.

4.5.1 Point Estimation

To obtain a point estimate of θ, one must select a summary statistic of p(θ|y) such as its mean, median, or mode. For example, the posterior mean is calculated as

$$\mu = \int \theta\, p(\theta \mid y)d\theta \tag{4.8}$$

It can be shown that the posterior mean is the Bayes estimate of θ under squared error loss and the posterior median is the Bayes estimate of θ under absolute error loss (DeGroot, 1970). The mode is usually easiest to calculate since it does not require normalization of the posterior distribution. If the prior distribution is flat, the posterior mode will be equal to the maximum likelihood estimate of θ.

4.5.2 Prediction

To make inferences about unknown observables, often called predictive inferences, the same methodology as used for point estimates is utilized. Before considering the data, the distribution of the observable but unknown y is

$$\begin{aligned} p(y) &= \int p(y,\theta)d\theta \\ &= \int p(\theta)p(y \mid \theta)d\theta \end{aligned} \tag{4.9}$$

This is sometimes called the marginal distribution of y or the prior predictive distribution. After observing y, an unknown observable y_f can be predicted using the same method. The distribution of y_f is called the posterior predictive distribution and may be expressed as

$$p(y_f \mid y) = \int p(y_f, \theta \mid y) d\theta \qquad (4.10)$$
$$= \int p(y_f \mid \theta) p(\theta \mid y) d\theta$$

where the second equation shows that the posterior predictive distribution may be expressed as an average of conditional predictions over the posterior distribution of θ. As such, one can consider parameter inference as an intermediate step in the process of observable prediction. Many statisticians argue that the emphasis on parameter inference is misguided in that reparameterization of a given model leads to different ranges of values for parameters which are in the final analysis, unobservable.

4.6 Model Assessment and Comparison

Previous sections have provided a brief overview of the Bayesian methodology. Upon choosing the model likelihood function and prior distribution, questions arise concerning these choices. The first question concerns the determination of whether a model is providing an adequate fit to the data, also

referred to as model assessment. The next question concerns the choice of a model among a group of models and may be referred to as model comparison. Each of these questions has a wide literature base, Bayesian and non-Bayesian alike. Sections 4.6.1 and 4.6.2 will briefly examine each of these questions in turn.

4.6.1 Model Assessment

Model assessment attempts to answer the question as to adequate fit of the data. As an example, in standard linear regression, the assumptions of normality, independence, linearity, and homogeneity of variance may be investigated. Some have advocated the use of the marginal distribution of the data, p(y). Values of $p(y_i)$ which are small are considered unlikely and thus, the associated y_i values may be considered as outliers. Too many outliers suggest model inadequacy. Criticisms of this approach include defining "small" and "too many." As such, many investigators have chosen to work with predictive distributions of which several variations have been proposed.

A model may be fit with a fitting sample of data, z, and then checked with an independent validation sample, y. Residuals, the difference between observed and fitted values, may be calculated as

$$r_i = y_i - E(Y_i \mid z) \tag{4.11}$$

Plotting residuals versus fitted values may reveal failure in normality or homogeneity of variance assumptions, and plotting residuals versus time may reveal a failure of independence. Summing the squares of residuals may provide an overall measure of fit. If independent data samples, z and y, are not available, an alternative may be a "cross-validatory" (or leave one out) approach (Stone, 1974; Gelfand et al., 1992). The fitted value for y_i is calculated conditional on all the data except y_i, written as $y_{(i)}$. Again, residuals may be calculated as

$$r_i = y_i - E(Y_i \mid y_{(i)}) \tag{4.12}$$

Cross-validation predictive densities are usually calculated by

$$p(y_i \mid y_{(i)}) = \int p(y_i \mid \theta, y_{(i)}) p(\theta \mid y_{(i)}) d\theta \tag{4.13}$$

where values of $p(y_i|y_{(i)})$ evaluated at the observed data are referred to as the Conditional Predictive Ordinates (CPOs). These can be plotted versus i to test for outliers. Additional expectations of functions using cross-validation techniques have been proposed (Gelfand et al, 1992) for model assessment.

Another approach for using predictive densities is that of posterior predictive checks (Rubin, 1984). The posterior predictive density, $p(y|y_{obs})$, is the

predictive density of a new independent set of observables given the actual observables:

$$p(y \mid y_{obs}) = \int p(y \mid \theta) p(\theta \mid y_{obs}) d\theta \tag{4.14}$$

4.6.2 Model Comparison

Model comparison, like model assessment, techniques span a wide spectrum ranging from strictly formal calculation of Bayes factors to various uses of other predictive distributions, to somewhat informal graphical techniques. Box described the role of predictive distributions as enabling "criticism of the entertained model in the light of current data" (Box, 1980). Several criticisms have arisen concerning the use of Bayes factors. Smith argued that a Bayes factor approach is strictly appropriate only when one of the entertained models is believed to be the "true" model (Smith, 1991). Another criticism concerns the use of improper prior distributions which then lead to improper marginal densities and either undefined or "uncalibrated" Bayes factors. Sensitivity to prior variance is yet another potential downside of the use of Bayes factors.

For these reasons, some investigators have turned to predictive densities. One such predictive density is the cross-validation predictive density as discussed in section 4.6.1. The product of CPOs has been used as a surrogate for the marginal density, expressed as the pseudo-Bayes factor (Geisser and Eddy, 1979; Gelfand et al., 1992)

$$\prod_{i=1}^{n} p(y_i \mid y_{(i)}) = \prod_{i=1}^{n} \frac{p(y_{i,obs} \mid y_{(i),obs}, M_1)}{p(y_{i,obs} \mid y_{(i),obs}, M_2)} \quad (4.15)$$

Likewise, comparison of models can be based on the negative cross-validatory log-likelihood

$$-\sum_{i=1}^{n} \ln(p(y_{i,obs} \mid y_{(i),obs}))$$

Plots of the conditional predictive ordinates for both models versus i can also indicate model preference.

Model assessment and comparison techniques span a wide range of formal and informal methodologies. The previous discussion is but a brief overview of some of the techniques found in the literature.

CHAPTER 5

MARKOV CHAIN MONTE CARLO TECHNIQUES

5.1 General

The single largest impediment to implementing the Bayesian statistical methodology for complex statistical problems has been the difficulty in performing required integrations for parameter and predictive inference. Revolutions in both computing hardware and software algorithms in the 1990's have allowed ever-more complex analyses. Methods for numerical integration include Gaussian quadrature, asymptotic approximation methods, lattice integration methods, and non-iterative Monte Carlo methods. Markov Chain Monte Carlo (MCMC) methods provide a powerful alternative to execute the integrations necessary for inference.

The most widely used MCMC simulation methods are the generalized Metropolis algorithm (Metropolis, et al., 1953; Hastings, 1970) and the Gibbs sampler (Geman and Geman, 1984). Gelfand and Smith pointed out the Gibbs sampler to the general statistics community as a method for sampling posterior distributions (Gelfand and Smith, 1990). The following sections provide a brief overview of Markov chain properties, distribution sampling methods, and MCMC convergence diagnostic techniques.

5.2 Markov Chains

Most simply stated, a Markov chain is a stochastic process where given the present state, past and future states are independent. This may be written more formally as

$$p[X_t \in A \mid X_0, X_1, \ldots X_{t-1}] = p[X_t \in A \mid X_{t-1}] \tag{5.1}$$

for a discrete time stochastic process $\{X_0, X_1, \ldots\}$. If the distribution of X_t is to converge to a stationary distribution, the Markov chain must satisfy three properties (Roberts, 1996). The first property to be satisfied is that of irreducibility. That is, from all starting values, the Markov chain can reach any non-empty set with positive probability in some number of iterations. The second property to be satisfied is that of aperiodicity. That is, the chain does not oscillate between states in a regular periodic movement. The last property is that a chain must be positive recurrent, which can be expressed in terms of the existence of a stationary distribution $\pi(.)$. If the initial value, X_0, is sampled from $\pi(.)$, all subsequent iterates will be distributed according to $\pi(.)$ or written as

$$\sum_i \pi(i) p_{ij}(t) = \pi(j) \tag{5.2}$$

for all j and $t \geq 0$. For all aperiodic positive-recurrent Markov chains, the stationary distribution is the limiting distribution of iterates from the chain.

Under these conditions, ergodic averages, written as

$$\overline{f_N} = \frac{\sum_{t=1}^{N} f(X_t)}{N} \tag{5.3}$$

converge to their expectations under the stationary distribution. MCMC output is usually summarized in terms of ergodic averages. This ergodic theorem, however, offers no solution as to how long the Markov chain must be run before iterations are distributed according to $\pi(.)$. Additional discussion of chain convergence will be addressed in section 5.6.

The goal of MCMC simulation is to create a Markov process for which the stationary distribution is the joint posterior distribution and to then run the simulation long enough such that the distribution of iterates is close to the stationary distribution. After constructing a model and its associated distributions, the next step is to sample from those distributions. The following sections describe three methodologies for sampling.

5.3 Gibbs Sampler

5.3.1 General

The Gibbs sampler is one of the most-widely used MCMC methodologies. This method was given its name (Geman and Geman, 1984) as it was used for analyzing Gibbs distributions on lattices. The Gibbs distribution may be described by its transition kernel, the density of going from one point, X, to

another, Y. The transition kernel is formed from the full conditional distributions, $\pi(X_i|X_{-i})$, the distribution of the i^{th} component of X conditioning on all remaining components. Full conditional distributions are formed as

$$\pi(X_i \mid X_{-i}) = \frac{\pi(X)}{\int \pi(X) dX_i} \tag{5.4}$$

The transition kernel is then given as

$$K(X,Y) = \prod_{i=1}^{d} \pi(Y_i \mid \{Y_j, j\{i\}, \{X_j, j > i\}\}) \tag{5.5}$$

the product of the conditional densities of the individual steps required to produce an iteration of the Gibbs sampler.

An important result is the derivation that the stationary distribution of a chain with the transition kernel given by equation (5.5) is the joint distribution of interest. Examples for both discrete and continuous cases are given by Gamerman (Gamerman, 1997). Under very mild conditions, the set of all full conditional distributions determine the joint distribution. Thus, the Markov chain with transition kernel given by equation (5.5) converges to the distribution of interest. Given an arbitrary set of starting values

$$\theta_1^{(0)}, \theta_2^{(0)}, \theta_3^{(0)}, \ldots, \theta_k^{(0)}$$

for the unknown quantities where the iteration number is given in parentheses, Gibbs sampling may be implemented using the following iterative procedure:

$$draw\,\theta_1^{(1)}\ from\ p(\theta_1 \mid x, \theta_2^{(0)}, ..., \theta_k^{(0)})$$

$$draw\,\theta_2^{(1)}\ from\ p(\theta_2 \mid x, \theta_1^{(1)}, \theta_3^{(0)}, ..., \theta_k^{(0)})$$

.

.

.

$$draw\,\theta_k^{(1)}\ from\ p(\theta_k \mid x, \theta_1^{(1)}, ..., \theta_{k-1}^{(1)})$$

$$draw\,\theta_1^{(2)}\ from\ p(\theta_1 \mid x, \theta_2^{(1)}, ..., \theta_k^{(1)})$$

.

.

.

These iterations are continued until convergence is reached with the resulting values of θ drawn from the stationary distribution. While this iterative procedure seems straightforward, sampling or drawing from the full conditional densities may not be easy.

5.3.2 Sampling from Full Conditional Densities

An important result for simplifying sampling from full conditional densities is that to construct the full conditional density for a given unknown, one only needs to consider terms from the joint density which contain the unknown. This may be shown with a simple application of the definition of conditional

densities. As an example, for a two parameter model with parameters, α and β, with observed data, y, the joint posterior of α and β, is given as

$$p(\alpha,\beta \mid y) = \frac{p(\alpha,\beta,y)}{p(y)} \tag{5.6}$$

The full conditional density of α is given by

$$p(\alpha \mid \beta) = \frac{p(\alpha,\beta \mid y)}{p(\beta \mid y)} \tag{5.7}$$

$$= \frac{p(\alpha,\beta,y)}{p(\beta,y)}$$

$$\propto p(\alpha,\beta,y)$$

where the denominator does not depend on α. Although this property greatly simplifies calculations, sampling from this less complex density still presents a computational challenge. Since full conditionals change from iteration to iteration as the conditioning changes, each full conditional calculation is used only once. As such, sampling methods must be as computationally efficient as possible. The following sections briefly describe some of these sampling methods.

5.3.3 Rejection Sampling

To perform rejection sampling, an envelope function, $g(\theta)$, must be defined for all θ for which $p(\theta,y)>0$. Samples are drawn from the density proportional to $g(\theta)$ with each sampled θ tested for acceptance or rejection. Draws are accepted with probability $p(\theta|y)/g(\theta)$ or else are rejected. This sampling continues until the required number of draws have been accepted. To reduce the number of rejections, the envelope function should be close to $p(\theta|y)$. Computational efficiencies may be gained by using "squeezing functions", $a(\theta)$ and $b(\theta)$, such that $a(\theta)\geq g(\theta)\geq b(\theta)$ where $a(\theta)$ and $b(\theta)$ are more efficiently evaluated than $g(\theta)$.

5.3.4 Adaptive Rejection Sampling

For those densities which are log-concave, envelope functions may be constructed with the aid of graphical techniques (Gilks and Wild, 1992). A density, $\pi(x)$, is said to be log-concave if the vector of the derivatives of its logarithm exists and has non-increasing components in x. Log-concavity may also be defined, in the univariate sense, as

$$\log\pi(x_1) - \log\pi(x_2) \leq \log\pi(x_2) - \log\pi(x_3) \tag{5.8}$$

for $x_1<x_2<x_3$. Gilks and Wild showed that for univariate X an envelope function could be constructed by drawing tangents to $\log\pi(.)$ at each given abscissa. The

envelope is constructed from these tangents. An alternative which does not require the calculation of derivatives was developed by Gilks (Gilks, 1992). This method uses secants rather than tangents. Both methods require starting abscissae to be placed on both sides of the mode. The adaptive portion of the algorithm stems from the use of sampling points, $\pi(x)$, calculated during the rejection step. Rejected points can be used for "tightening" the envelope by incorporating a new tangent line. The envelope function then better approximates $\pi(x)$ and thus, reduces the number of rejections. The use of tangent lines in the univariate case may be extended to tangent planes and hyperplanes for higher dimension cases.

5.4 Metropolis-Hastings Sampling

The Metropolis-Hastings algorithm (Hastings,1970) is a generalization of the Metropolis method. At each time, t, the next state X_{t+1} is chosen by sampling a candidate point, Y, from a proposal distribution $q(.|X_t)$. The candidate point Y is accepted with probability $\alpha(X_t,Y)$ given by

$$\alpha(X,Y) = \min(1,\frac{\pi(Y)q(X \mid Y)}{\pi(X)q(Y \mid X)}) \qquad (5.9)$$

If the candidate point is accepted, $X_{t+1}=Y$. If the candidate point is rejected, $X_{t+1}=X_t$. Variations of the Metropolis-Hastings algorithm are usually defined by the properties of the proposal distribution. Two widely-used versions are the independence sampler and the random walk Metropolis algorithms.

The independence sampler uses $q(X,Y)=q(Y)$. Although it seems that the independence from the previous state, X, disagrees with the Markov property of the chain, q is a proposal distribution that must be combined with an acceptance probability to give the transition kernel. As such, the Markov property remains valid.

The random walk algorithm uses $q(X,Y)=f_w(Y-X)$ where f_w is symmetric around the current state. The most widely used choices for f_w are the normal (Muller, 1991) and the Student's t (Geweke, 1992) distributions. The magnitude of the variances then dictate the efficiency of the chain for reaching convergence to the stationary distribution. A large variance allows wide moves in the parameter space with high rejection rates, and a small variance allows small moves in the parameter space with low acceptance rates.

5.5 Slice Sampling

To utilize Gibbs sampling, methods must be developed to sample from non-standard, univariate, full conditional distributions. To utilize Metropolis-Hastings sampling, an appropriate proposal distribution must be found. An alternative class of sampling methods, called "slice sampling", has been developed (Neal, 1997) to overcome these potential disadvantages. Slice sampling methods originate from the idea that a univariate distribution may be sampled uniformly from the region under the curve of its density function. Subsequently, only the horizontal coordinates of the sample points need to be

considered. A Markov chain that converges to this uniform distribution can be constructed by alternately sampling uniformly from the vertical interval defined by the density at the current point and from the horizontal slice defined by the union of intervals through the density at the point chosen from the vertical interval. Multivariate distributions can be sampled by looking at each variable in turn.

If f(x) is a function proportional to the probability density for variable X, the procedure to update the current value x_0 with a new value x, is as follows:

(1) Draw a value y uniformly from $(0,f(x_0))$. This defines a horizontal slice, $S=\{x:y<f(x)\}$

(2) Find an interval $I=\{L,R\}$ around x_0 that contains a large part of the slice

(3) Draw the new point, x_1, from the part of the slice within the interval, I.

The slice sampling method provides a valuable tool, in addition to the Gibbs and Metropolis-Hastings methods, for sampling complex distributions.

5.6 Convergence Diagnostics

Convergence diagnostics are used to determine if the MCMC simulation has been run for enough iterations to allow convergence to the stationary distribution. These initial iterations are often referred to as "burn-in". Some convergence diagnostic algorithms have been constructed to consider not only

whether convergence has been reached but also to consider the independence of successive iterates. Two general methods have been developed to study the convergence of Markov chains. The first method is theoretical and attempts to measure variation distances and establish bounds on distribution functions generated by a Markov chain. In general, this approach is difficult and has not been fully explored. Most practical work has approached the study of convergence from a statistical approach in that properties of the chain output are analysed. Three such approaches are briefly discussed next.

The Gelman-Rubin convergence diagnostic may be used for the analysis of two or more parallel chains. This diagnostic (Gelman and Rubin, 1992) is based on the comparison of the within and between chain variance for each variable. The comparison is used to estimate the potential scale reduction factor, the multiplicative factor by which the estimate of the posterior distribution scale parameter might be reduced if the chains were run to infinity. Calculation of these reduction factors is based on analysis of variance and sampling from the normal distribution.

The Raferty-Lewis convergence diagnostic (Raferty and Lewis, 1992) attempts to detect convergence to the stationary distribution and to provide a way of bounding the variance of estimates of quantiles of functions of parameters. This approach is based on two-state Markov chain theory and standard sample size formulas involving binomial variance. A binary sequence is formed with a

0/1 indicator for each iteration as to whether the quantity of interest is less than the specified cutoff. This diagnostic provides the smallest skip interval for which the behavior of a new binary sequence approximates that of a first-order Markov chain, as well as the number of iterations to approach within some specified value of the estimated stationary distribution.

The Heidelberger-Welch convergence diagnostic (Heidelberger and Welch, 1983) may also be used for the analysis of single chains. This stationarity test is based on Brownian bridge theory. A halfwidth test is performed on the portion of the chain that passes the stationarity test. Spectral density estimation is used to compute the asymptotic standard error of the mean. This mean is estimated with acceptable accuracy if the halfwidth of the confidence interval for the mean is less than a specified accuracy of the mean.

5.7 Forming the Sample

After choosing the method of sampling the target distribution and determining the convergence diagnostic to be utilized, one must decide how to form the sample. Several methods have been proposed, with no consensus reached by the statistics community. The independent sampling approach (Gelfand and Smith, 1990) forms n chains in parallel until convergence, with the last iterate from each of the n chains used to form the sample. Using independent initial values with large dispersion helps to establish independent values in the sample.

Another method is to form a single chain and utilize ergodic results (Geyer, 1992). All chain values have marginal distributions given by the equilibrium distribution, and the sample is formed from the n successive iterates (after burn-in) of the chain. These sample iterates are not independent due to chain dependence, but ergodic theorems ensure that inference based on the sample is valid. If chain autocorrelation is too high, this method may take a long time to adequately sample the parameter space.

Yet another method to consider is to "thin" the chain (Raferty and Lewis, 1992) by taking every k^{th} iteration of the chain after convergence. For larger k, chain values become less correlated, and the samples may be said to be "quasi-independent". This method is advantageous if computer storage is limited although there is no gain in efficiency as compared to retaining all chain values. Single chain proponents argue that independent samples are not required for ergodic averages. Multiple chain proponents argue that multiple chains may reveal that chains have not reached stationarity. Debate continues as to the need for running multiple chains versus a single chain.

CHAPTER 6

METHODOLOGY AND RESULTS FOR INDIVIDUAL SPE NON-LINEAR REGRESSION MODELS

6.1 Computational Techniques

MCMC techniques for sampling distributions of interest were implemented with the Bayesian Inference Using Gibbs Sampling (BUGS) software package (Spiegelhalter, et al., 1999; Spiegelhalter, et al., 2000). BUGS allows construction of a probability model consisting of a joint distribution over all observed and unobserved quantities. BUGS allows many standard distributions and utilizes a variety of sampling techniques including (1) direct sampling using standard algorithms, (2) derivative-free adaptive rejection sampling, (3) slice sampling, and (4) point Metropolis. The method of sampling depends on the mathematical form of the full conditional distributions.

MCMC convergence diagnostics were implemented with either BUGS or the Bayesian Output Analysis (BOA) software package (Smith, 2000). The modified Gelman-Rubin diagnostic, as revised by Brooks and Gelman (Gelman and Rubin, 1992; Brooks and Gelman, 1998) is included in the BUGS software package. The Raferty-Lewis diagnostic (Raferty and Lewis, 1992) and the Heidelberger-Welch diagnostic (Heidelberger and Welch, 1983) are included in the BOA software package.

Posterior predictive intervals and checking functions, as described in section 4.6.2, were used for model assessment and were calculated using BUGS. Conditional predictive ordinates for model comparison/selection were calculated using BUGS. A Monte Carlo estimate of $p(y_i|y_{(i)})$ is obtained as a harmonic mean of $p(y_i|y_{(i)},\theta)$ using

$$\frac{1}{p(y_i \mid y_{(i)})} = \int \frac{1}{p(y_i \mid y_{(i)}, \theta)} p(\theta \mid y) d\theta \qquad (6.1)$$

(Gelfand and Dey, 1994) which may be sampled using BUGS. Negative cross-validatory log-likelihood values and pseudo Bayes factors were used for model comparison/selection.

6.2 Investigations Utilizing Individual SPE Non-Linear Regression Models

Initial efforts at fitting and prediction of asymptotic dose, dose-time profiles, and dose rate-time profiles utilized individual SPE non-linear regression models. Data from an individual SPE, a growth curve model likelihood as described in section 4.3, uniform growth curve parameter prior distributions formed from estimations of the parameter space based on earlier work, and normally distributed errors are used to form models in these preliminary investigations.

6.2.1 Fitting of Organ Doses Using Alternative Growth Curves

Previous work (Zapp et al., 1998) had fit various organ doses using a Weibull growth curve and least squares regression techniques. The asymptotic dose was treated as a known rather than as an unknown parameter. As there was nothing to suggest a preference for any given member of the non-linear sigmoidal curve family, investigations to examine the adequacy of other non-linear sigmoidal growth curves were conducted (Neal and Townsend, 2000). Weibull, Gompertz, and logistic growth curves

$$D = D_{\infty}(1 - \exp(-(\alpha t)^{\gamma})) \tag{6.2}$$

$$D = \exp(\alpha - \beta\gamma^{t}) \tag{6.3}$$

$$D = \frac{K}{1 + C\exp(-rt)} \tag{6.4}$$

were used in conjunction with non-linear regression models for fitting individual skin and eye data sets for the (1) March 23, 1991, (2) June 4, 1991, and (3) August 4, 1972 SPEs. Proton flux was transported through 2 g/cm^2 of aluminum and 100 cm of water (assumed to be soft tissue equivalent) prior to entering the organs of interest. Data sets are presented in Tables A.1 through A.3. Raferty - Lewis and Heidelberger-Welch convergence diagnostics were used for convergence monitoring.

Assuming a Weibull growth curve, the model may be represented as

$$
\begin{aligned}
& y_i = D_\infty(1-\exp(-\alpha t_i)^\gamma)) + \varepsilon_i \\
& \varepsilon_i \sim N(0,\tau) \\
& D_\infty \sim U(0,10000) \\
& \alpha \sim U(0,5) \\
& \gamma \sim U(0,20) \\
& \tau \sim Ga(0.001,0.001)
\end{aligned}
\tag{6.5}
$$

where N(.), U(.), and Ga(.) indicate the Normal, Uniform, and Gamma probability distributions, respectively. Assuming a Gompertz growth curve, the model may be represented as

$$
\begin{aligned}
& y_i = \exp(\alpha - \beta\gamma^{t_i}) + \varepsilon_i \\
& \varepsilon_i \sim N(0,\tau) \\
& \alpha \sim U(-5,10) \\
& \beta \sim U(0,50) \\
& \gamma \sim U(0,1) \\
& \tau \sim Ga(0.001,0.001)
\end{aligned}
\tag{6.6}
$$

Assuming a logistic growth curve, the model may be represented as

$$
\begin{aligned}
& y_i = \frac{K}{1 + C\exp(-rt_i)} + \varepsilon_i \\
& \varepsilon_i \sim N(0,\tau) \\
& K \sim U(0,10000) \\
& C \sim U(0,40000) \\
& r \sim U(0,20) \\
& \tau \sim Ga(0.001,0.001)
\end{aligned}
\tag{6.7}
$$

Tables 6.1 through 6.6 present posterior parameter mean values for each of the three growth curves. Dose time profiles were generated using posterior parameter mean values and the respective growth curve function. Figures 6.1 through 6.6 present dose-time profiles.

Model assessment was originally performed (Neal and Townsend, 2000) using (1) the standardized residual, (2) the chance of getting a more extreme observation, and (3) the predictive ordinate of each observation. The same data sets were analyzed again using posterior predictive checks. The percentage of observations which fell into the 50% and 95% predictive intervals are presented in Table A.4. These models generally support the predictive intervals and indicate adequate fits of the data.

Model comparison used the negative cross-validatory log-likelihood statistic. As this statistic is an accumulation of the negative logarithm of likelihoods over observations, a smaller value of the negative cross-validatory log-likelihood indicates preference for a model. Table 6.7 presents the model comparison statistics. The Weibull model was preferred for the March 23, 1991 and the August 4, 1972 SPEs for both skin and eye dose. The Gompertz model was preferred for the June 4, 1991 SPE for both skin and eye dose.

Table 6.1. Weibull growth curve posterior parameter means and 95% confidence intervals for skin dose.

SPE	D_∞ (cGy)	α	γ
March 23, 1991	140.8 (139.6, 142.0)	.9540 (.9467, .9611)	5.865 (5.584, 6.169)
June 4, 1991	22.10 (21.54, 22.66)	1.025 (.9849, 1.067)	2.141 (1.940, 2.364)
August 4, 1972	707.6 (688.4, 727.2)	.09588 (.09278, .09896)	2.536 (2.306, 2.777)

Table 6.2. Weibull growth curve posterior parameter means and 95% confidence intervals for eye dose.

SPE	D_∞ (cGy)	α	γ
March 23, 1991	81.64 (81.08, 82.22)	.9526 (.9469, .9583)	5.856 (5.643, 6.079)
June 4, 1991	16.34 (15.91, 16.77)	1.058 (1.012, 1.103)	2.097 (1.894, 2.324)
August 4, 1972	529.3 (517.0, 541.9)	.09849 (.09572, .1014)	2.527 (2.317, 2.739)

Table 6.3. Gompertz growth curve posterior parameter means and 95% confidence intervals for skin dose.

SPE	α	β	γ
March 23, 1991	4.968 (4.929, 5.007)	43.81 (31.05, 49.82)	.01413 (.0110, .0206)
June 4, 1991	3.103 (3.086, 3.120)	6.6 (5.727, 7.582)	.06326 (.0518, .0768)
August 4, 1972	6.586 (6.55, 6.62)	8.399 (6.551, 11.34)	.7585 (.7291, .7821)

Table 6.4. Gompertz growth curve posterior parameter means and 95% confidence intervals for eye dose.

SPE	α	β	γ
March 23, 1991	4.424 (4.386, 4.461)	43.93 (30.07, 49.82)	.01423 (.01112, .02134)
June 4, 1991	2.801 (2.782, 2.820)	6.4 (5.441, 7.497)	.05997 (.0470, .0748)
August 4, 1972	6.294 (6.263, 6.323)	8.51 (6.736, 10.98)	.7512 (.7261, .7734)

Table 6.5. Logistic growth curve posterior parameter means and 95% confidence intervals for skin dose.

SPE	K (cGy)	C	r
March 23, 1991	141.2 (139.4, 143.1)	5331 (2882, 10590)	8.709 (8.132, 9.469)
June 4, 1991	21.74 (20.97, 22.53)	38.07 (22.21, 67.24)	4.355 (3.72, 5.136)
August 4, 1972	707.8 (687.8, 728.3)	45.72 (32.13, 64.44)	.4174 (.3782, .4589)

Table 6.6. Logistic growth curve posterior parameter means and 95% confidence intervals for eye dose.

SPE	K (cGy)	C	r
March 23, 1991	81.89 (80.98, 82.79)	5367 (3058, 9814)	8.713 (8.179, 9.38)
June 4, 1991	16.07 (15.47, 16.68)	36.31 (20.07, 71.39)	4.421 (3.708, 5.414)
August 4, 1972	529.1 (514.7, 543.4)	45.81 (31.87, 65.81)	.4293 (.3881, .474)

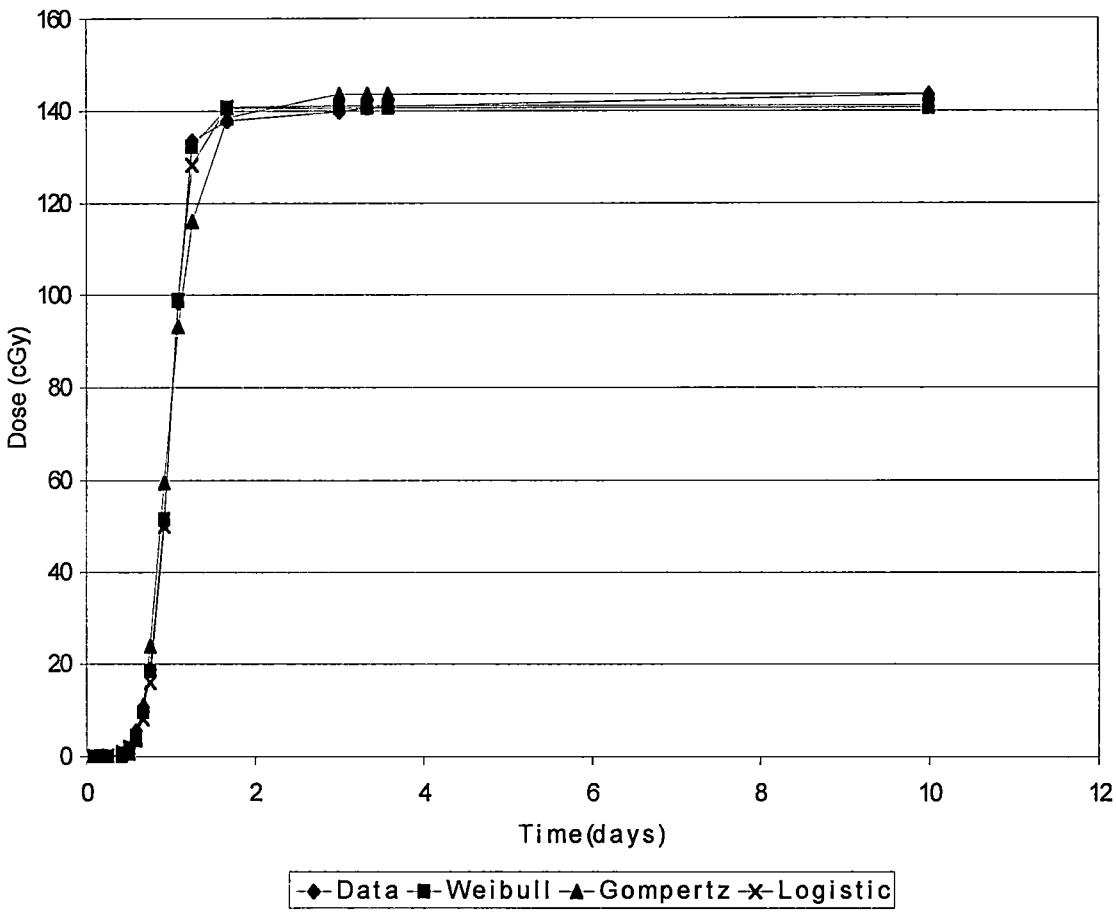


Figure 6.1. Skin dose-time profile fits using posterior parameter means for the March 23, 1991 SPE.

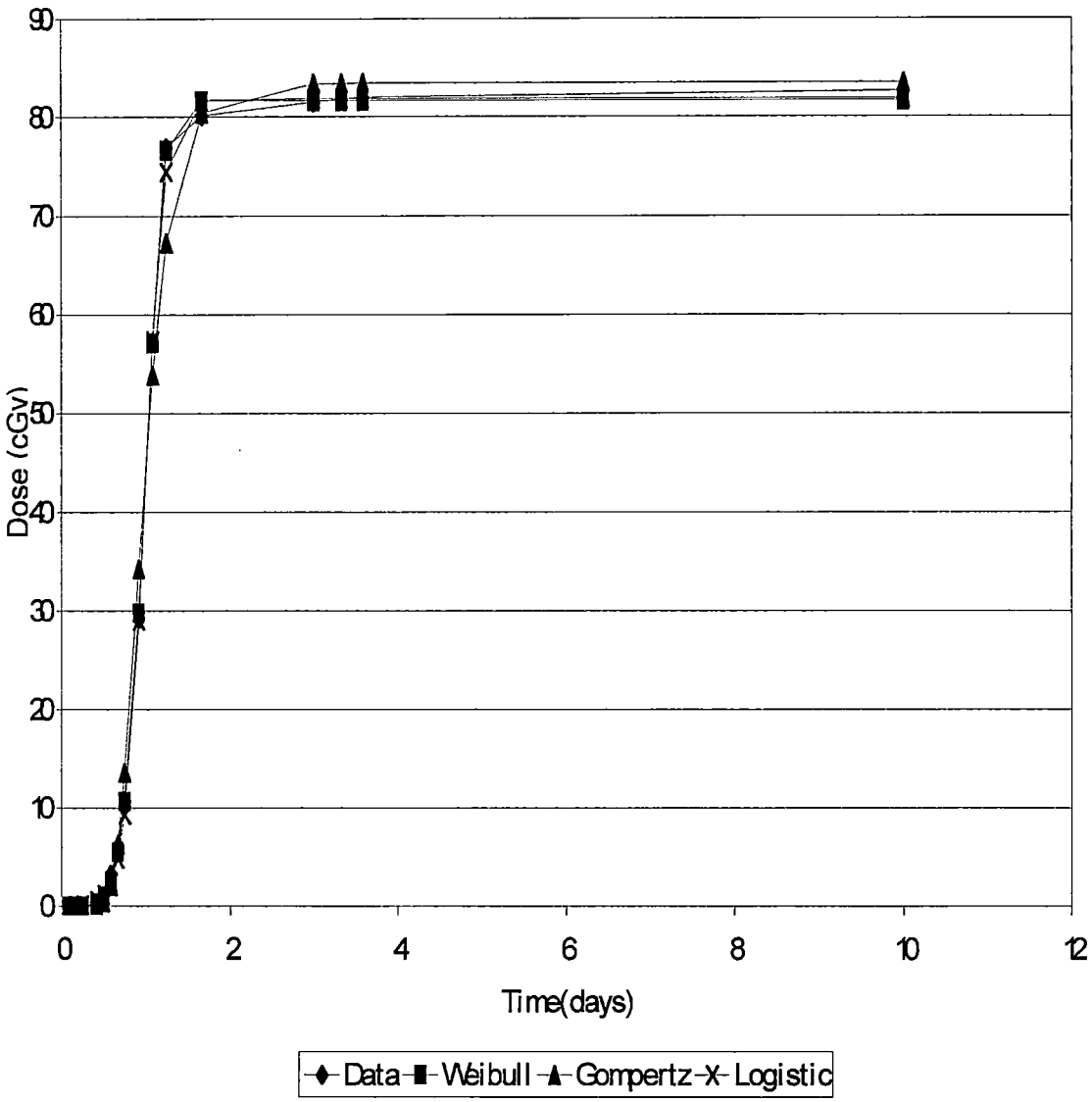


Figure 6.2. Eye dose-time profile fits using posterior parameter means for the March 23, 1991 SPE.

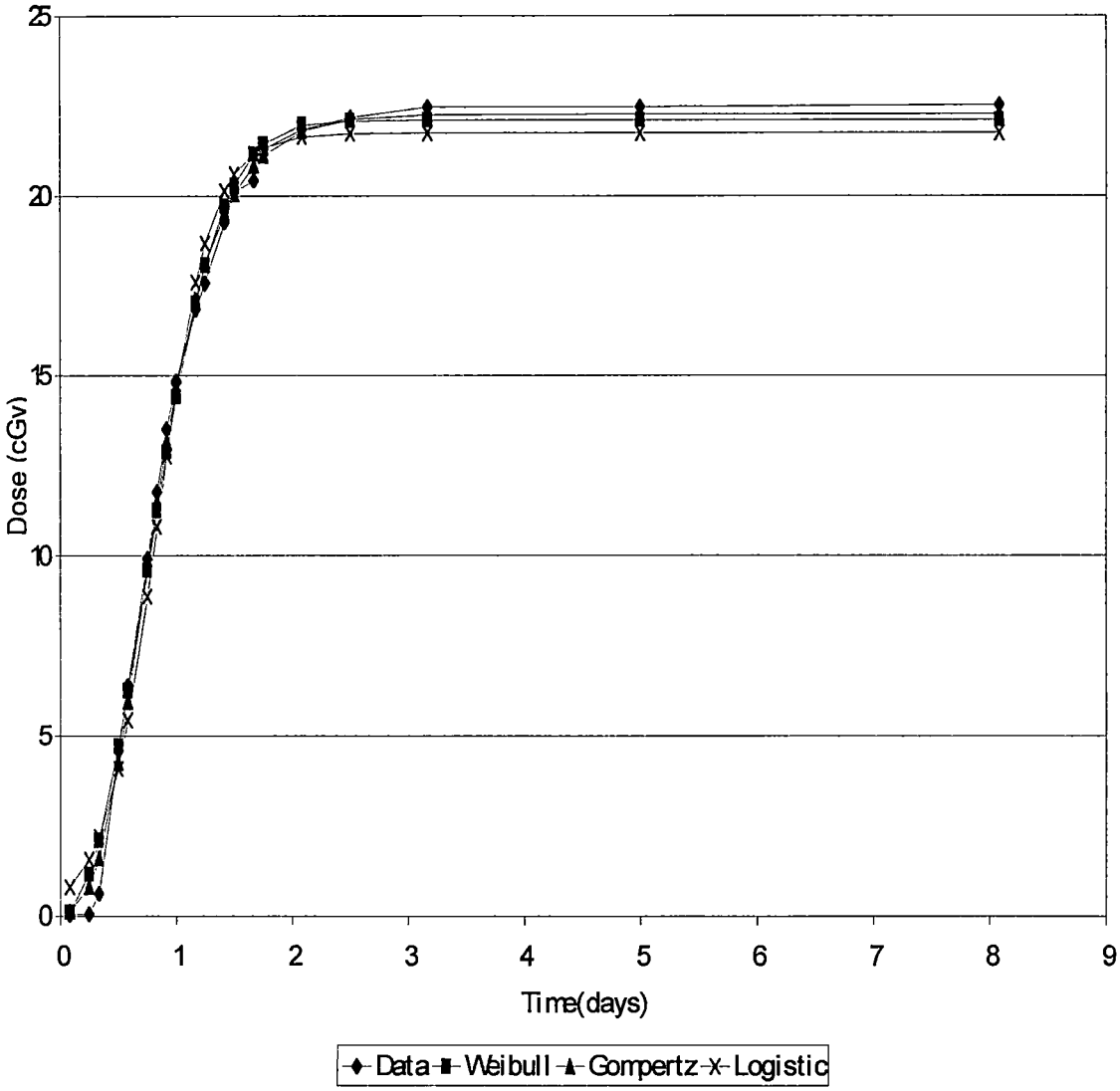


Figure 6.3. Skin dose-time profile fits using posterior parameter means for the June 4, 1991 SPE.

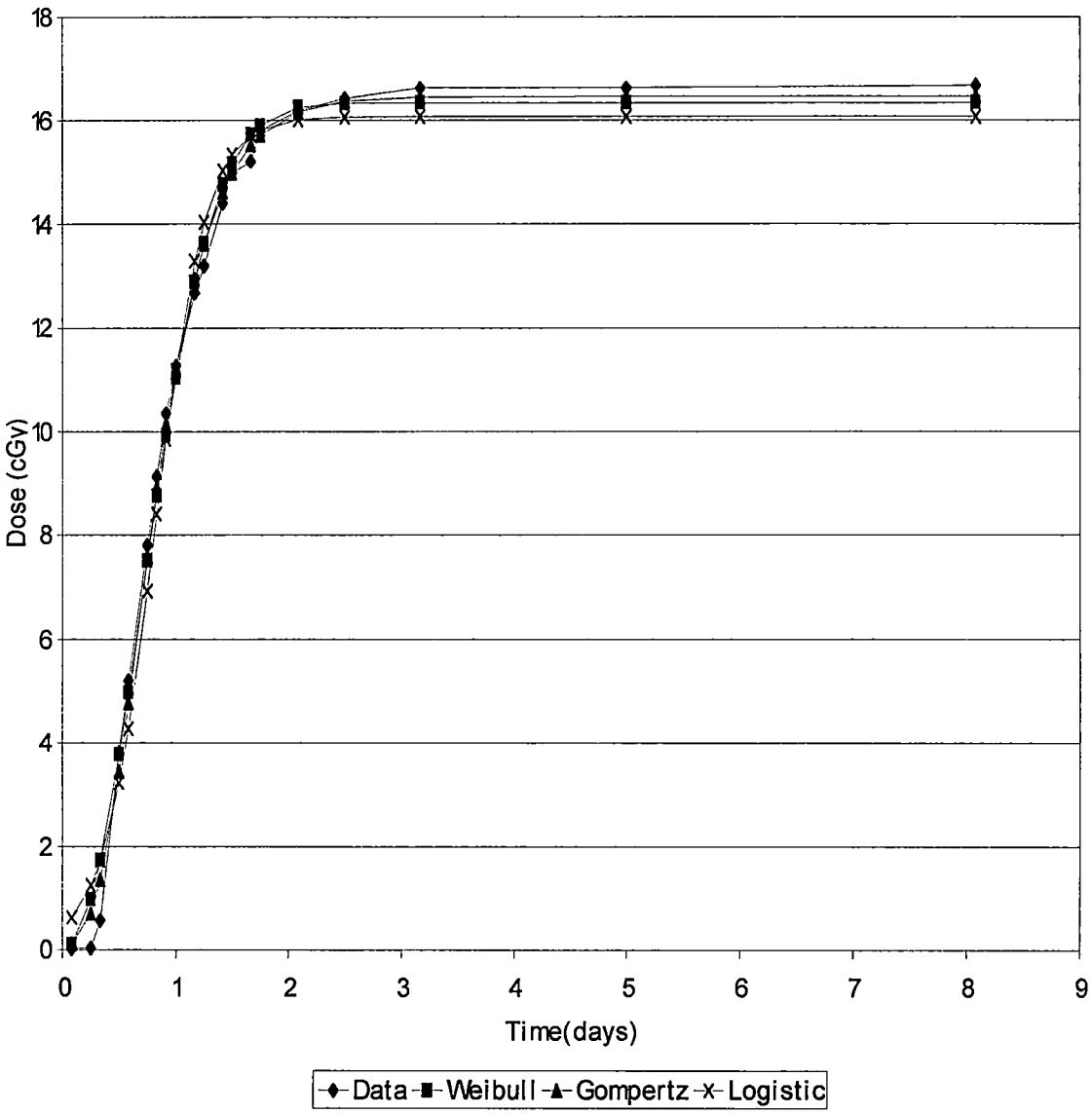


Figure 6.4. Eye dose-time profile fits using posterior parameter means for the June 4, 1991 SPE.

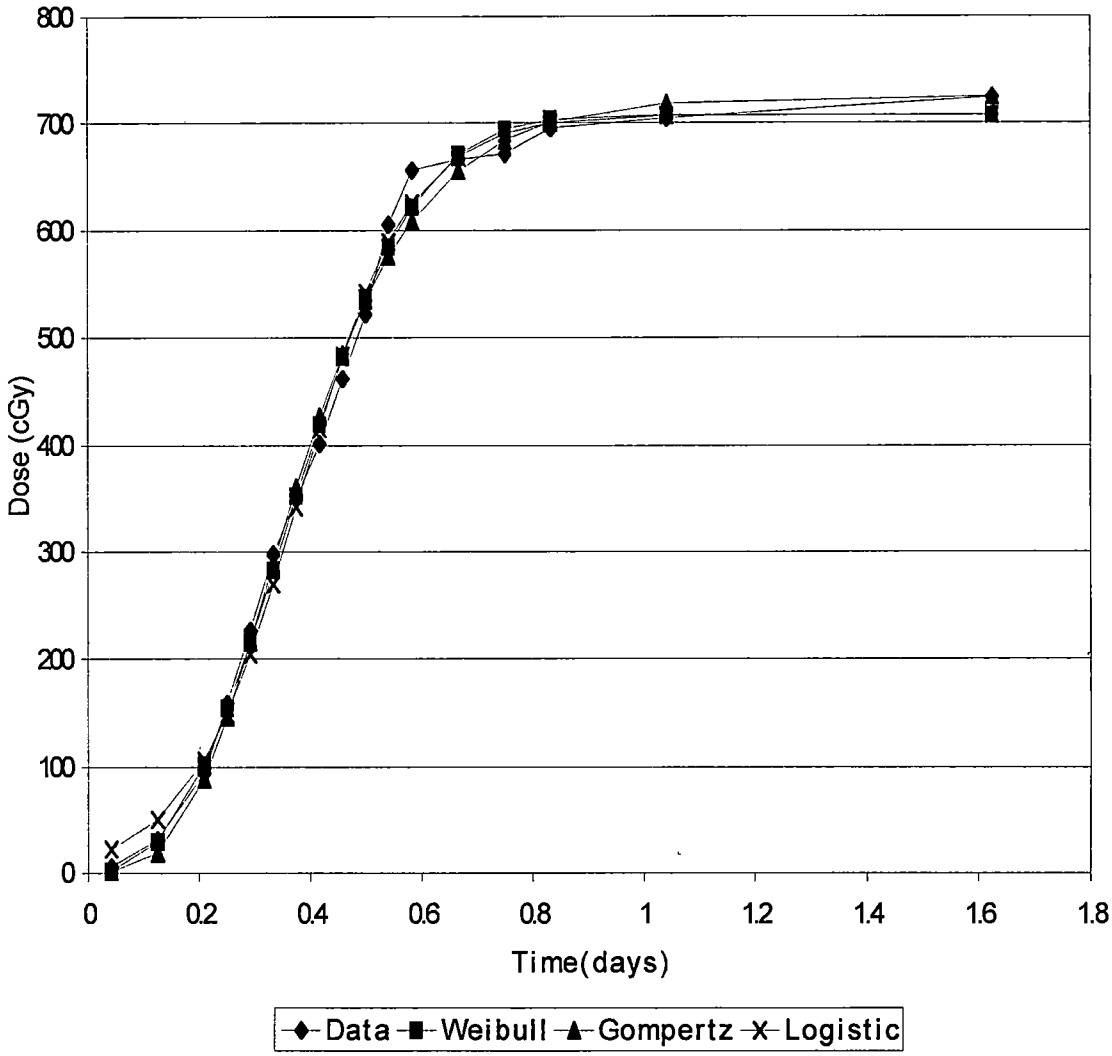


Figure 6.5. Skin dose-time profile fits using posterior parameter means for the August 4, 1972 SPE.

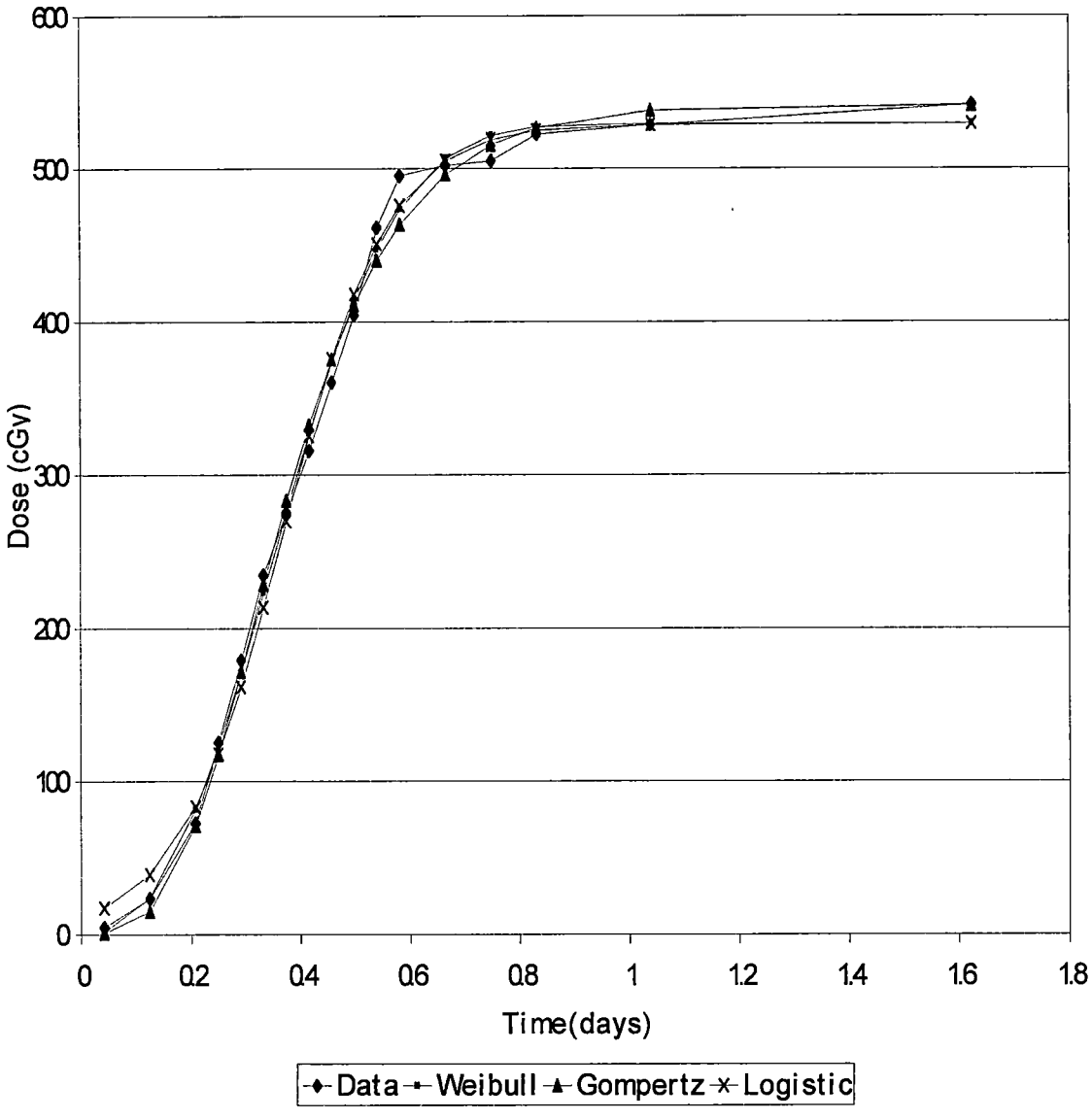


Figure 6.6. Eye dose-time profile fits using posterior parameter means for the August 4, 1972 SPE.

Table 6.7. Calculated negative cross-validatory log-likelihood values of skin and eye dose-time profile fits. Smaller values indicate model preference.

SPE	Weibull	Gompertz	Logistic
March 23, 1991 skin	31.28	57.6	38.61
June 4, 1991 skin	21.08	14.08	29.21
August 4, 1972 skin	75.37	78.36	76.56
March 23, 1991 eye	19.43	46.63	27.97
June 4, 1991 eye	16.36	10.72	24.42
August 4, 1972 eye	68.41	71.44	71.08

Results indicate the adequacy of the three growth curves for fitting individual SPE dose-time profiles. As such, it seems reasonable to consider all of these growth curves in future efforts to make parameter inferences and to predict dose and dose rate-time profiles.

6.2.2 Calculation of Doses in Water

In addition to investigating alternative growth curves, doses in water were calculated in order to determine if the non-linear sigmoidal shape of dose-time profiles was unique to organ dose-time profiles. Proton fluxes were transported through 1 g/cm^2 of aluminum shielding prior to the water. Non-linear regression models using growth curves, as given by equations (6.2) and (6.4), as

well as a reparameterized version of equation (6.3),

$$D = \exp(\alpha - \beta \exp(-\gamma t)) \tag{6.8}$$

were used to fit dose data for the (1) May 6, 1989, (2) January 31, 1991, (3) March 23, 1991, (4) June 4, 1991, and (5) August 26, 1991 SPEs. Data sets are presented in Tables B.1 through B.5. Raferty-Lewis and Heidelberger-Welch convergence diagnostics were used for convergence monitoring. Assuming a Weibull growth curve, the model may be represented as

$$\begin{aligned} y_i &= D_\infty (1 - \exp(-\alpha t_i)^\gamma)) + \varepsilon_i \\ \varepsilon_i &\sim N(0, \tau) \\ D_\infty &\sim U(0,10000) \\ \alpha &\sim U(0,5) \\ \gamma &\sim U(0,20) \\ \tau &\sim Ga(2,0.001) \end{aligned} \tag{6.9}$$

Assuming a Gompertz growth curve, the model may be represented as

$$\begin{aligned} y_i &= \exp(\alpha - \beta \exp(-\gamma t_i) + \varepsilon_i \\ \varepsilon_i &\sim N(0, \tau) \\ \alpha &\sim U(-5,10) \\ \beta &\sim U(0,50) \\ \gamma &\sim U(0,1) \\ \tau &\sim Ga(2,0.001) \end{aligned} \tag{6.10}$$

Assuming a logistic growth curve, the model may be represented as

$$y_i = \frac{K}{1 + C\exp(-rt_i)} + \varepsilon_i \qquad (6.11)$$

$$\varepsilon_i \sim N(0,\tau)$$

$$K \sim U(0,10000)$$

$$C \sim U(0,40000)$$

$$r \sim U(0,20)$$

$$\tau \sim Ga(2,0.001)$$

Tables 6.8 through 6.10 present parameter posterior mean sample values for each of the three growth curves. Dose-time profiles were generated using posterior parameter mean values and the respective growth curve function. Figures 6.7 through 6.11 present these dose-time profiles. These results indicate the adequacy of the non-linear sigmoidal growth curves for fitting water dose data. Further efforts to predict dose and dose rate-time profiles using these growth curves seems reasonable.

Table 6.8. Weibull growth curve posterior parameter means and 95% confidence intervals for water dose.

SPE	D_∞ (cGy)	α	γ
May 6,1989	.1113 (.09927, .1283)	.02585 (.01921, .0317)	1.131 (.9754, 1.301)
January 31, 1991	.3325 (.3201, .3449)	.142 (.1201, .1696)	1.542 (.9744, 2.346)
March 23, 1991	799.8 (791.2, 808.6)	.05089 (.05032, .05147)	3.985 (3.792, 4.198)
June 4, 1991	55.52 (54.05, 57.17)	.01029 (.009998, .01057)	2.988 (2.82, 3.164)
August 26, 1991	.873 (.8076, .9413)	.03536 (.03148, .03939)	2.362 (1.621, 3.526)

Table 6.9. Gompertz growth curve posterior parameter means and 95% confidence intervals for water dose.

SPE	α	β	γ
May 6, 1989	-2.309 (-2.383, -2.233)	2.921 (2.572, 3.357)	.06016 (.0501, .07138)
January 31, 1991	-1.106 (-1.14, -1.075)	4.757 (2.352, 13.9)	.3224 (.2175, .5693)
March 23, 1991	6.702 (6.682, 6.722)	21.59 (16.02, 29.98)	.1919 (.1743, .2129)
June 4, 1991	4.13 (4.075, 4.192)	8.779 (7.387, 10.69)	.02796 (.02487, .03142)
August 26, 1991	-.1218 (-.2049, -.04519)	9.477 (3.744, 34.64)	.101 (.06822, .1635)

Table 6.10. Logistic growth curve posterior parameter means and 95% confidence intervals for water dose.

SPE	K (cGy)	C	r
May 6, 1989	.09444 (.08704, .1024)	10.35 (7.649, 14.44)	.1018 (.08194, .1256)
January 31, 1991	.3239 (.3064, .3399)	11450 (8.358, 33510)	1.585 (.3635, 2.517)
March 23, 1991	802.5 (794.1, 811.1)	396.6 (312.5, 498.8)	.3336 (.3198, .3482)
June 4, 1991	55.5 (54.65, 56.37)	107.2 (92.98, 123.3)	.0541 (.0521, .05619)
August 26, 1991	.8651 (.7989, .9194)	665.5 (17.04, 8532)	.164 (.1144, .3685)

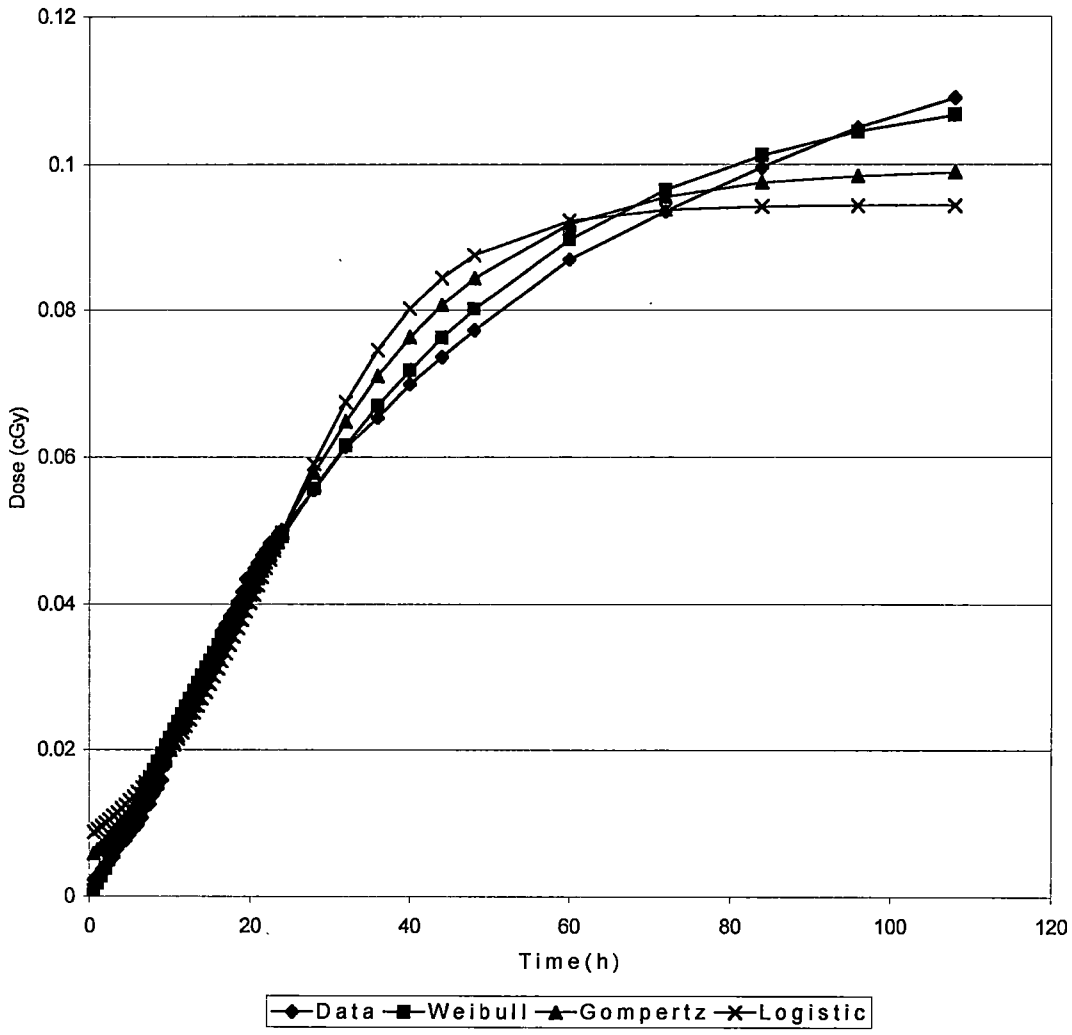


Figure 6.7. Water dose-time profile fits using posterior parameter means for the May 6, 1989 SPE.

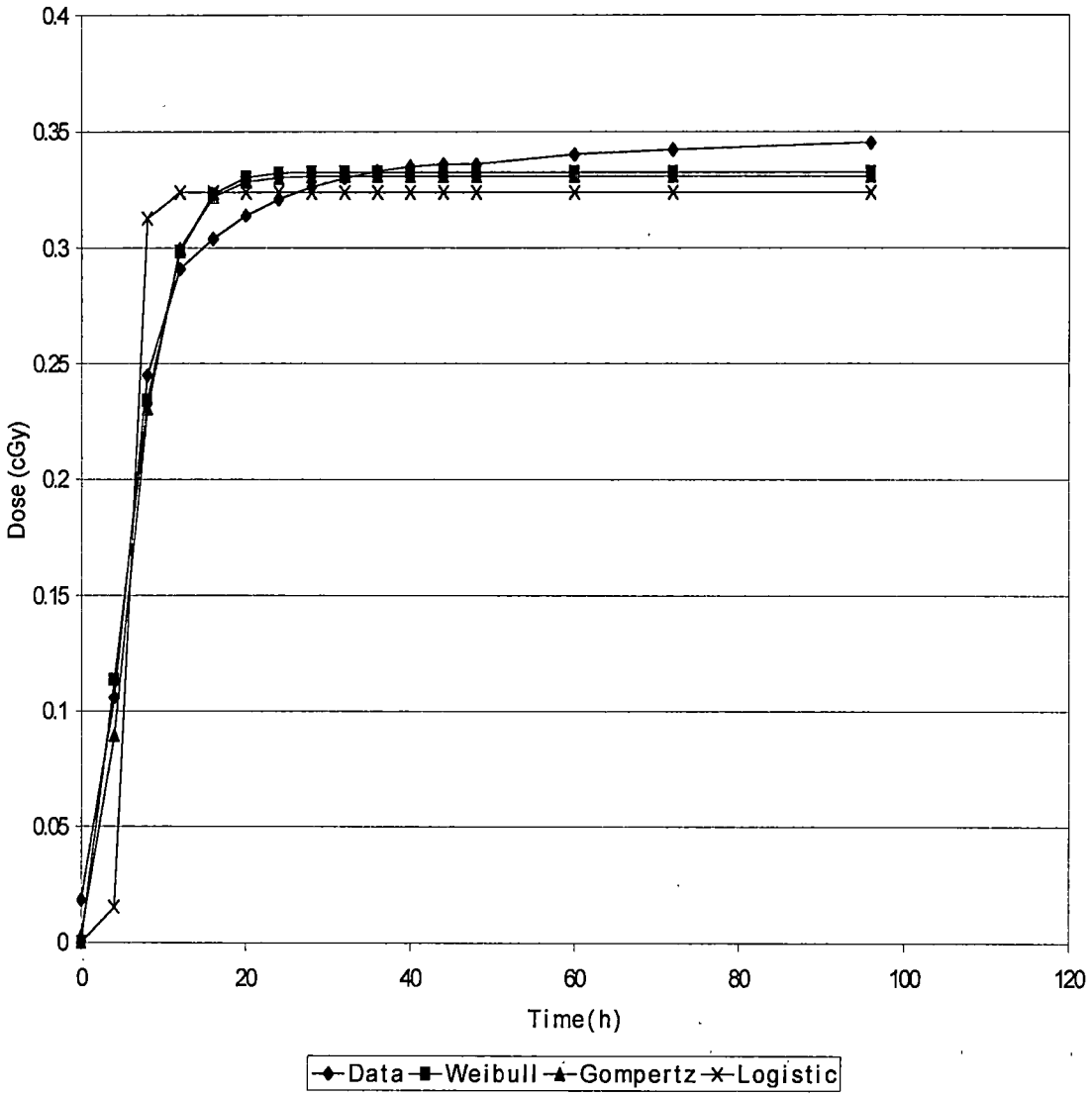


Figure 6.8. Water dose-time profile fits using posterior parameter means for the January 31, 1991 SPE.

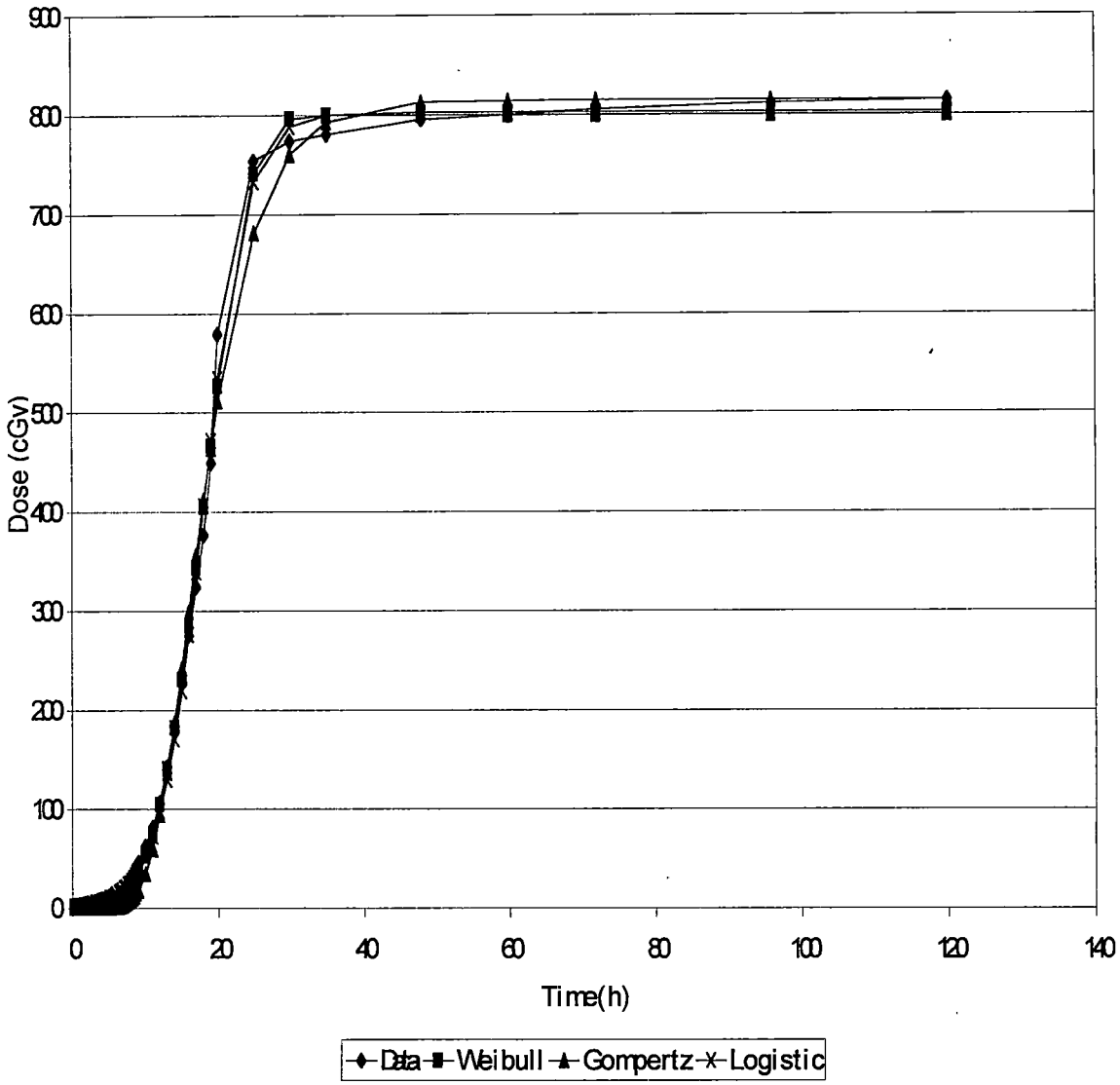


Figure 6.9. Water dose-time profile fits using posterior parameter means for the March 23, 1991 SPE.

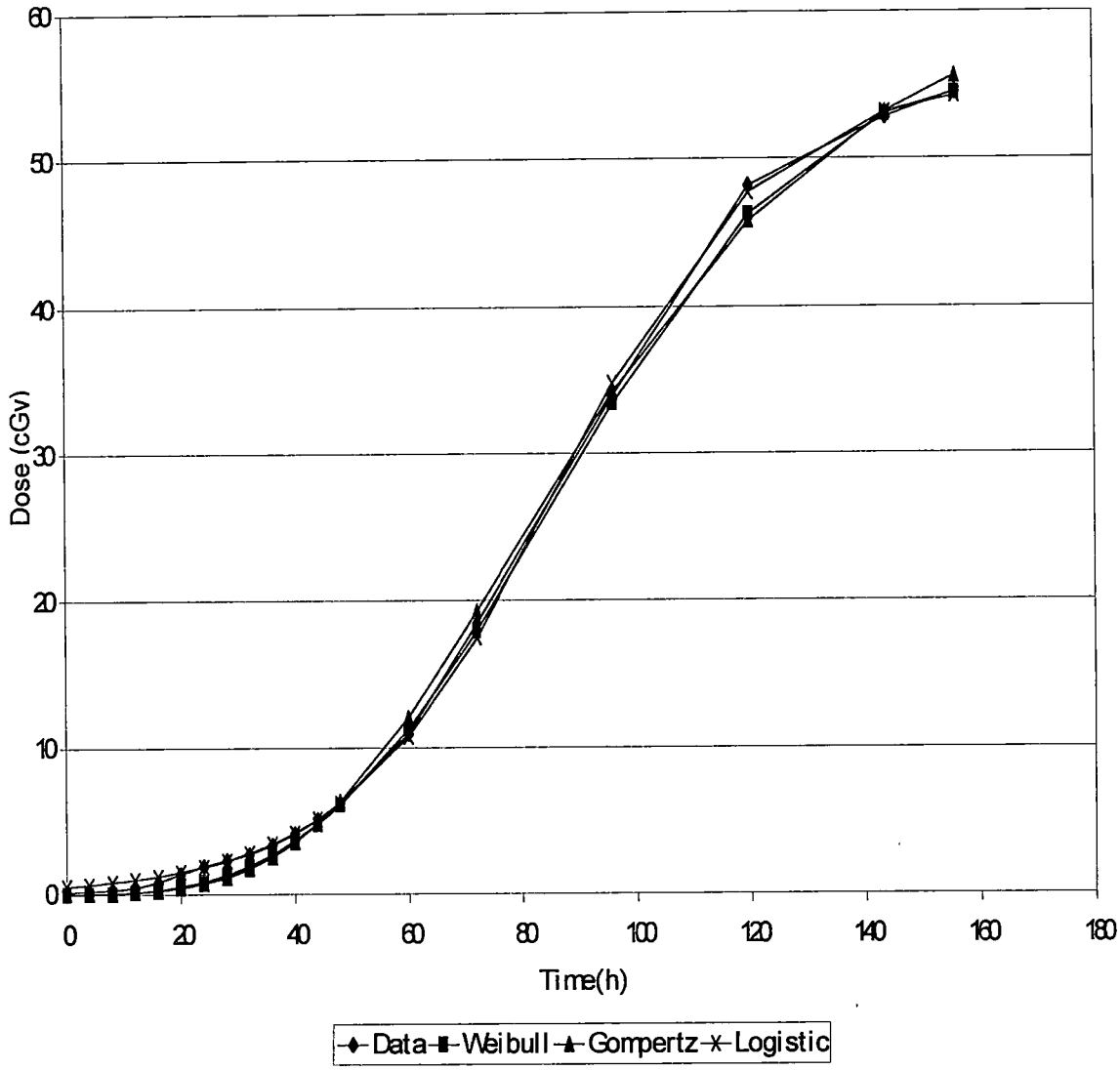


Figure 6.10. Water dose-time profile fits using posterior parameter means for the June 4, 1991 SPE.

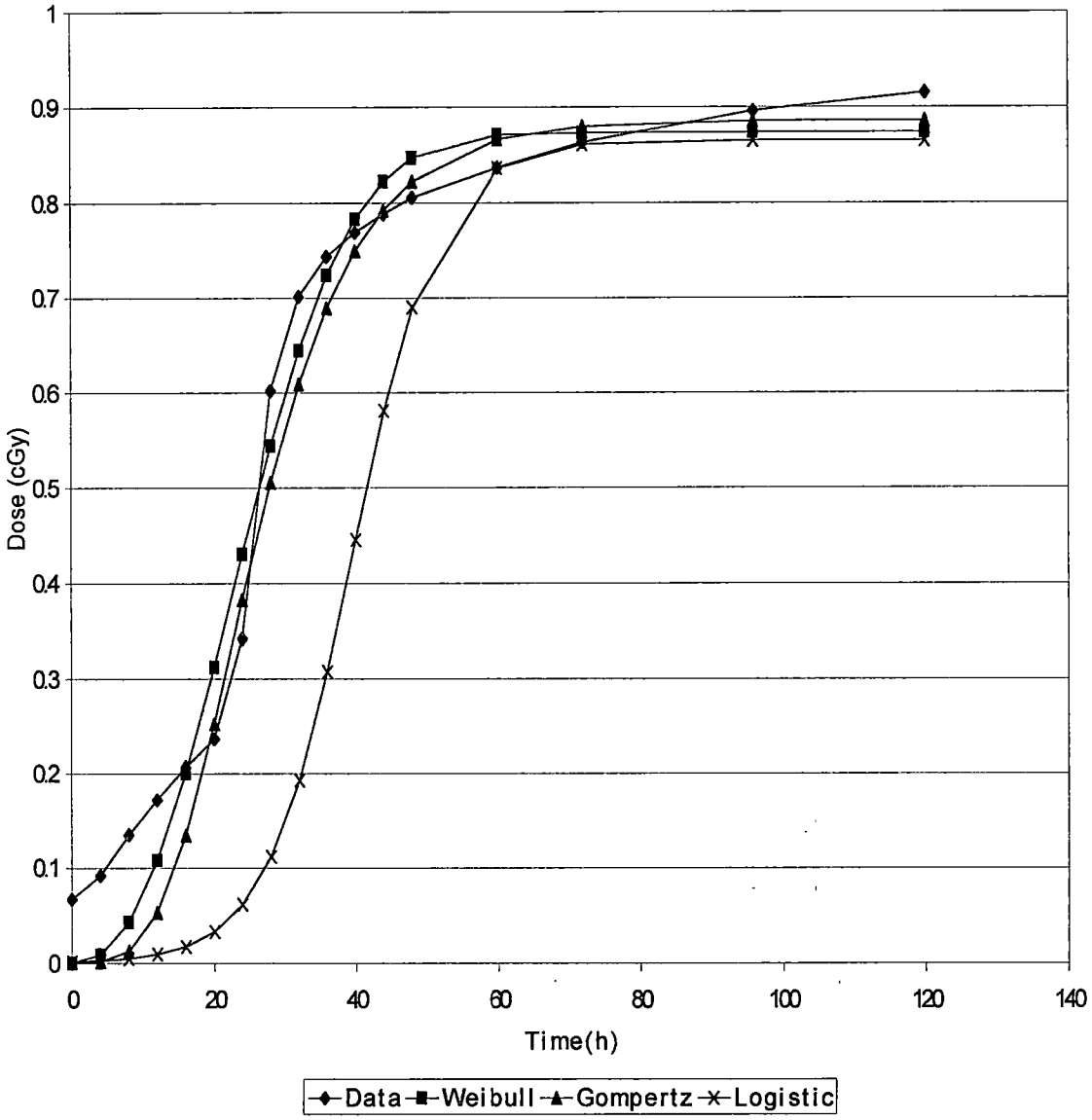


Figure 6.11. Water dose-time profile fits using posterior parameter means for the August 26, 1991 SPE.

6.2.3 Prediction of Dose-Time Profiles

Data for dose in water from the March 23, 1991 and September 29, 1989 SPEs were used to make parameter inferences and predictions of dose-time profiles (Townsend et al., 2001) at various times in the evolution of the SPEs. Proton flux was transported through 1 g/cm^2 of aluminum shielding prior to transport through the water. Prediction of asymptotic doses was inadequate and a lack of convergence for several runs precluded prediction.

Instead of using a single long chain of iterates, the November 8, 2000 and September 29, 1989 SPE data sets were next analyzed using three chains and the Gelman-Rubin convergence diagnostic for convergence monitoring. Data are presented in Tables C.1 and C.2. Models are represented by Equations (6.9) through (6.11). Dose time profiles were generated using dose predictive mean values rather than using parameter posterior means and the respective growth curves. Figures 6.12 through 6.17 present these dose-time profiles. These figures display the data throughout the event and the predicted dose-time profile(s) at the specified dose and time. Individual curves are labeled by the dose/time to indicate at what point in the evolution of the SPE the prediction was made. As an example, the curve labeled "178.2cGy/5h" in Figure 6.12 indicates the predicted dose-time profile when the observed dose was 178.2 cGy which occurred 5 hours into the event.

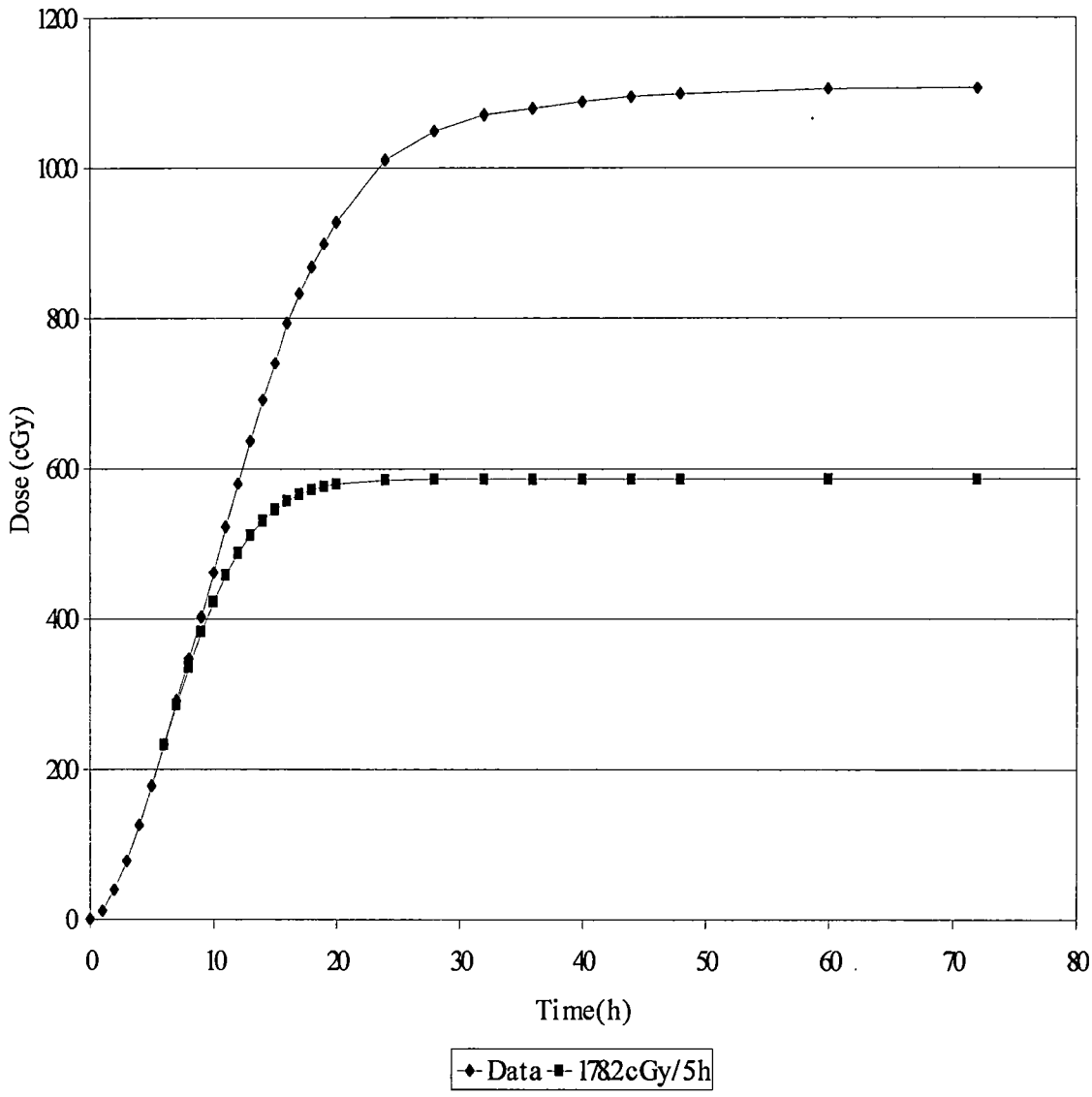


Figure 6.12. Water dose-time profile prediction using posterior predictive means for the November 8, 2000 SPE and Weibull growth curves.

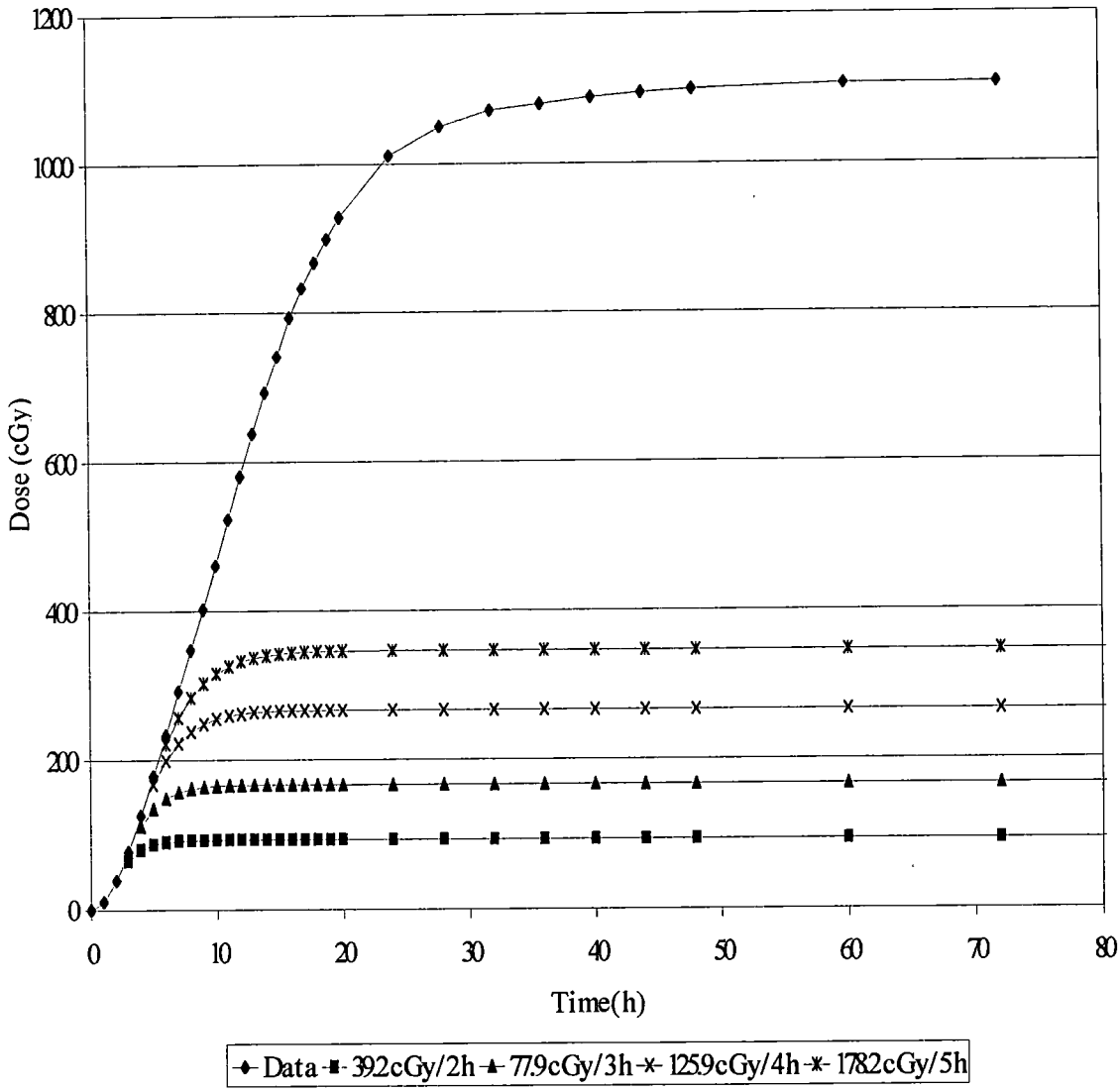


Figure 6.13. Water dose-time profile prediction using posterior predictive means for the November 8, 2000 SPE and Gompertz growth curves.

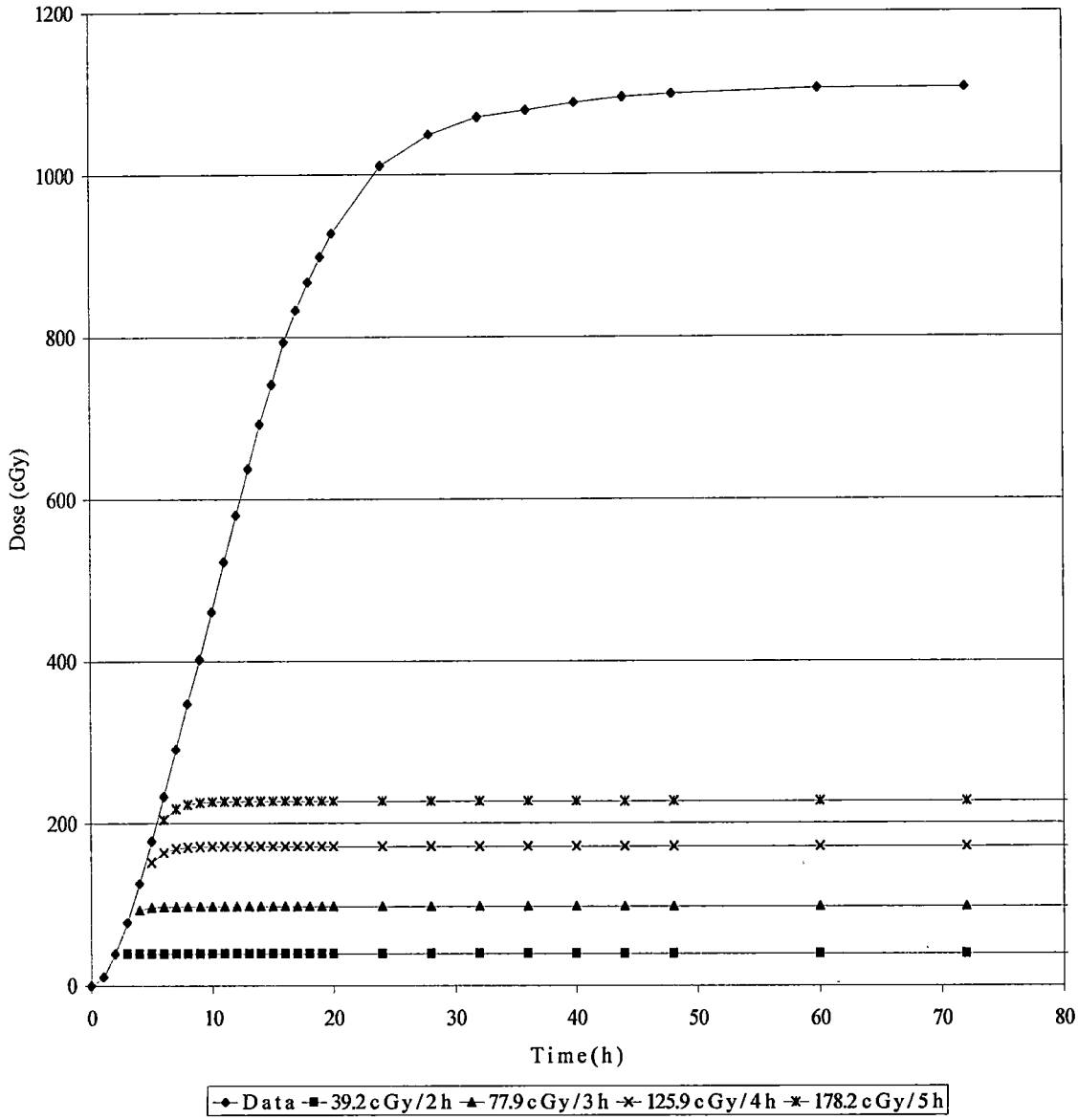


Figure 6.14. Water dose-time profile prediction using posterior predictive means for the November 8, 2000 SPE and logistic growth curves.

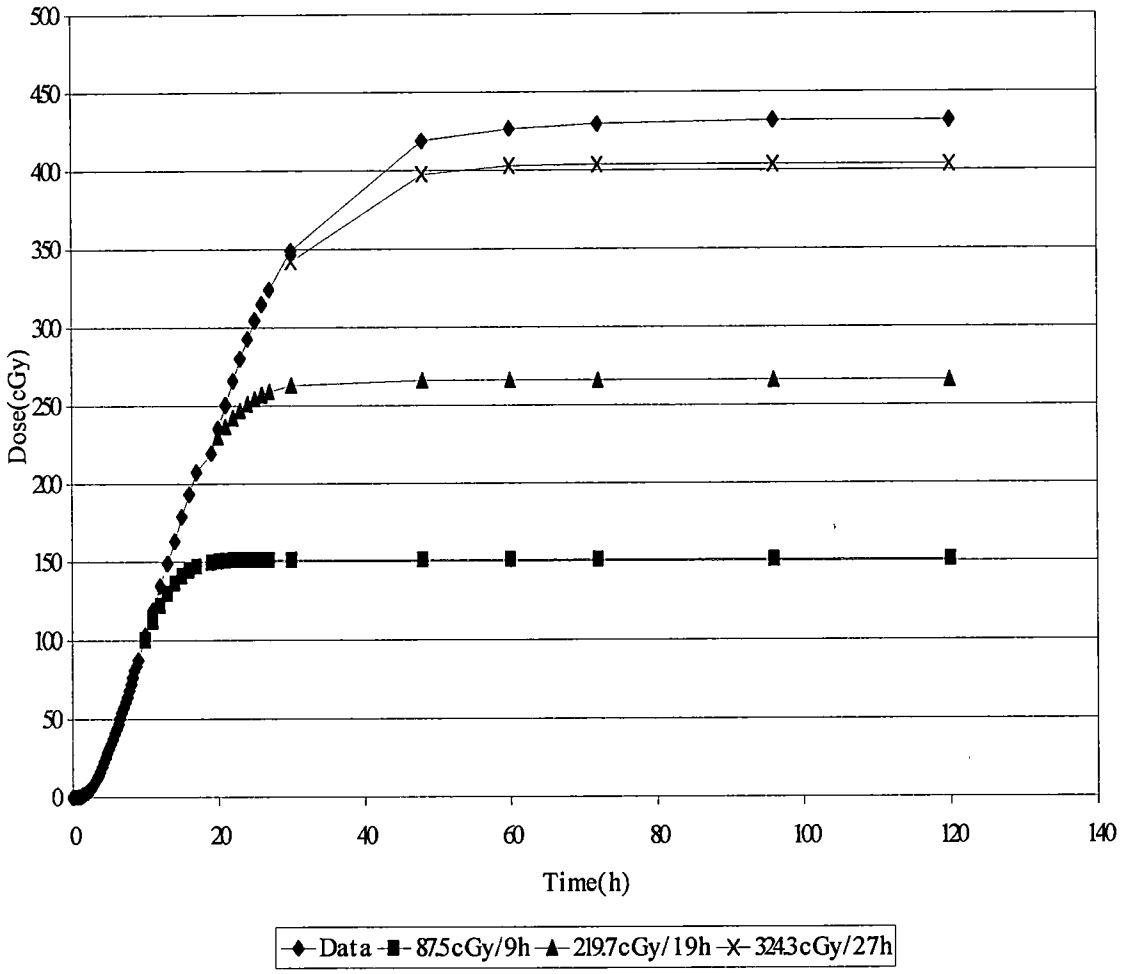


Figure 6.15. Water dose-time profile prediction using posterior predictive means for the September 29, 1989 SPE and Weibull growth curves.

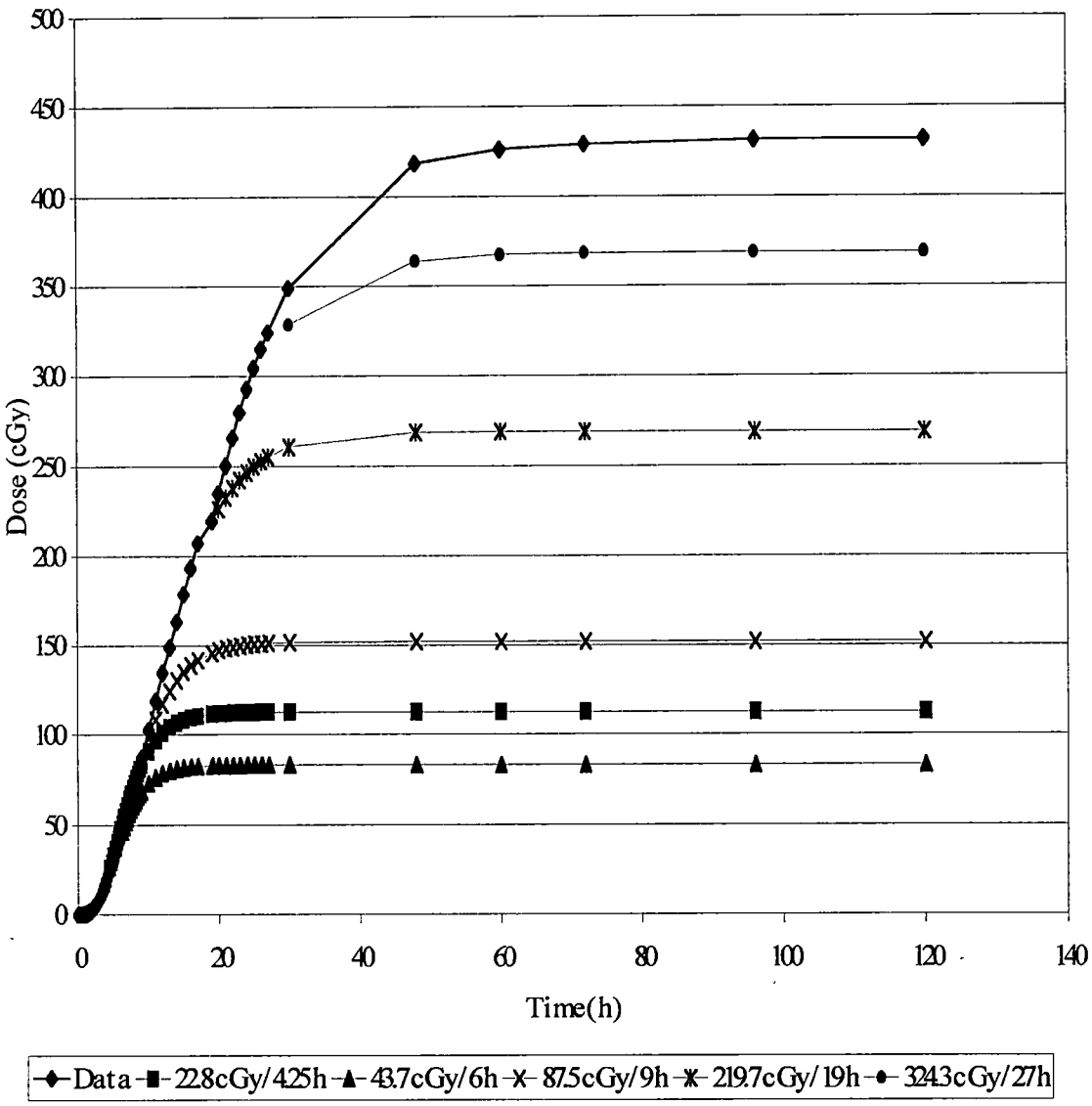


Figure 6.16. Water dose-time profile prediction using posterior predictive means for the September 29, 1989 SPE and Gompertz growth curves.

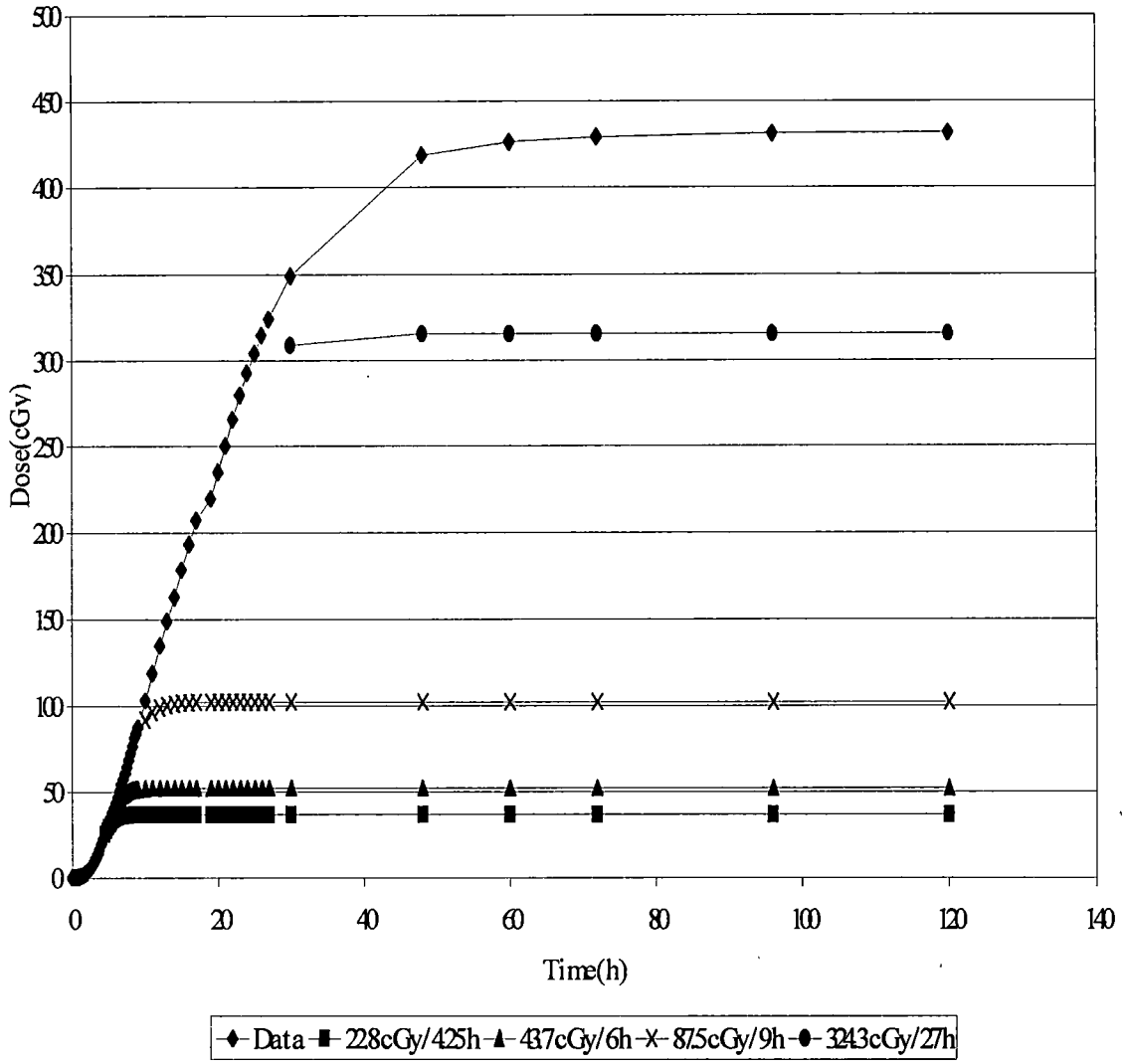


Figure 6.17. Water dose-time profile prediction using posterior predictive means for the September 29, 1989 SPE and logistic growth curves.

Model assessment was performed using posterior predictive checks. The percentage of observations which fell into the 50% and 95% predictive intervals are presented in Tables C.3 and C.4. All models generally supported the predictive intervals for the November 8, 2000 and September 29, 1989 SPEs and thus indicated adequate fits for the data.

Model comparison used the pseudo Bayes factor or the ratio of the product of conditional predictive ordinates. Tables 6.11 and 6.12 present the model comparison results for the November 8, 2000 and September 29, 1989 SPEs.

Table 6.11. Calculated product of conditional predictive ordinate values for November 8, 2000 SPE predictions. NC indicates Non Convergence of the chain.

Hours into event	Weibull	Gompertz	Logistic
2	NC	1.46e-2	7.42e-1
3	NC	9.75e-5	8.76e-7
4	NC	4.16e-6	1.89e-9
5	1.93e-3	2.41e-8	1.28e-10

Table 6.12. Calculated product of conditional predictive ordinate values for September 29, 1989 SPE predictions. NC indicates Non Convergence of the chain.

Hours into event	Weibull	Gompertz	Logistic
4.25	NC	1.58	1.27e-4
6	NC	2.11	6.76e-12
9	2.32e-19	5.62e-24	2.21e-35
19	1.06e-37	1.33e-46	1.22e-121
27	2.96e-66	9.56e-77	1.11e-90

Model comparison results indicate that the Weibull model, when chain convergence criteria were met, consistently best met the comparison criteria for both the November 8, 2000 and September 29, 1989 SPEs. The Gompertz model better meets the comparison criteria than the logistic model for both SPEs, with the exception of the first prediction for the November 8, 2000 SPE at 2 hours.

Prediction of dose-time profiles indicates a limited forecasting ability for these models. The predicted asymptotic dose is typically greater than the current dose value by 5-20% of the actual asymptotic dose. Convergence of MCMC sampling chains is inadequate for some of the runs.

6.2.4 Conclusions on the Use of Individual Non-Linear Regression Models

While the Weibull, Gompertz, and logistic growth curves seemed to provide adequate fits of SPE data, it was not clear that the individual non-linear regression models adequately used information from other SPEs, as expressed by uniform prior distributions based on previous estimations of parameters, to make forecasts of future doses. As such, it seems reasonable to investigate hierarchical models which assume partial exchangeability among data sets and allow new predictions to borrow strength from previous similar SPEs. Individual SPE model parameters would then be viewed as samples from population distributions for similar SPEs.

CHAPTER 7

METHODOLOGY AND RESULTS FOR HIERARCHICAL NON-LINEAR REGRESSION MODELS

7.1 Investigations Utilizing Hierarchical Non-Linear Regression Models

7.1.1 Categorization of SPE

Upon further examination of SPE water dose and dose rate-time profiles and a review of previous organ dose and dose rate-time profiles, it was noted that SPEs with relatively large asymptotic doses were associated with (1) relatively large dose rates early in an event and (2) relatively large maximum dose rates. As such, SPE dose in water data were placed in one of four groups as determined by the asymptotic dose and maximum dose rate for the SPE. Group characteristics and initial SPE members are presented in Table 7.1. Tables D.1 through D.10 present data for these initial SPE members.

Categorization for new events was based on observed dose rates from times early in the event. The maximum dose rate observed by the fifth hour of the event was used to categorize the new event. Since Group 1 SPEs are the most significant events from a radiological standpoint, it was considered prudent to begin making predictions for these events earlier in the evolution of the SPE. If the observed dose rate exceeded the initial categorization criterion for Group 1 prior to the fifth hour of the SPE, predictions would be made before the fifth hour of the event. Criteria for categorization of new events are presented in Table 7.2.

Table 7.1. Hierarchical model group characteristics and initial SPE members.

Group Number	Asymptotic Dose Range (cGy)	Maximum Dose Rate(cGy/hr)	Initial SPE Members
1	500-5000	>40	July 14, 2000 March 23, 1991
2	100-500	10-40	October 19, 1989 September 29, 1989
3	1-100	0.1-10	June 4, 1991 March 19, 1990 November 30, 1989
4	0-1	0-0.1	August 26, 1991 January 31, 1991 November 8, 1987

Table 7.2. Criteria for categorization of new events.

Group Number	Maximum Dose Rate after 5 Hours into Event (cGy/hr)
1	>15
2	0.1-15
3	0.05-0.1
4	0-0.05

7.1.2 Hierarchical Non-Linear Regression Models

A hierarchical, non-linear regression model was assumed for each of the four groups. Assuming a Weibull growth curve, the model may be represented by the following:

$$y_{i,j} = D_{\infty_i}(1-\exp(-\alpha_i t_j)^{\gamma_i})) + \varepsilon_{i,j} \qquad (7.1)$$
$$\varepsilon_{i,j} \sim N(0,\tau_i)$$

$$D_{\infty_i} \sim N(D_\infty.\mu, D_\infty.\tau)$$
$$\alpha_i \sim N(\alpha.\mu, \alpha.\tau)$$
$$\gamma_i \sim N(\gamma.\mu, \gamma.\tau)$$
$$\tau_i \sim Ga(\tau.shape, \tau.scale)$$

$$D_\infty.\mu \sim U(a,b)$$
$$D_\infty.\tau \sim U(c,d)$$
$$\alpha.\mu \sim U(e,f)$$
$$\alpha.\tau \sim U(g,h)$$
$$\gamma.\mu \sim U(k,l)$$
$$\gamma.\tau \sim U(m,n)$$
$$\tau.shape \sim U(1e-4, 1e3)$$
$$\tau.scale \sim Ga(2, 1e-3)$$

Hyperprior distribution constants for the Weibull growth curve hierarchical model are presented in Table 7.3.

Table 7.3. Hyperpriors distribution for groups 1 through 4 Weibull growth curve hierarchical models.

Distribution constant	Group 1	Group 2	Group 3	Group 4
a	500	100	1	0
b	10000	500	100	1
c	0.00001	0.00001	0.00001	0.00001
d	1000	1000	1000	1000
e	0.00001	0.00001	0.00001	0.00001
f	10	10	10	10
g	0.00001	0.00001	0.00001	0.00001
h	1000	1000	1000	1000
k	0.00001	0.00001	0.00001	0.00001
l	20	20	20	20
m	0.00001	0.00001	0.00001	0.00001
n	1000	1000	1000	1000

Assuming a Gompertz growth curve, the model may be represented by the following:

$$y_{i,j} = \exp(\alpha_i - \beta_i \exp(-\gamma_i t_j)) + \varepsilon_{i,j} \qquad (7.2)$$
$$\varepsilon_{i,j} \sim N(0, \tau_i)$$

$$\alpha_i \sim N(\alpha.\mu, \alpha.\tau)$$
$$\beta_i \sim N(\beta.\mu, \beta.\tau)$$
$$\gamma_i \sim N(\gamma.\mu, \gamma.\tau)$$
$$\tau_i \sim Ga(\tau.shape, \tau.scale)$$

$$\alpha.\mu \sim U(p, q)$$
$$\alpha.\tau \sim U(r, s)$$
$$\beta.\mu \sim U(t, u)$$
$$\beta.\tau \sim U(v, w)$$
$$\gamma.\mu \sim U(x, z)$$
$$\gamma.\tau \sim U(aa, bb)$$
$$\tau.shape \sim U(1e-4, 1e3)$$
$$\tau.scale \sim Ga(2, 1e-3)$$

Hyperprior distribution constants for the Gompertz growth curve hierarchical model are presented in Table 7.4.

Table 7.4. Hyperpriors distribution for groups 1 through 4 Gompertz growth curve hierarchical models.

Distribution constant	Group 1	Group 2	Group 3	Group 4
p	6.215	4.605	0	-5
q	8.517	6.215	4.605	0
r	0.0001	0.00001	0.00001	0.00001
s	1000	1000	1000	1000
t	0.00001	0.00001	0.00001	0.00001
u	100	100	100	100
v	0.00001	0.00001	0.00001	0.00001
w	1000	1000	1000	1000
x	0.00001	0.00001	0.00001	0.00001
z	1	1	1	1
aa	0.00001	0.00001	0.00001	0.00001
bb	1000	1000	1000	1000

Assuming a logistic growth curve, the model may be represented by the following:

$$y_{i,j} = \frac{K_i}{1 + C_i \exp(-r_i t_j)} + \varepsilon_{i,j} \qquad (7.3)$$

$$\varepsilon_{i,j} \sim N(0, \tau_i)$$

$$K_i \sim N(K.\mu, K.\tau)$$
$$C_i \sim N(C.\mu, C.\tau)$$
$$r_i \sim N(r.\mu, r.\tau)$$
$$\tau_i \sim Ga(\tau.shape, \tau.scale)$$

$$K.\mu \sim U(cc, dd)$$
$$K.\tau \sim U(ee, ff)$$
$$C.\mu \sim U(gg, hh)$$
$$C.\tau \sim U(kk, ll)$$
$$r.\mu \sim U(mm, nn)$$
$$r.\tau \sim U(pp, qq)$$
$$\tau.shape \sim U(1e-4, 1e3)$$
$$\tau.scale \sim Ga(2, 1e-3)$$

Hyperprior distribution constants for the logistic growth curve hierarchical model are presented in Table 7.5.

Table 7.5. Hyperpriors distribution for groups 1 through 4 logistic growth curve hierarchical models.

Distribution constant	Group 1	Group 2	Group 3	Group 4
cc	500	100	1	0
dd	5000	500	100	1
ee	0.00001	0.00001	0.00001	0.00001
ff	1000	1000	1000	1000
gg	0.0001	0.0001	0.0001	0.0001
hh	40000	40000	40000	40000
kk	0.00001	0.00001	0.00001	0.00001
ll	1000	1000	1000	1000
mm	0.00001	0.00001	0.00001	0.00001
nn	20	20	20	20
pp	0.00001	0.00001	0.00001	0.00001
qq	1000	1000	1000	1000

Initial efforts with the logistic model indicated convergence difficulties for the C_i and r_i parameters. Posterior distributions appeared to be insensitive to a wide range of values for C_i. The logistic growth curve represented by equation (7.3) was reparameterized to a two parameter growth curve by assuming C_i=20000.

Convergence diagnosis was performed using the modified Gelman-Rubin diagnostic for three sampling chains. At least 4000 iterations were used for burn-in for all runs. Each of the three parallel chains was run for 5000 iterations. Plots of parameter iterates were reviewed for each run as an informal determination of convergence.

Model assessment utilized posterior predictive intervals, 50% and 95%, to assess the percentage of water dose observations that fell within these predictive intervals. Model comparison/selection utilized the pseudo Bayes factor from section 4.6.3 to determine which of the three growth curve models best met the comparison criteria at each prediction step. Predictive 50% and 95% interval widths were examined to determine if (1) interval widths increased as predictions were made farther into the future for a set time in the evolution of an SPE and (2) interval widths decreased for predictions made later in the evolution of an SPE.

7.2 November 2000 SPE

The November 8, 2000 SPE started at 2350 Universal Time (UT). Particle flux reached a maximum of 14,800 particle flux units (pfu=1 proton-cm^{-2}-sr^{-1}-s^{-1}) at 1600 UT on November 9, 2000. The associated solar flare reached a

maximum at 2328 UT on November 8, 2000. The associated coronal mass ejection was first observed at 2306 UT as a large, bright loop front over the northwest limb and later developed into a full halo (Schenk, 2000). The average plane-of-sky speed was estimated to be 2035 km/s.

Data used in this analysis were collected by the GOES-8 satellite and are presented in Table D.11. Dose rate data used for categorization of the event are presented in Table D.12. The dose rate exceeded the 15 cGy/hr threshold for Group 1 one hour into the event.

Individual curves are labeled by the dose/time to indicate at what point in the evolution of the SPE the prediction was made. As an example, the curve labeled "39.2cGy/2h" in Figure 7.1 indicates the predicted dose-time profile when the observed dose was 39.2 cGy which occurred 2 hours into the event. As the posterior predictive distributions for dose were highly skewed to the right for the Gompertz models, posterior predictive median values were used in the dose and dose rate-time profiles.

The Weibull model dose-time profiles provided a fairly tight grouping of predictions, within approximately ± 10% of the observed data, up to hour 20 of the event with the exception of the 39.2cGy/2h prediction. The Weibull model consistently over-predicted the asymptotic dose, which would be considered conservative from a radiological standpoint. Dose rate-time profiles reflected the

tight grouping of the dose time profiles up to hour 20 and over-prediction later in the event.

Gompertz model dose-time profiles first under-predicted, then over-predicted, then gradually decreased toward the observed asymptotic dose. Asymptotic dose predictions were within ± 10% of the observed asymptotic dose. With the exception of the 39.2cGy/2h prediction, dose rate-time profiles over-predicted up to hour 10 and then provided a mixture of over and under-prediction later in the event.

The logistic model under-predicted the asymptotic dose by 1% to 3% of the observed asymptotic dose. While the two parameter logistic model provided outstanding asymptotic dose predictions, a lag in forecasting the dose-time profile provided poor predictions early in the event. Dose rate predictions up to hour 28 were poor with significant over-prediction of maximum dose rate for several of the predictions. Dose rate predictions after hour 28 were reasonable as the event had nearly reached asymptotic dose values. Dose and dose rate time profiles for each of the three growth curve models are presented in Figures 7.1 through 7.6.

Model assessment results are presented in Tables D.13 through D.15. Model assessment indicated that all of the models supported the predictive intervals for the November 8, 2000 SPE. These statistics indicate that the models adequately fit the data.

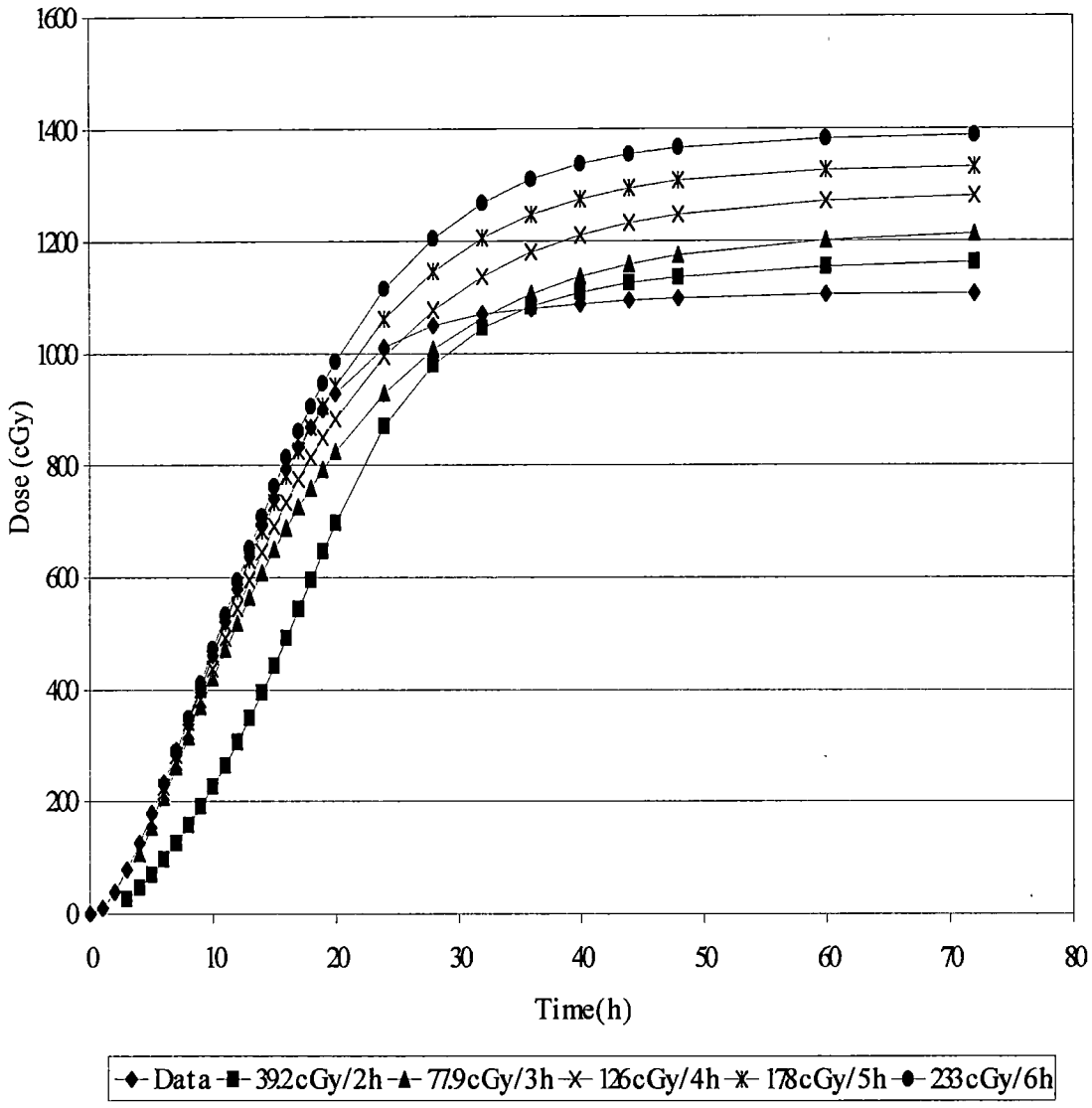


Figure 7.1. Water dose-time profile prediction using posterior predictive means for the November 8, 2000 SPE and Weibull growth curves.

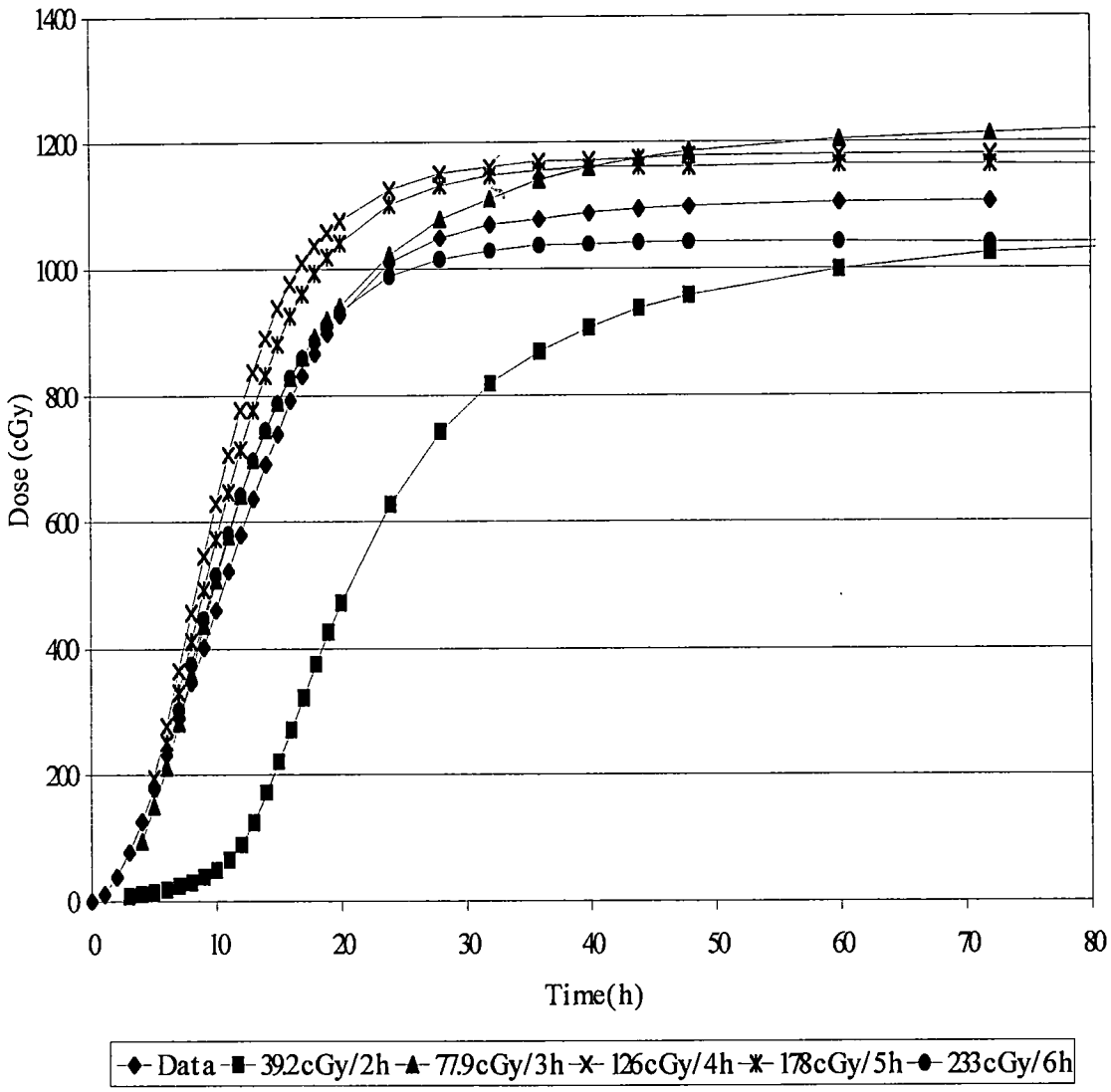


Figure 7.2. Water dose-time profile prediction using posterior predictive medians for the November 8, 2000 SPE and Gompertz growth curves.

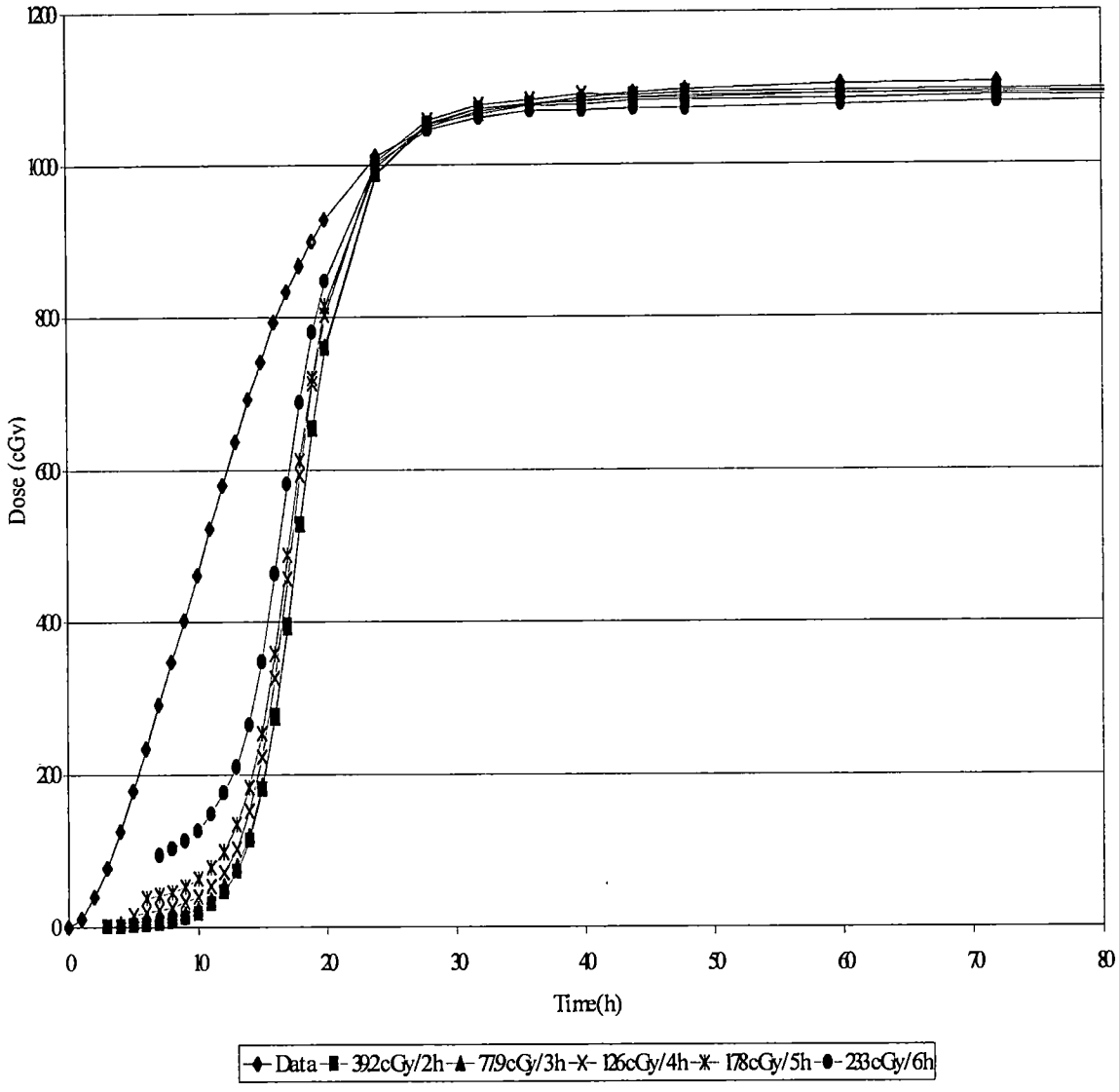


Figure 7.3. Water dose-time profile prediction using posterior predictive medians for the November 8, 2000 SPE and logistic growth curves.

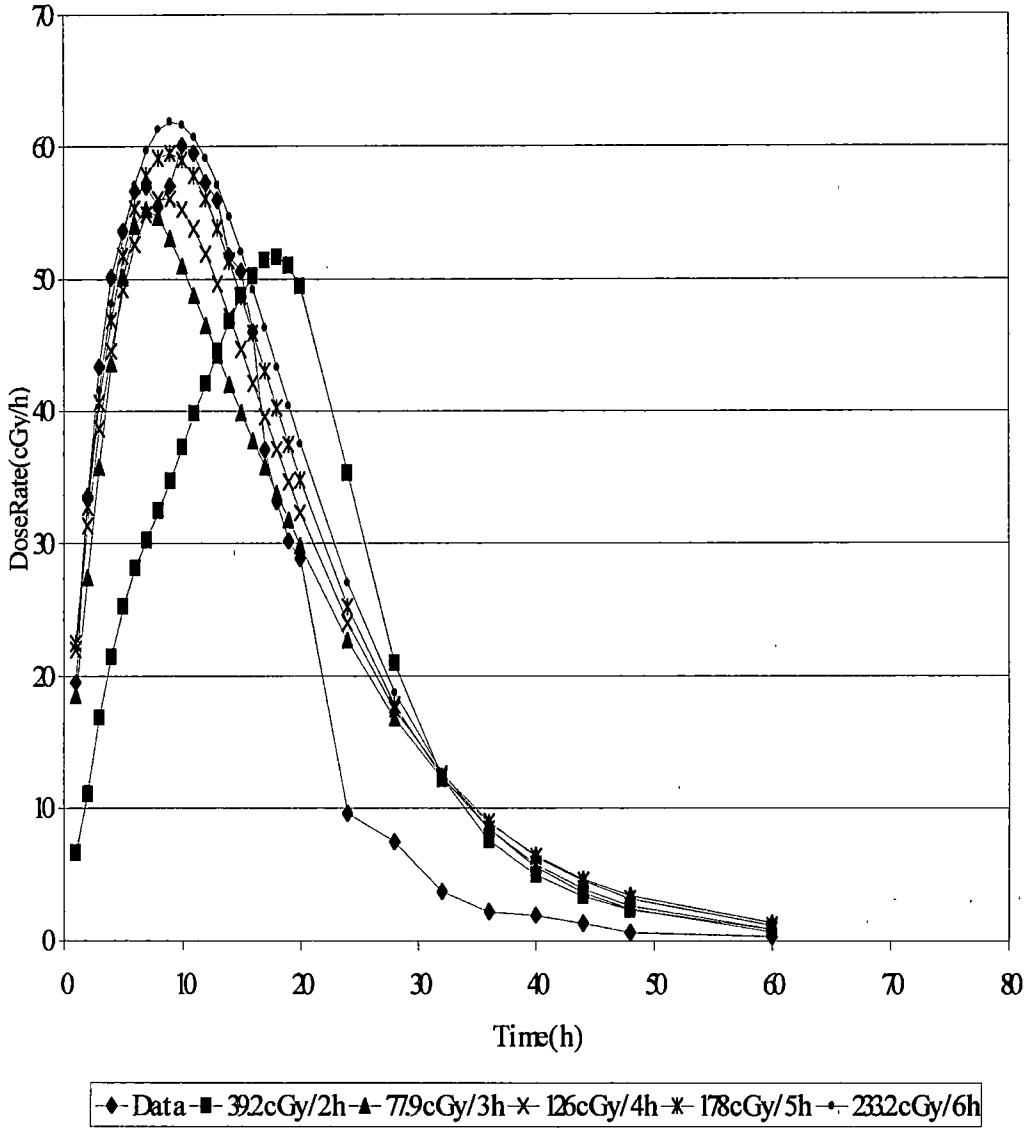


Figure 7.4. Water dose rate-time profile prediction using posterior predictive means for the November 8, 2000 SPE and Weibull growth curves.

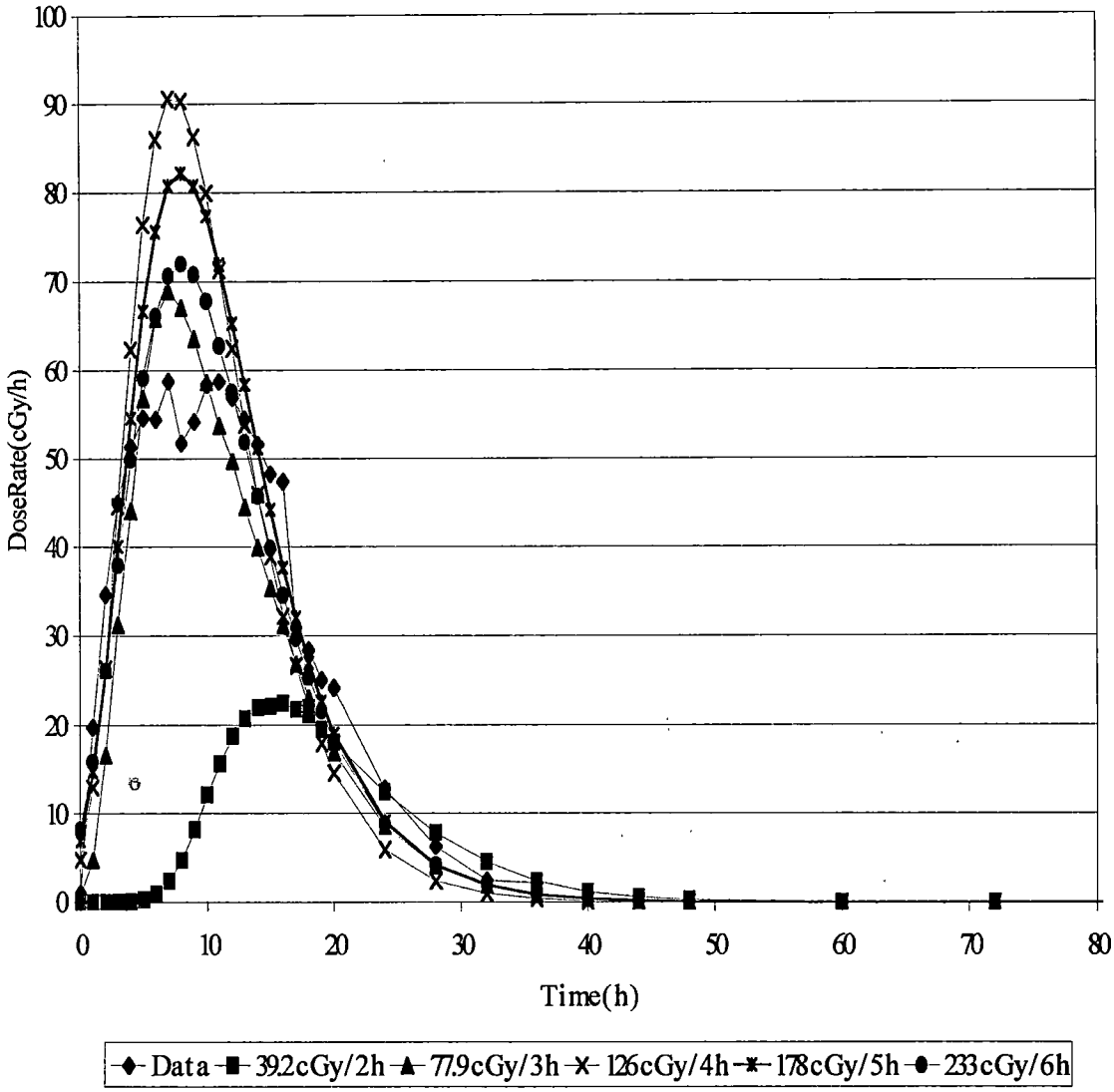


Figure 7.5. Water dose rate-time profile prediction using posterior predictive medians for the November 8, 2000 SPE and Gompertz growth curves.

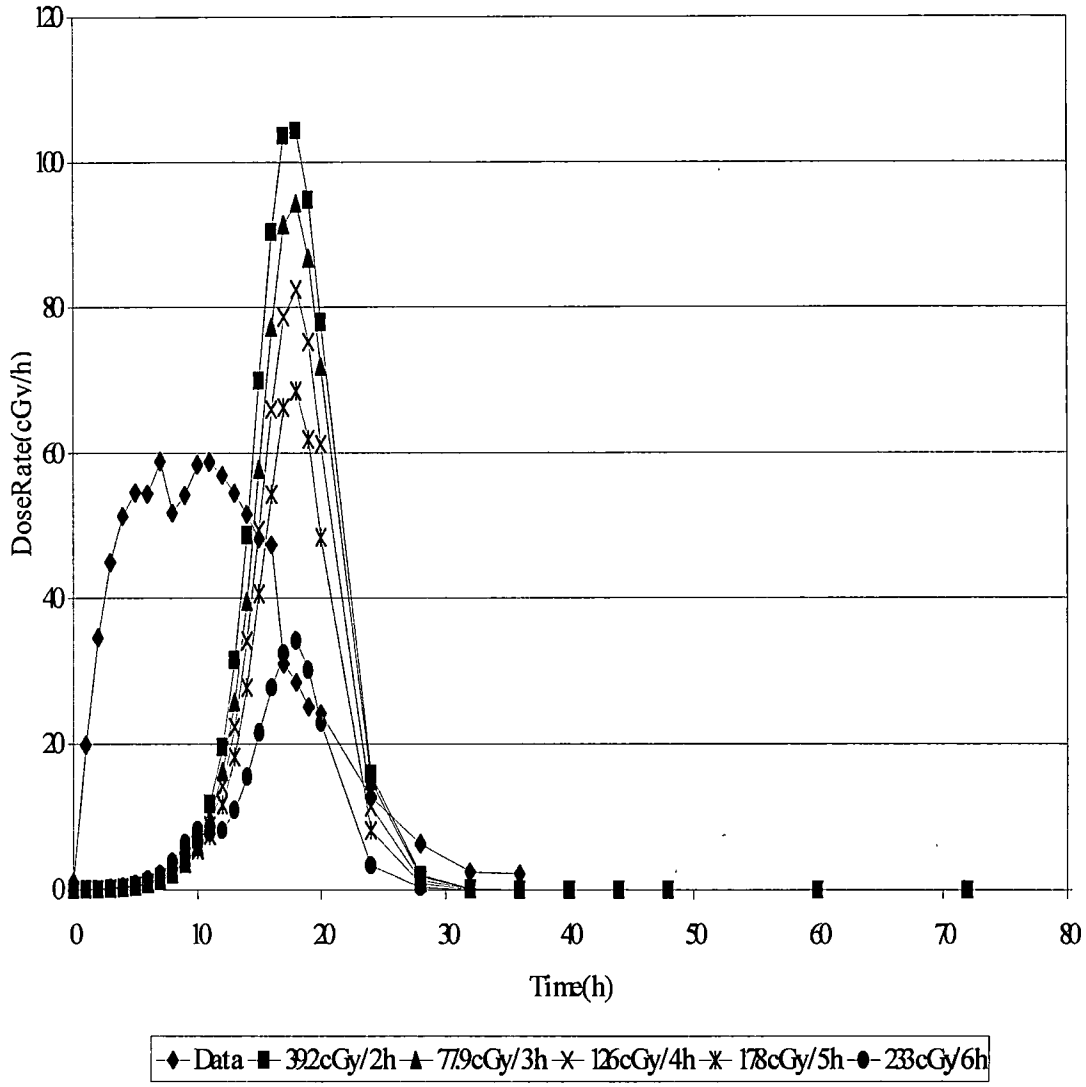


Figure 7.6. Water dose rate-time profile prediction using posterior predictive medians for the November 8, 2000 SPE and logistic growth curves.

Model comparison results are presented in Table 7.6. As this statistic is an accumulation of likelihoods over observations, a larger value of the product of conditional predictive ordinates indicates preference between two models. Because this statistic is uncalibrated, its magnitude has no meaning other than in a relative sense for comparison of two models. The ratio of the product of conditional predictive ordinate values, the pseudo Bayes factor, indicated that the Weibull model was preferred to the Gompertz and logistic models. The Gompertz model was consistently preferred over the logistic model. It is important to note that the comparison criteria are a measure of internal consistency for a given model for observed data and not a measure of forecasting ability.

Predictive dose 50% and 95% interval widths are presented in Figures 7.7 through 7.12. Predictive interval widths for the Weibull and Gompertz models indicated that interval widths increased, as expected, as predictions were made farther into the future with a given set of data. Predictive interval widths mimicked the asymptotic nature of the growth curves. Predictive interval widths generally decreased, as expected, as more data became available. Notable exceptions were the 50% and 95% interval widths for the Gompertz model at three hours into the SPE.

Table 7.6 Calculated product of conditional predictive ordinate values for November 8, 2000 SPE predictions.

Hours into event	Weibull	Gompertz	Logistic
2	1.23e-134	1.96e-145	1.85e-166
3	1.03e-135	5.06e-148	1.67e-169
4	8.30e-137	4.12e-149	1.00e-172
5	1.39e-138	1.40e-150	6.03e-176
6	1.32e-139	1.05e-152	3.75e-179

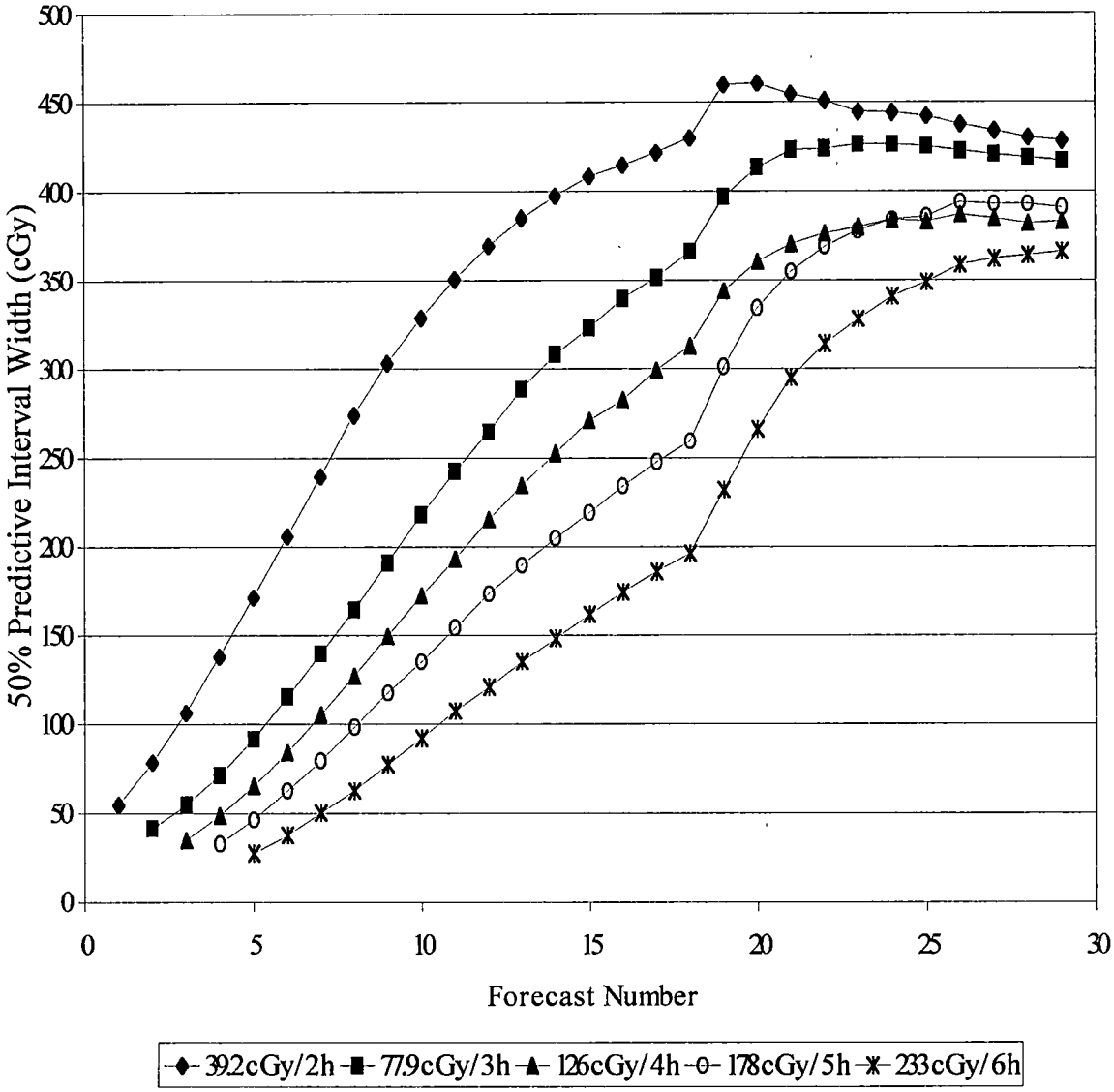


Figure 7.7. Weibull model 50% predictive interval widths for November 8, 2000 SPE.

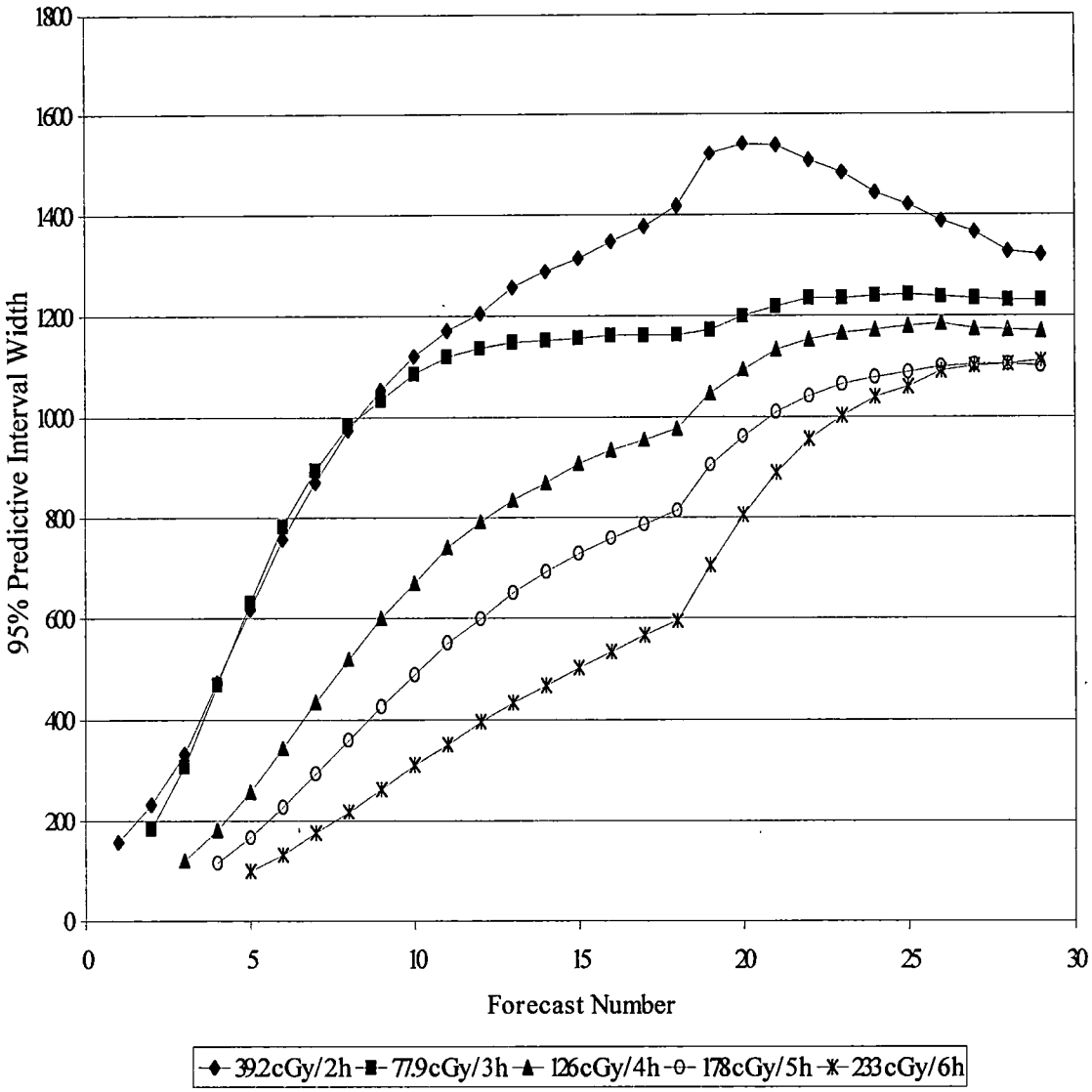


Figure 7.8. Weibull model 95% predictive interval widths for November 8, 2000 SPE.

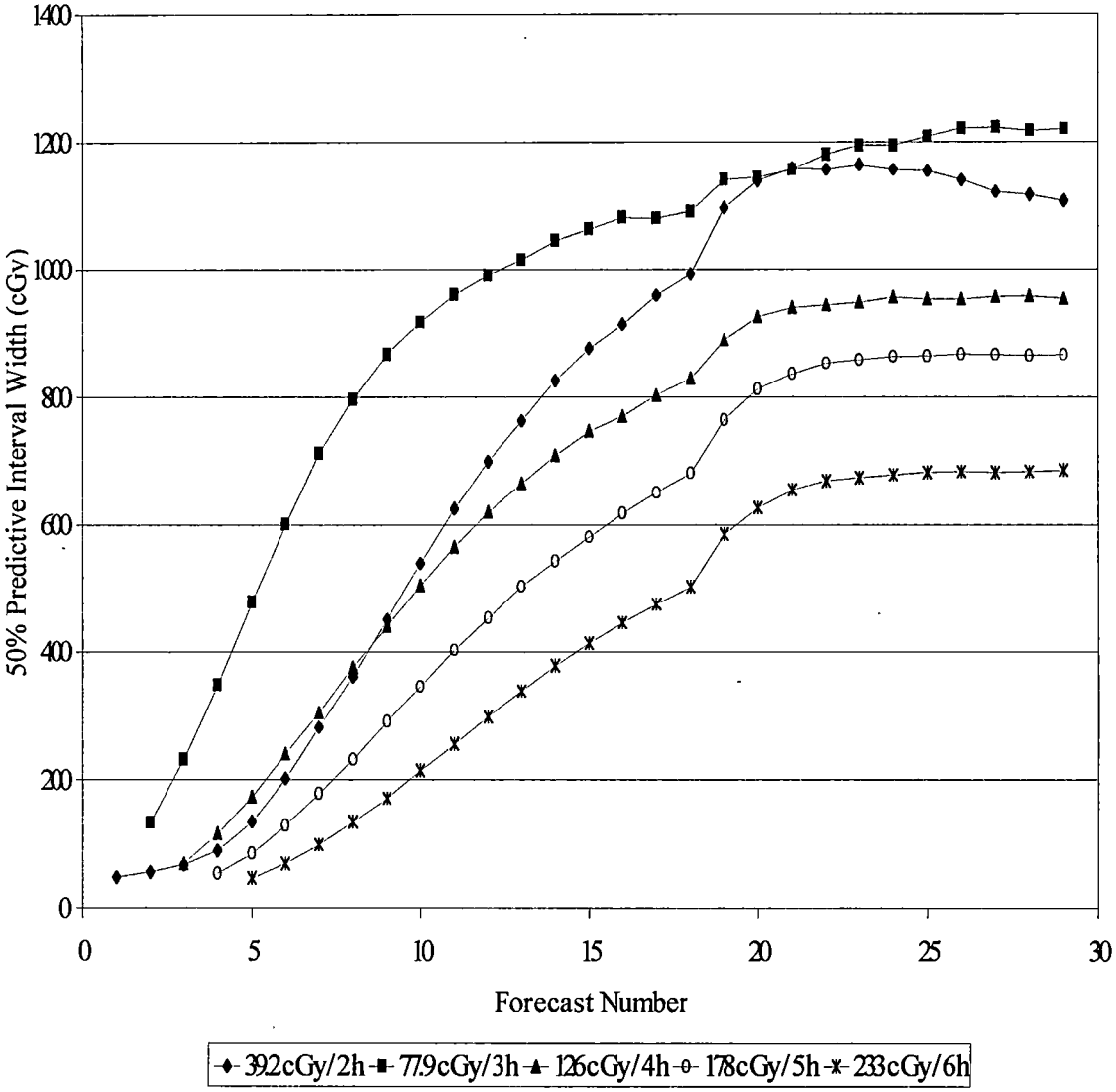


Figure 7.9. Gompertz model 50% predictive interval widths for November 8, 2000 SPE.

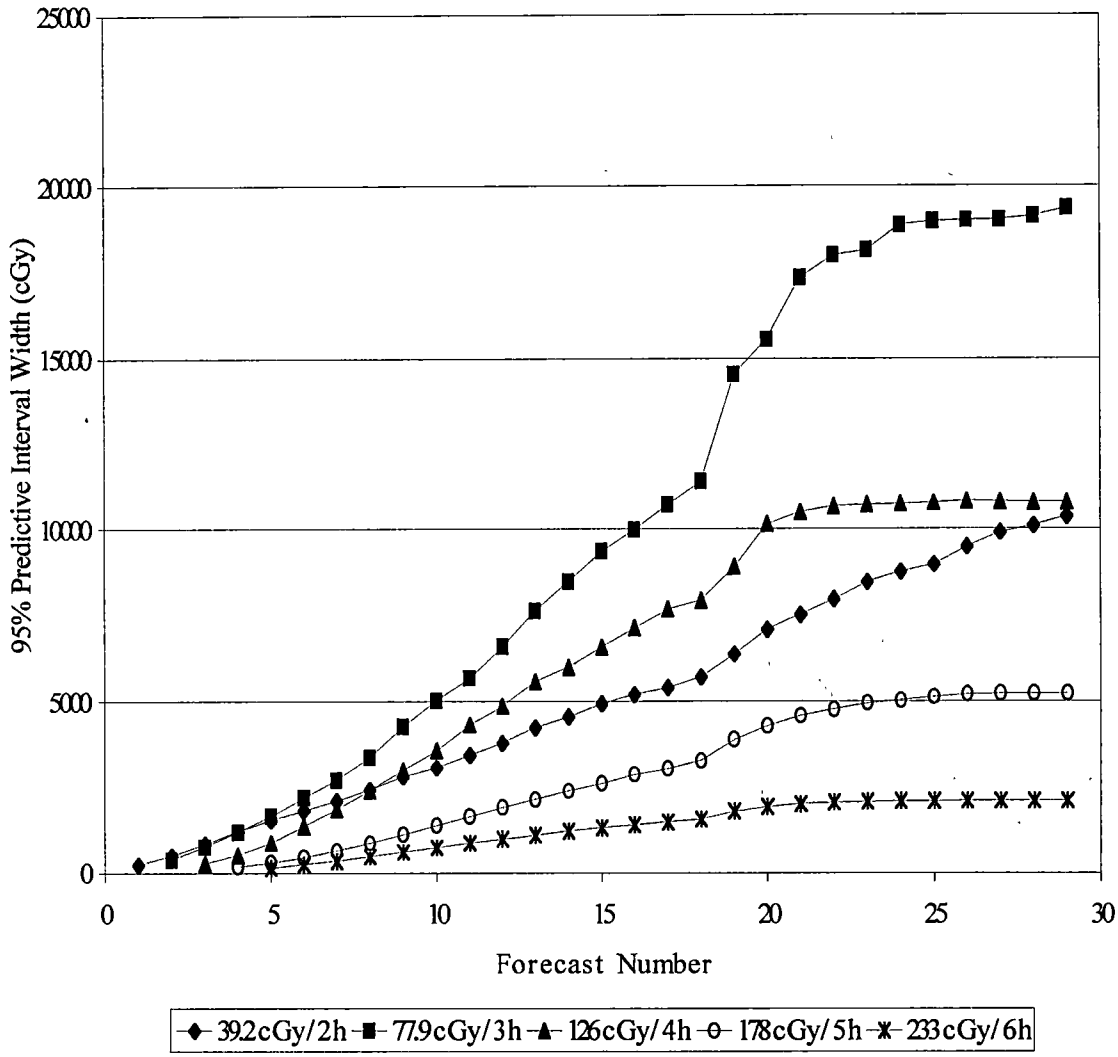


Figure 7.10. Gompertz model 95% predictive interval widths for November 8, 2000 SPE.

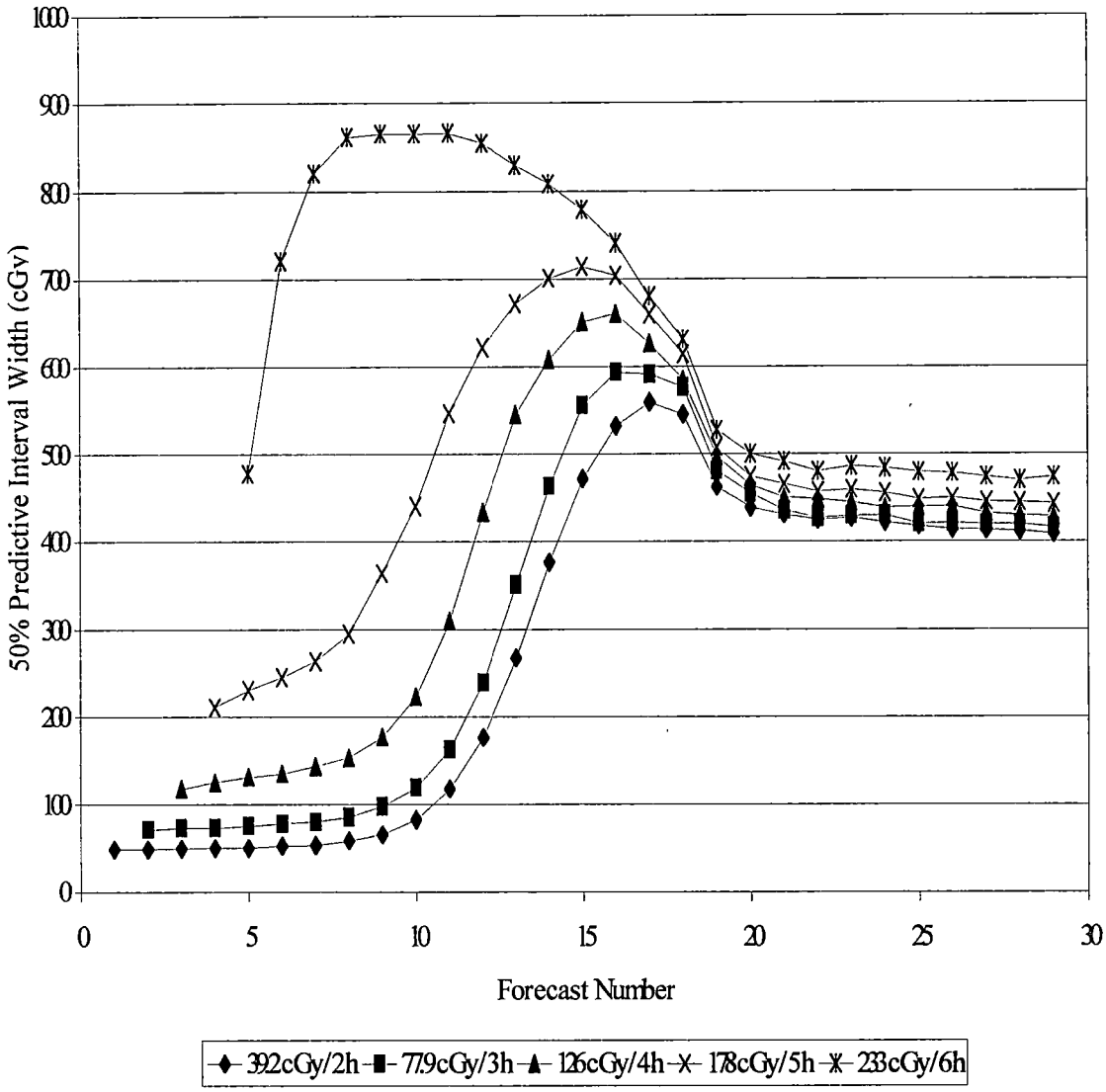


Figure 7.11. Logistic model 50% predictive interval widths for November 8, 2000 SPE.

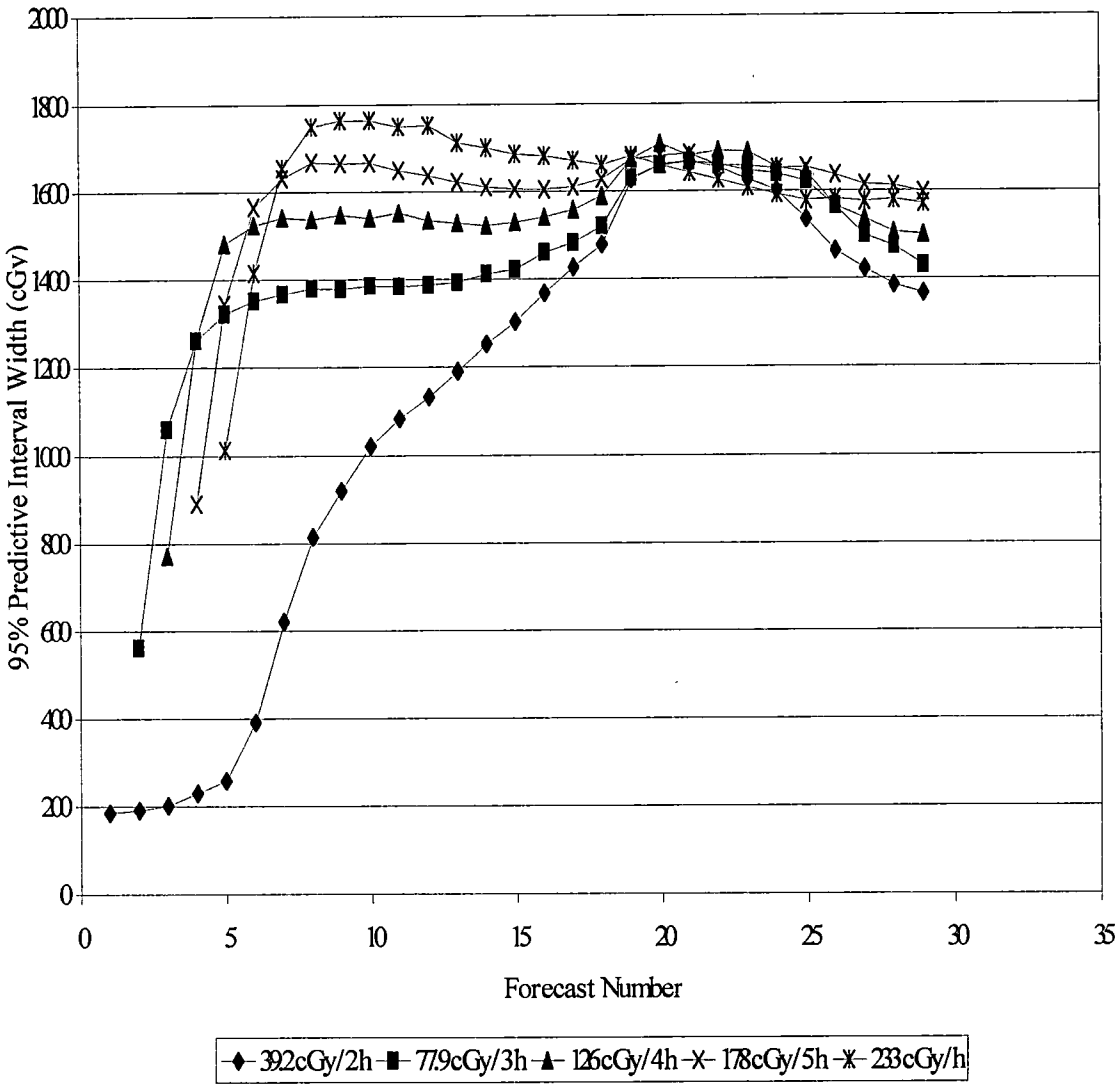


Figure 7.12. Logistic model 95% predictive interval widths for November 8, 2000 SPE.

Predictive interval widths for the logistic model decreased after forecast number 15, contrary to expectations, as predictions were made farther in the future with a given set of data. An examination of the posterior predictive distributions revealed shapes that were initially symmetric, then became skewed to the right as the distribution gained mass near the predicted asymptote, and then tended towards symmetric. This behavior is reflected in the initial gain in uncertainty, as expected, and then decreasing uncertainties after forecast number 15. Contrary to expectations, predictive interval widths increased as more data became available. Posterior predictive distributions made later in the evolution of the event tended to look bimodal. This spreading out of the distribution mass led to larger predictive intervals as more data became available.

7.3 August 1989 SPE

The August 12, 1989 SPE started at 1600 UT. Particle flux reached a maximum of 9,200 pfu at 0710 UT on August 13, 1989. The associated flare began at 1357 UT and reached a maximum at 1424 UT. The first associated CME was observed at 1445 UT, centered at approximately 3° South with a width of at least 85° (Kahler, 1993). A lower limit on the CME speed was established to be 1200km/s. A second CME was observed with a calculated onset time of 1645-1710 UT and a plane-of-sky speed of ~304 km/s. The ~90 MeV proton flux began a significant increase about 1820 UT. As the second CME intrinsic speed may have been significantly higher than the plane-of-sky speed, it has been

suggested that additional particle acceleration was caused by shocks driven by the second CME. This occurrence of two CMEs from the same spatial region in a short period of time is unusual. These conditions resulted in a complex SPE flux profile (Kahler, 1993).

Data used in this analysis were collected by the GOES-7 satellite and are presented in Table D.16. Dose rate data used for categorization of the event are presented in Table D.17. Dose rate exceeded the 0.1 cGy/hr threshold for Group 2 two hours into the event.

The Weibull model consistently under-predicted the dose. The model under-predicted dose rate up to hour 28 of the event. The 64.0cGy/11h prediction, or when observed dose was 13% of asymptotic dose, under-predicted the asymptotic dose by 4% of the observed asymptotic dose. The hour 5 to hour 9 predictions seem to group towards a common asymptote at approximately 300 cGy. The hour 10 and hour 11 predictions then increase towards the observed asymptote of 484 cGy. This behavior may be attributed to the second CME accelerating event and the subsequent complex flux profile.

Like the Weibull model, the Gompertz model consistently under-estimated the dose throughout the event. The model under-predicted dose rate up to hour 24 for all of the predictions, but then closely matched observations for the 45.0cGy/10h and 64.0cGy/11h predictions. The 64.0cGy/11h prediction, or when observed dose was 13% of asymptotic dose, under-predicted the asymptotic dose

by 9% of the observed asymptotic dose. Again, there is a grouping among the hour 5 to hour 9 predictions towards an asymptote of approximately 300 cGy with a subsequent increase towards the observed asymptote.

The logistic model did not exhibit the same initial grouping of predictions towards an asymptote of approximately 300 cGy, but rather, provided a more consistent increase towards the observed asymptote. The 33.5cGy/9h prediction, or when observed dose was 7% of asymptotic dose, under-predicted the asymptotic dose by 22% of the observed asymptotic dose. Initial predictions under-predicted dose up to hour 24, and later predictions over-predicted dose up to hour 24. Dose rate predictions were a mixture of under and over-predictions up to hour 16. After hour 16, all predictions were significantly less than the observed dose rate. Dose and dose rate time profiles for each of the three growth curve models are presented in Figures 7.13 through 7.18.

Model assessment results are presented in Tables D.18 through D.20. Model assessment indicated that the first three 95% predictive intervals for the logistic model were too dispersed. Otherwise, the models supported the predictive intervals for the August 12, 1989 SPE. These statistics indicate that the models adequately fit the data.

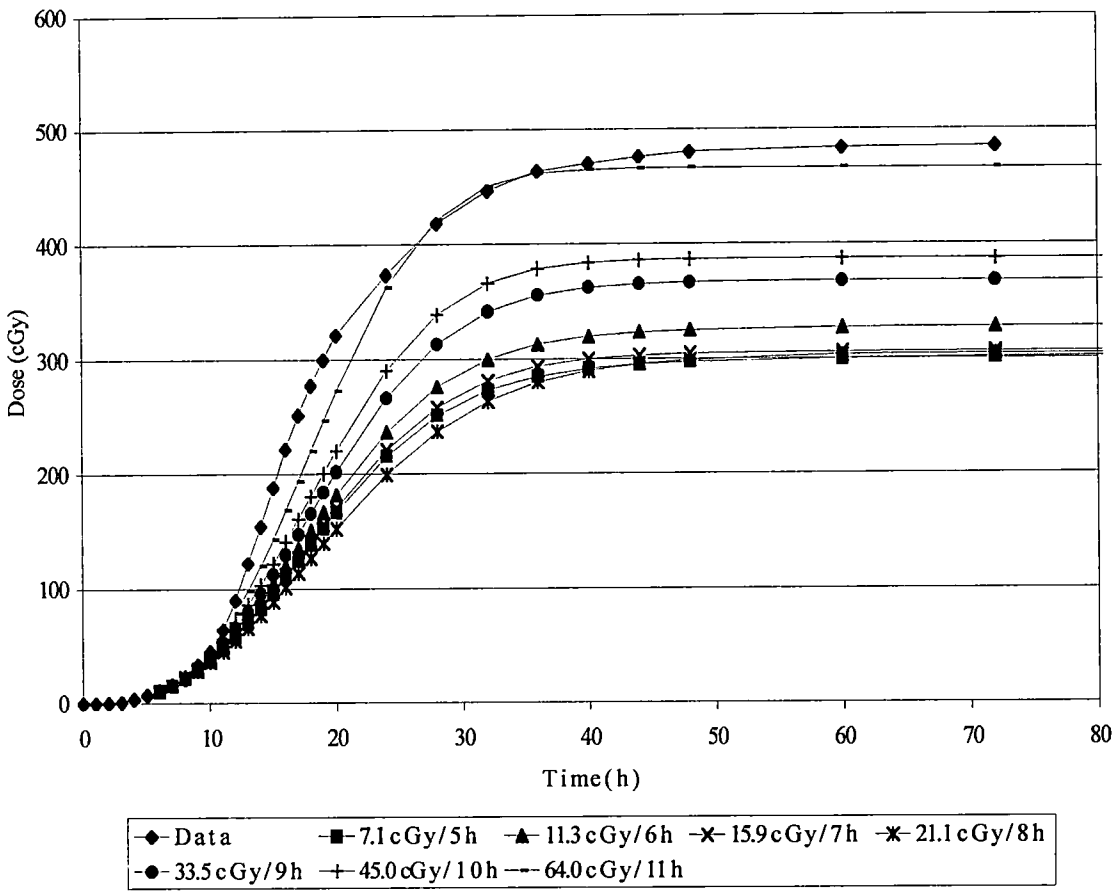


Figure 7.13. Water dose-time profile prediction using posterior predictive means for the August 12, 1989 SPE and Weibull growth curves.

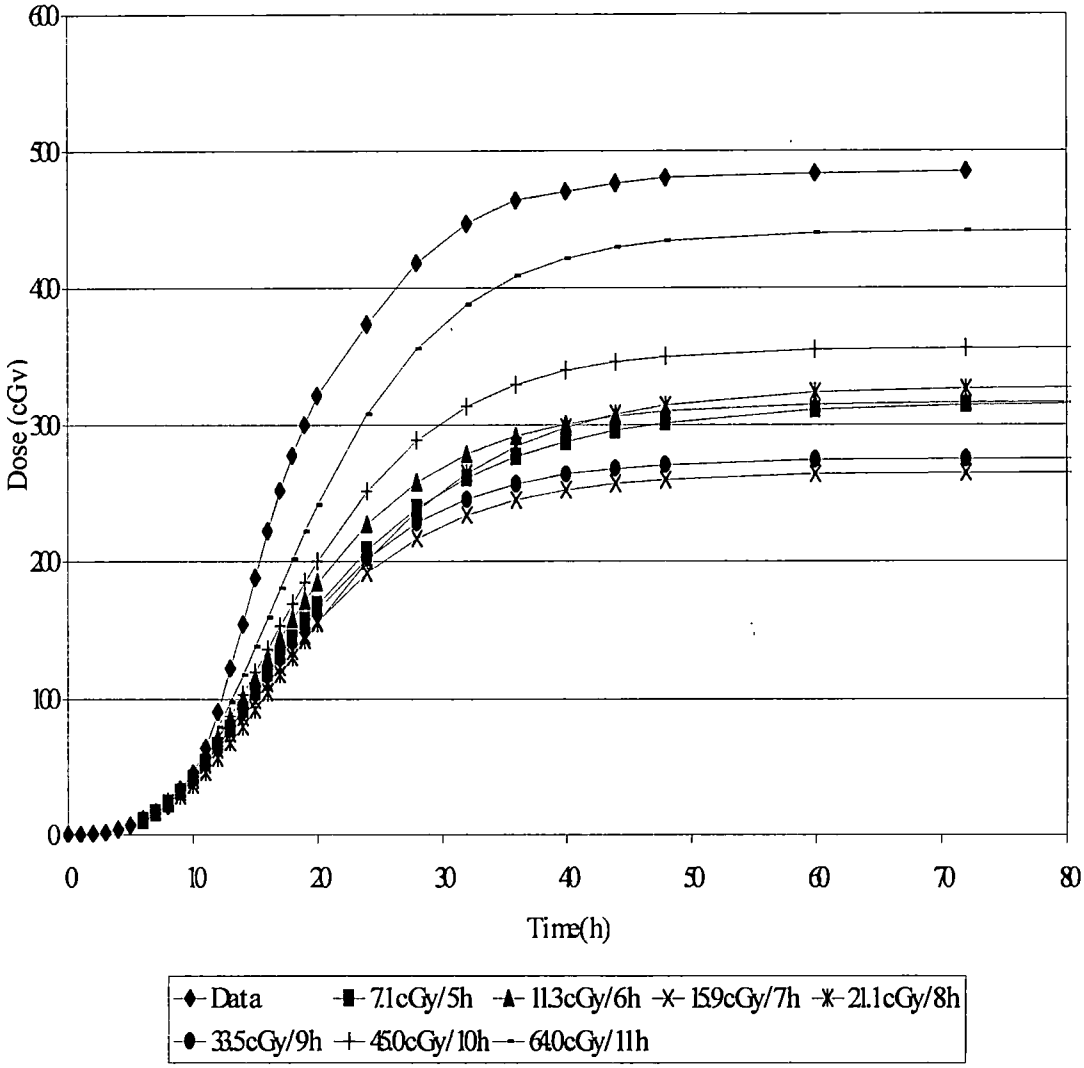


Figure 7.14. Water dose-time profile prediction using posterior predictive means for the August 12, 1989 SPE and Gompertz growth curves.

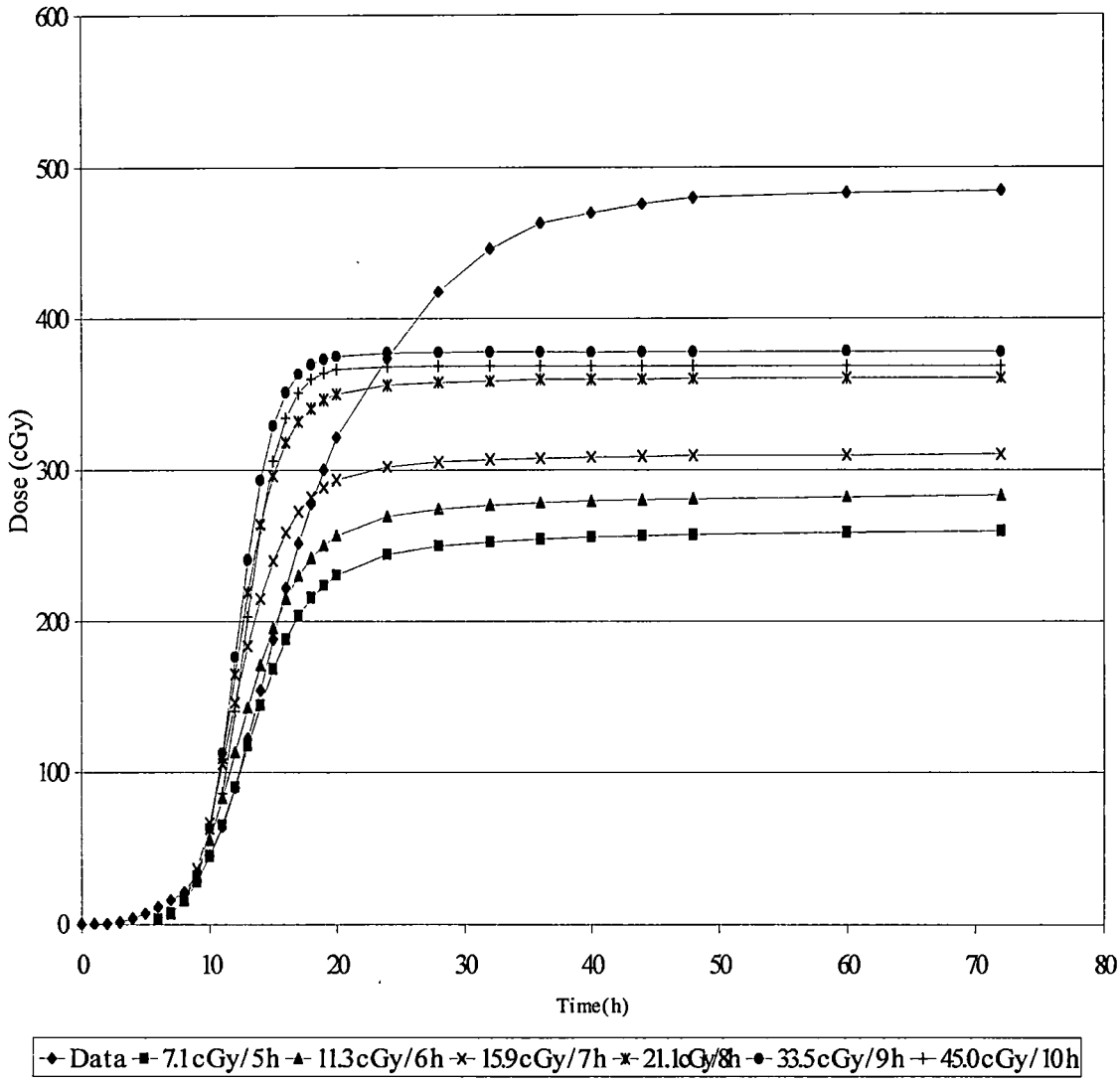


Figure 7.15. Water dose-time profile prediction using posterior predictive means for the August 12, 1989 SPE and logistic growth curves.

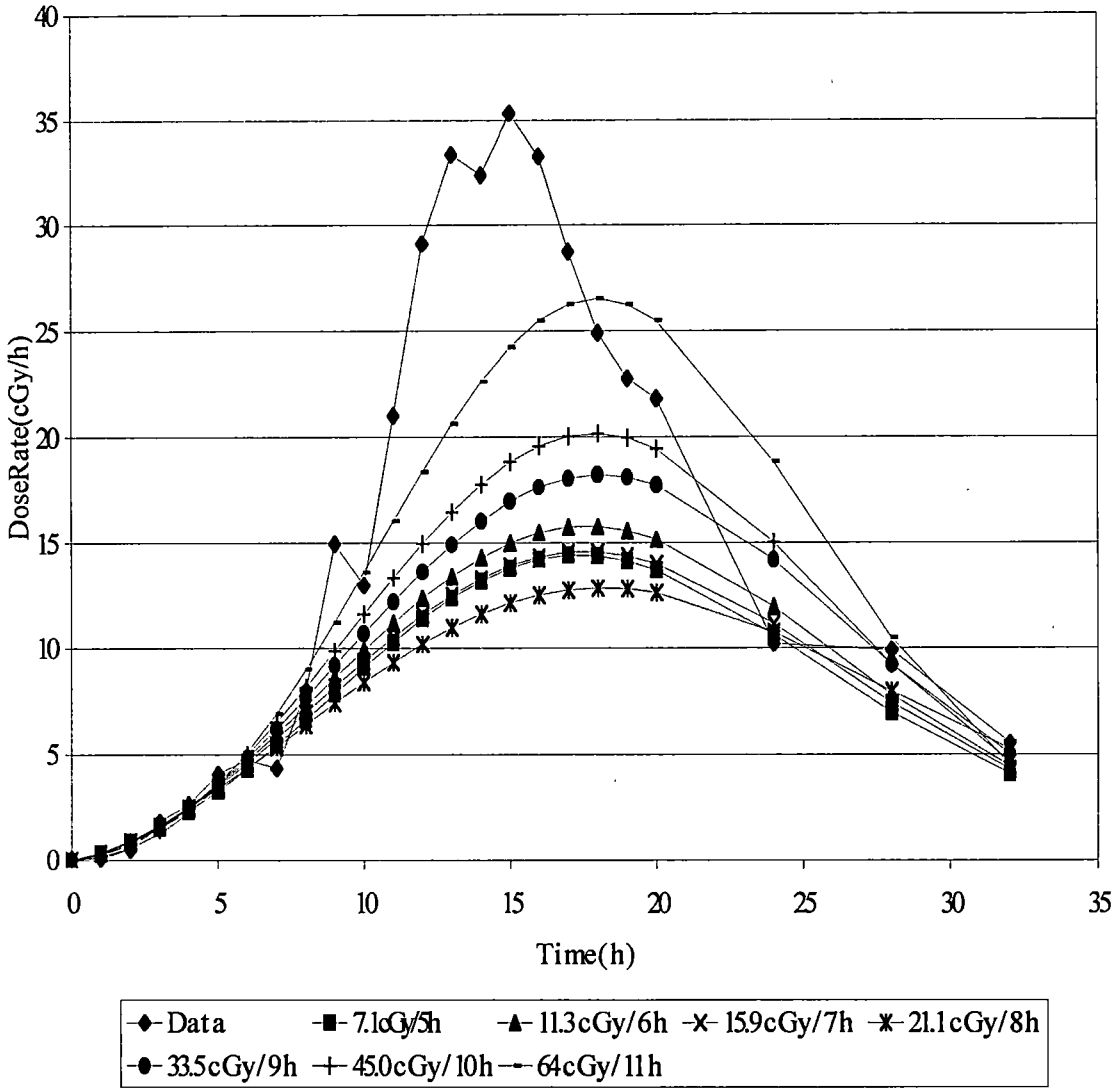


Figure 7.16. Water dose rate-time profile prediction using posterior predictive means for the August 12, 1989 SPE and Weibull growth curves.

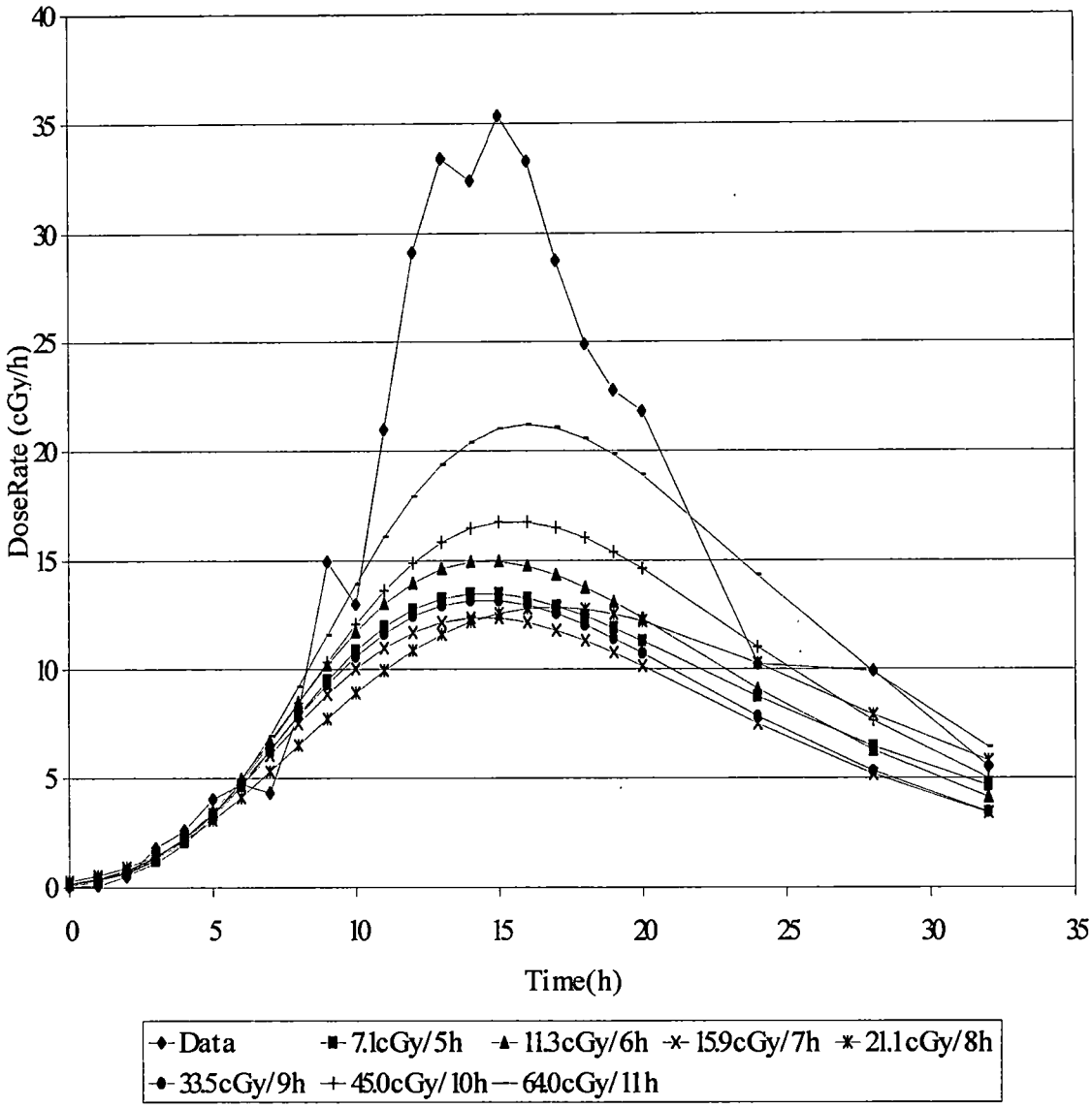


Figure 7.17. Water dose rate-time profile prediction using posterior predictive means for the August 12, 1989 SPE and Gompertz growth curves.

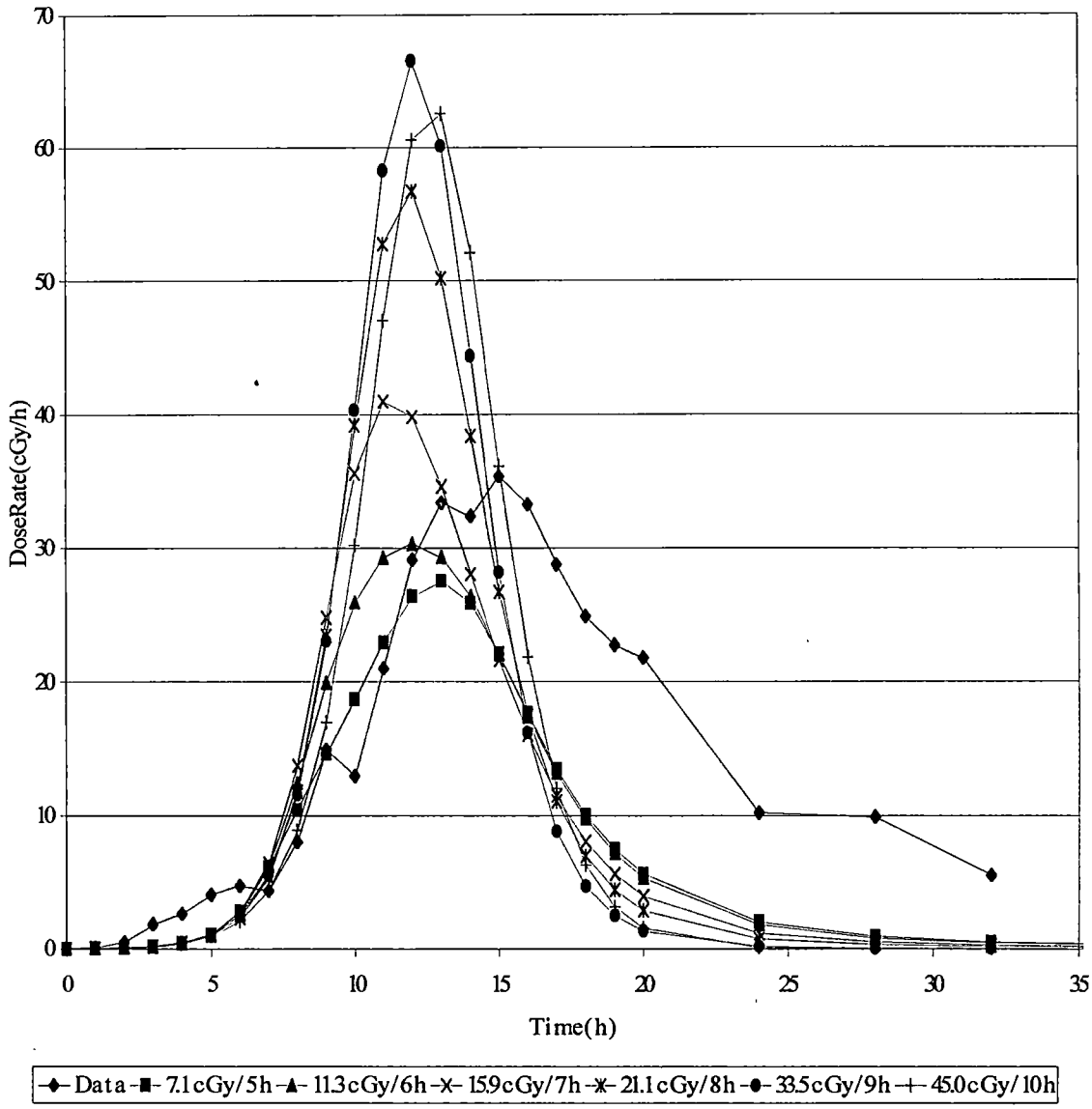


Figure 7.18. Water dose rate-time profile prediction using posterior predictive means for the August 12, 1989 SPE and logistic growth curves.

Model comparison results are presented in Table 7.7. The ratio of the product of conditional predictive ordinates, the pseudo Bayes factor, indicated that the Weibull model was preferred to the Gompertz and logistic models. The Gompertz model was consistently preferred over the logistic model.

Predictive dose 50% and 95% interval widths are presented in Figures 7.19 through 7.24. Predictive interval widths for all models indicated that interval widths increased, as expected, as predictions were made farther into the future with a given set of data. Predictive intervals mimicked the asymptotic nature of the growth curves. Predictive interval widths after 8 hours did not generally decrease, but rather, oscillated as the SPE evolved. The complex nature of the dose rate between 7 and 10 hours probably contributed to these anomalies.

7.4 Conclusions

The Weibull, Gompertz, and logistic models provided useful forecasts of the dose-time profile for the November 8, 2000 SPE. Dose rate-time profiles for the Weibull and Gompertz models were reasonable, but the logistic model significantly over-predicted and temporally lagged dose rate observations. Predictive interval widths for the Weibull and Gompertz models indicated more certain forecasts as additional observations were made. The logistic model indicated less certain forecasts as additional observations were made. This behavior was due to skewed and/or bimodal posterior predictive distributions and their associated uncertainties.

Table 7.7 Calculated product of conditional predictive ordinate values for August 12, 1989 SPE predictions. NC indicates non-convergence of chain.

Hours into event	Weibull	Gompertz	Logistic
5	3.41e-67	5.53e-71	6.1e-128
6	3.1e-63	2.31e-71	1.43e-129
7	4.4e-64	3.11e-72	2.66e-131
8	6.4e-64	1.67e-73	6.59e-133
9	1.33e-70	3.09e-75	2.87e-134
10	3.53e-73	2.82e-75	1.83e-136
11	3.61e-75	6.87e-80	NC

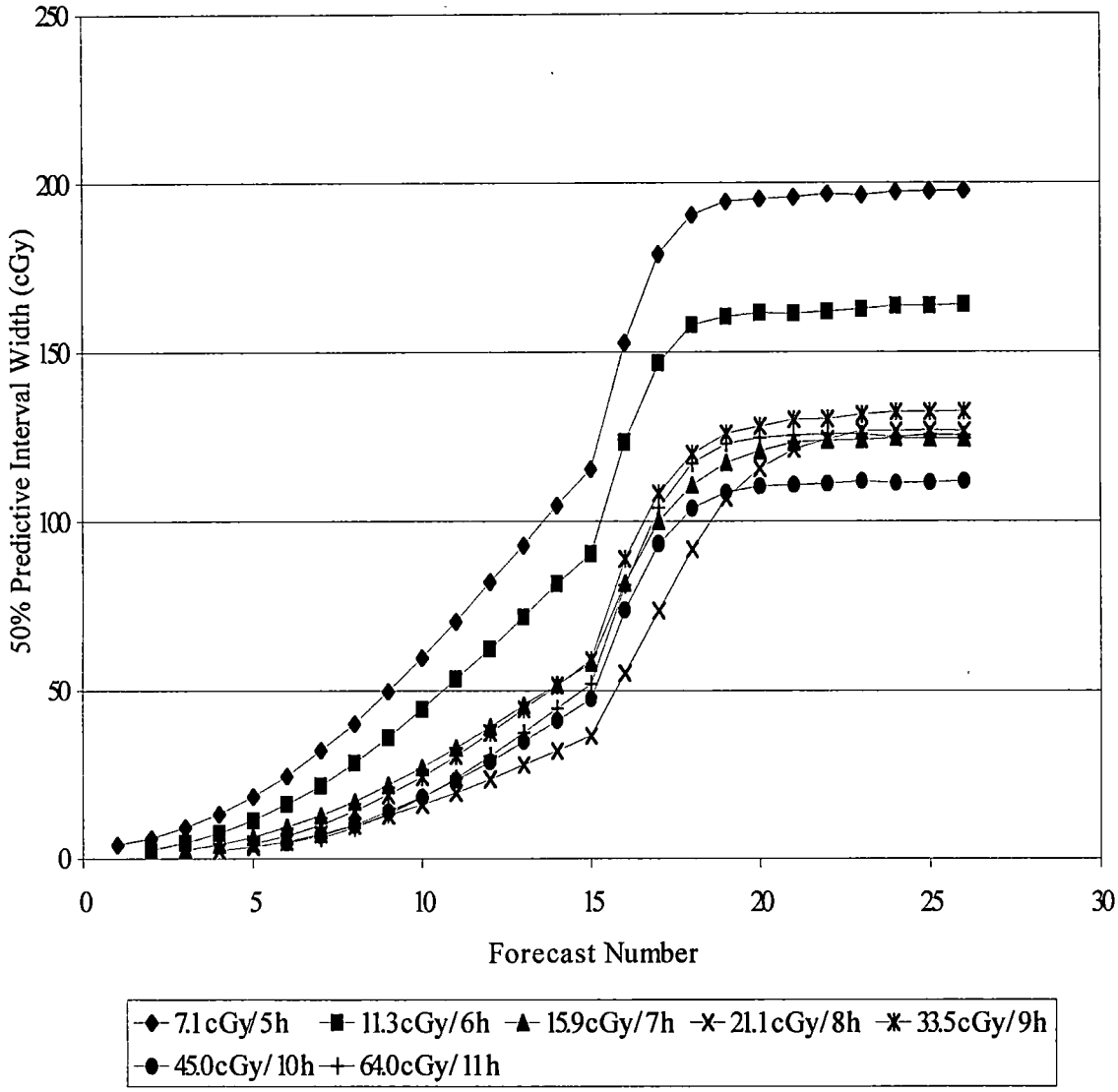


Figure 7.19. Weibull model 50% predictive interval widths for August 12, 1989 SPE.

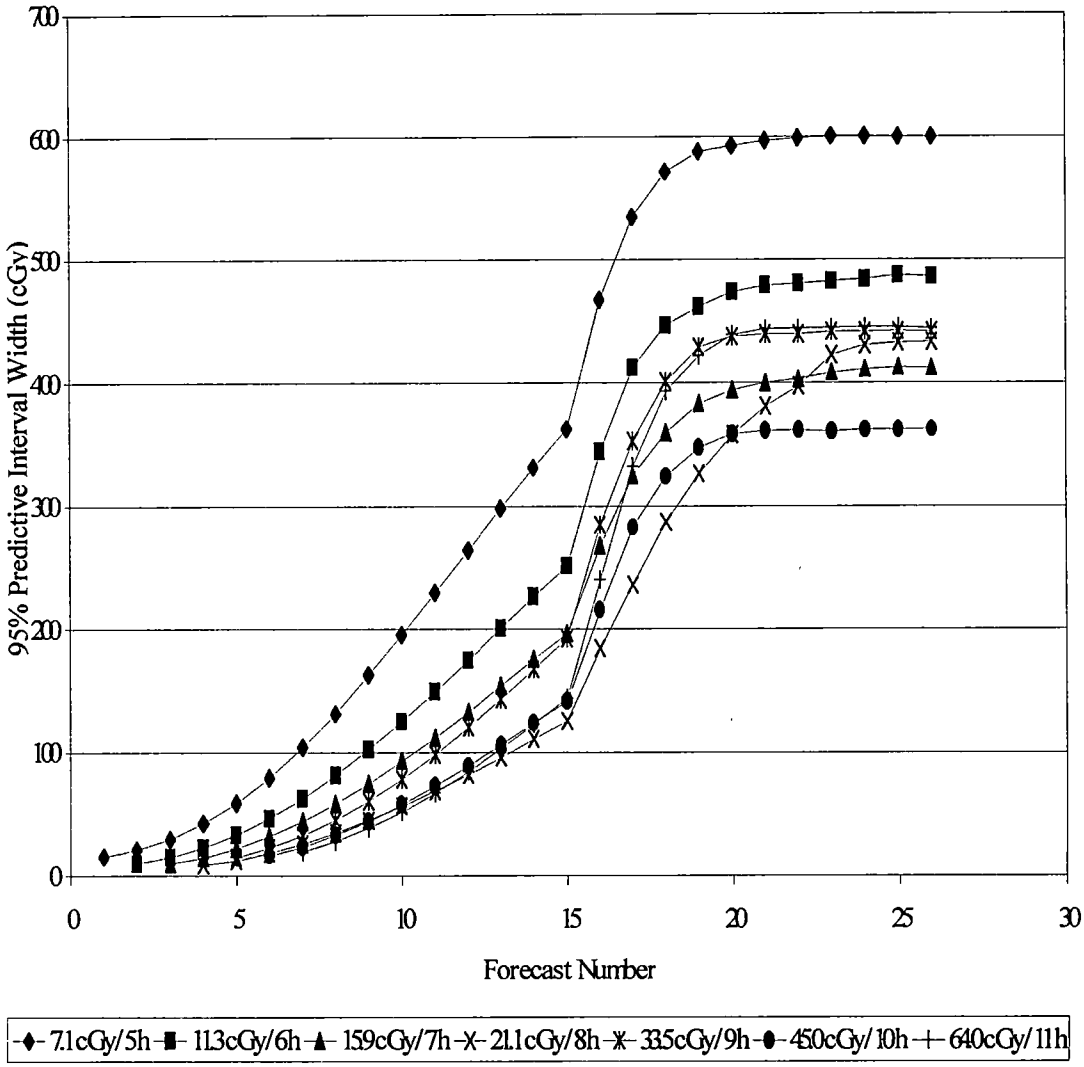


Figure 7.20. Weibull model 95% predictive interval widths for August 12, 1989 SPE.

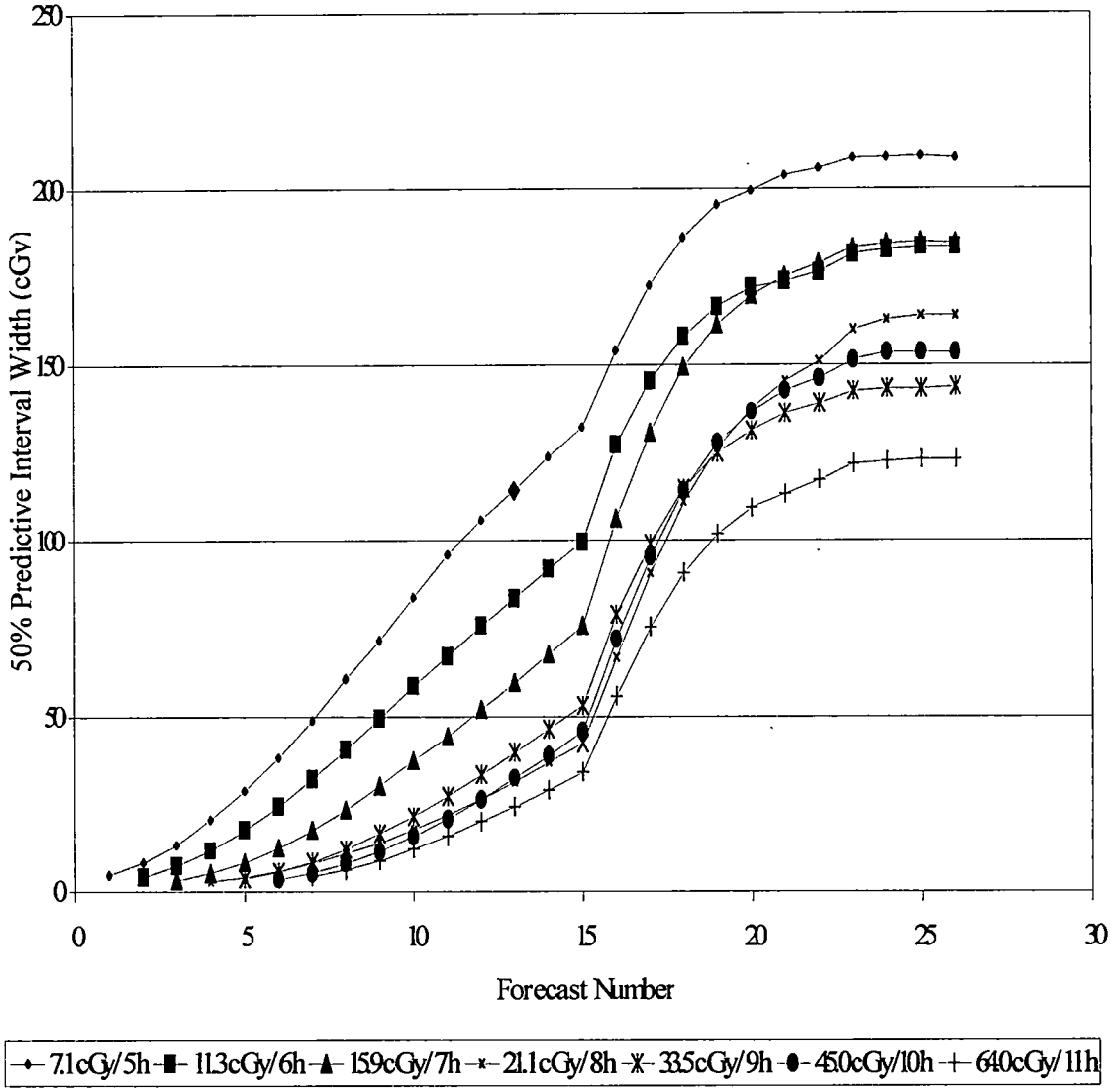


Figure 7.21. Gompertz model 50% predictive interval widths for August 12, 1989 SPE.

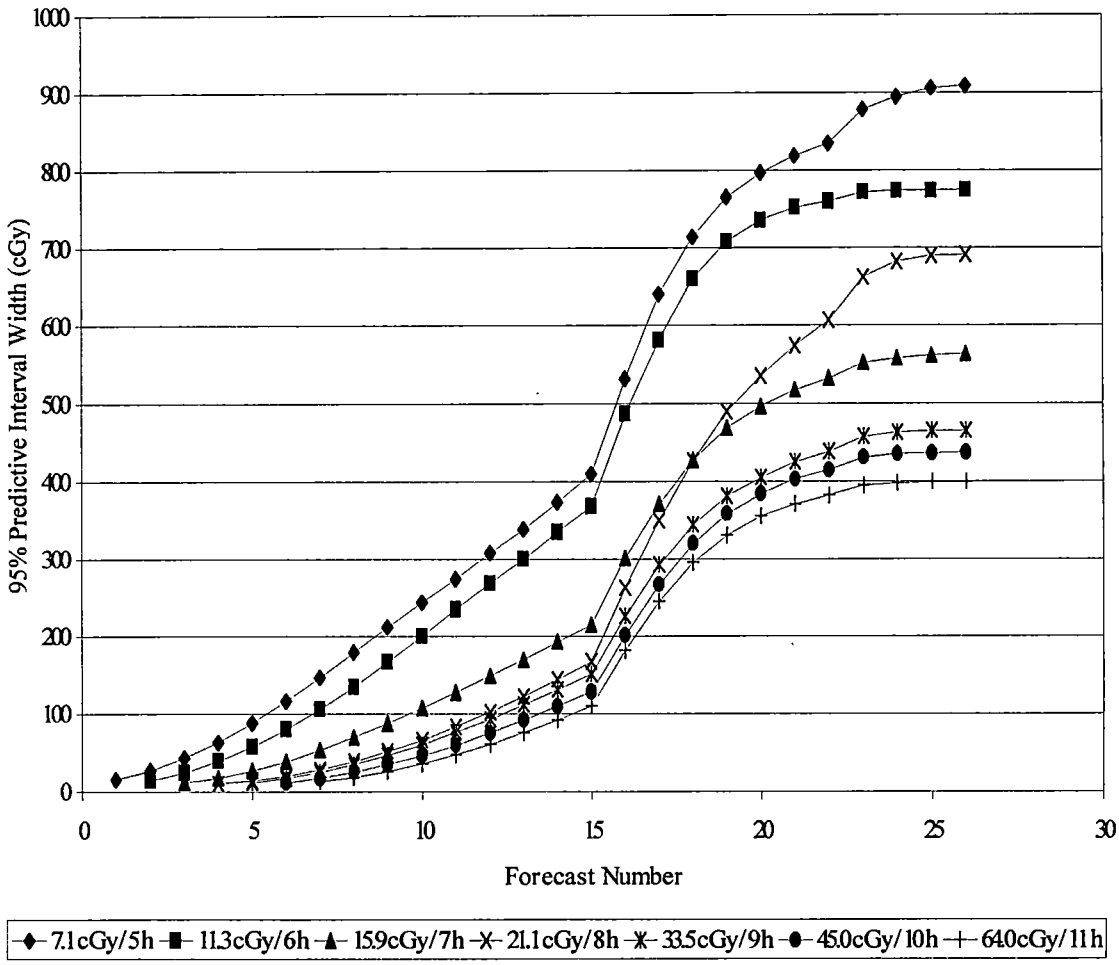


Figure 7.22. Gompertz model 95% predictive interval widths for August 12, 1989 SPE.

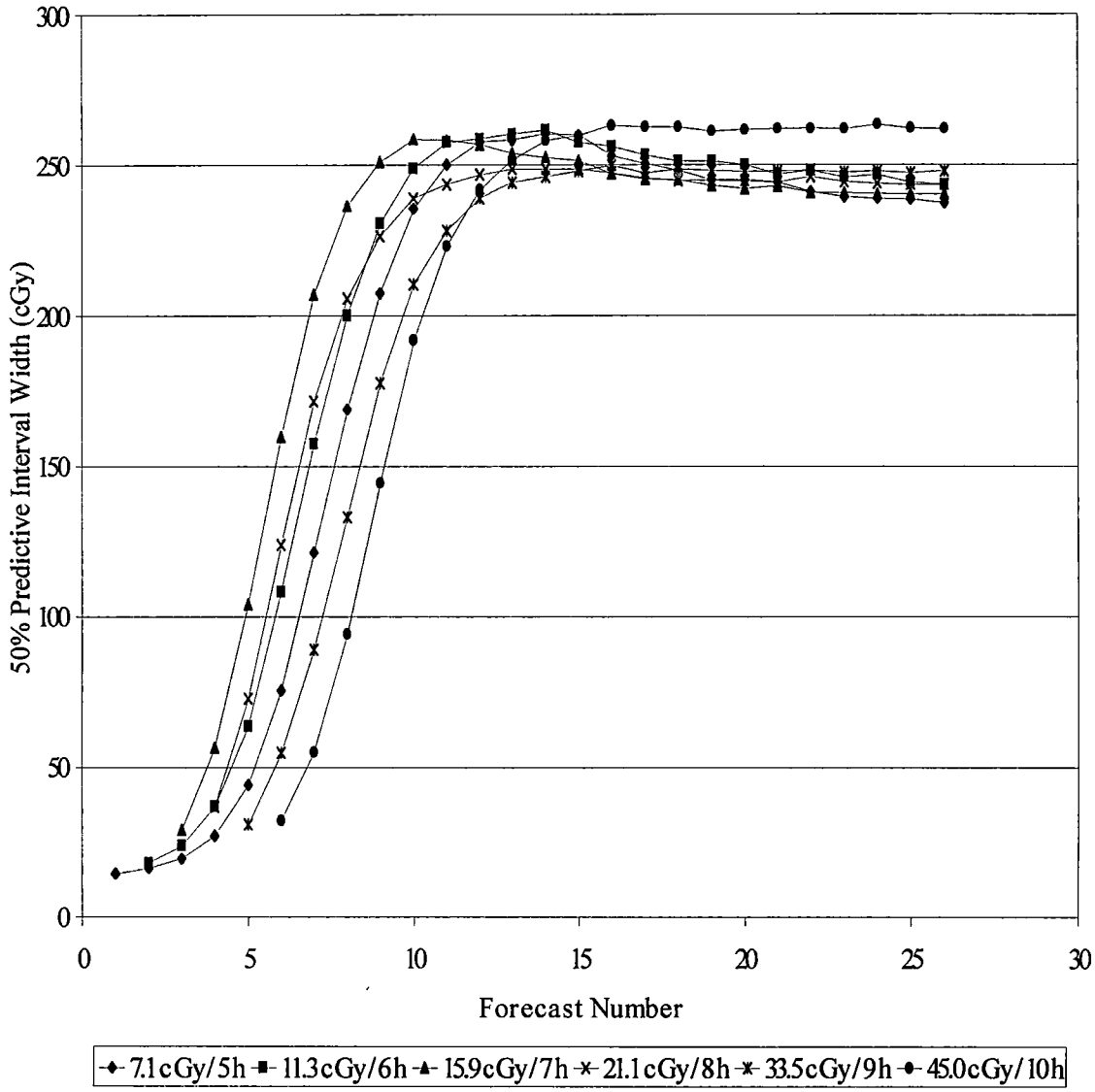


Figure 7.23. Logistic model 50% predictive interval widths for August 12, 1989 SPE.

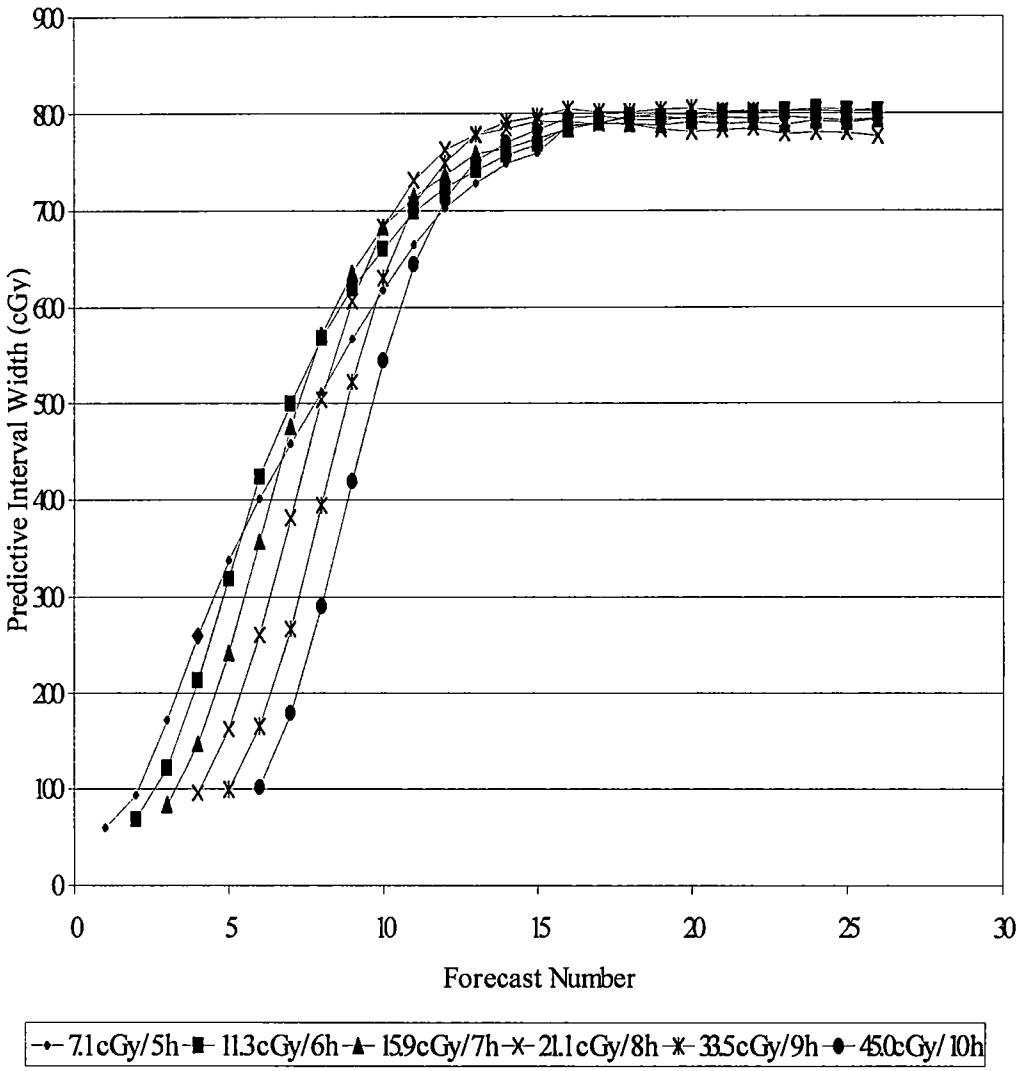


Figure 7.24. Logistic model 95% predictive interval widths for August 12, 1989 SPE.

All models provided adequate forecasts of the dose-time profile for the August 12, 1989 SPE. The Weibull and Gompertz models exhibited grouping of early predictions towards an asymptote of approximately 300 cGy, as compared to the observed asymptote of 484 cGy. The logistic model provided predictions which generally increased towards the observed asymptote. Weibull and Gompertz models consistently under-predicted dose rate. Logistic model predictions after the 11.3cGy/6h prediction over-predicted dose rate early in the event and under-predicted dose rate late in the event. Predictive interval widths did not consistently indicate less uncertainty in predictions as additional observations were made. Forecasts of dose and dose rate were influenced by the occurrence of a second CME which led to complex dose and dose-rate time profiles.

The Weibull and Gompertz models provided similar dose and dose rate-time profiles as well as predictive interval widths. Some of the differences in logistic model results may be attributed to the use of fewer fitting parameters for the logistic hierarchical non-linear regression model. Generally, fewer fitting parameters allow less flexibility for fitting and subsequently, forecasting the evolution of a curve. Reparameterization of the three parameter logistic growth curve might avoid the convergence problems encountered with Equation 7.3 while allowing additional flexibility for fitting and forecasting.

CHAPTER 8

CONCLUSIONS AND RECOMMENDATIONS FOR FUTURE WORK

This work demonstrated the potential for Bayesian inference methods to make forecasts of dose and dose rate-time profiles early in the evolution of SPEs. Bayesian inference methods provide a coherent methodology for quantifying uncertainty. Hierarchical models provide a natural framework to build an ever-evolving historical database to be used for the prediction of new SPE dose and dose rate-time profiles. Forecasts provide a valuable tool to space operations planners when making recommendations concerning operations in which radiation exposure might jeopardize personal safety or mission completion. While a previous attempt to use artificial neural networks was successful in predicting asymptotic dose, it provided no information concerning the uncertainty of those predictions, the temporal evolution of the SPE, or the dose rate-time profile of an event. These predictions are a new feature of this work.

Dose time profile predictions using hierarchical non-linear regression models and Bayesian inference methods provided significant improvements in forecasting over the individual SPE non-linear regression models discussed in Chapter 6 of this work. This methodology provides prediction of the temporal evolution of an event, dose rate prediction, and a measure of the uncertainty for the predictions.

Analysis of the November 8, 2000 SPE provided adequate forecasts of the dose-time profile for the Weibull, Gompertz, and logistic growth curve models. The Weibull and Gompertz models provided adequate forecasts of the dose rate-time profile, while the logistic model forecasts lagged temporally and significantly over-predicted the magnitudes of the observed dose rates. Predictive interval widths for the Weibull and Gompertz models behaved as expected, while the logistic model predictive interval widths indicated more uncertain forecasts as additional data became available.

Analysis of the August 12, 1989, SPE provided adequate forecasts of the dose-time profile for the Weibull, Gompertz, and logistic growth curve models. While forecasts were not as accurate as those for the November 8, 2000, SPE, these forecasts were influenced by a second CME accelerating event which led to a complex flux profile and subsequently, complex dose and dose rate-time profiles. The Weibull and Gompertz models under-predicted dose rate while the logistic model significantly over-predicted the dose rate after seven hours into the event. Predictive interval widths for all models reflected the complex nature of the event, in that widths did not consistently indicate less uncertainty in predictions as additional data became available.

The following research is recommended to improve and extend this methodology:

(1) Investigate convergence problems associated with the logistic growth curve model to allow a three parameter model. This may provide better flexibility in fitting and subsequent forecasting.

(2) Investigate other methods of model comparison in an attempt to capture a given model's ability to forecast rather than to fit observed data.

(3) Investigate hierarchical, dynamic models in an attempt to capture the temporal evolution of parameters.

(4) Continue the search for physical solar observables which relate to the subsequent dose and dose rate evolution of an event.

(5) Graphically show the uncertainty for dose predictions for different times.

WORKS CONSULTED

REFERENCES

Adams, J. H., Jr., Silberberg, R., Tsao, C.H., 1981. Cosmic Ray Effects on Microelectronics. Part I – The Near-Earth Particle Environment. NRL Memo. Rep. 4506-Pt. I, U.S. Navy.

Bethe, H., 1930. Zur Theorie des Durchgangs schneller Korpuskularstrahlen durch Materie. Annals Physik 5, 325-400.

Birnbaum, A., 1962. On the Foundations of Statistical Inference. Journal of the American Statistical Association 57, 269-306.

Box, G. E. P., 1980. Sampling and Bayes Inference in Scientific Modeling and Robustness. Journal of the Royal Statistical Society A 143, 383-430.

Box, G.E.P., and Jenkins, G.M., 1976. Time Series Analysis: Forecasting and Control (2^{nd} ed.). Holden-Day, San Francisco.

Brooks, S. P., Gelman, A., 1998. Alternative Methods for Monitoring Convergence of Iterative Simulations. Journal of Computational and Graphical Statisitics 7, 434-455.

Canfield, R. C.,Hudson, H.S., McKenzie, D.E., 1999. Sigmoidal Morphology and Eruptive Solar Activity. Geophysical Research Letters 26, 627-630.

DeGroot, M. H., 1970. Optimal Statistical Decisions. New York: McGraw Hill.

Fearn, T., 1975. A Bayesian Approach to Growth Curves. Biometrika 62, 89-100.

Gamerman, D., 1997. Markov Chain Monte Carlo. Chapman and Hall, Great Britain.

Geisser, S., Eddy, W. F., 1979. A Predictive Approach to Model Selection. Journal of the American Statistical Association 74, 153-160.

Gelfand, A. E., Dey, D. K., 1994. Bayesian Model Choice: Asymptotics and Exact Calculations. Journal of the Royal Statistical Society B 56, 501-514.

Gelfand, A. E., Dey, D. K., Chang, H., 1992. Model Determination using Predictive Distributions with Implementation via Sampling-Based Methods. Bayesian Statisitics 4, 147-167.

Gelfand, A. E., Smith A. F. M., 1990. Sampling Based Approaches to Calculating Marginal Densities. Journal of the American Statistical Association, 85, 398-409.

Gelman, A., Rubin, D. B., 1992. Inference from Iterative Simulation Using Multiple Sequences. Statistical Science 7, 457-511.

Geman, S. and Geman, D., 1984. Stochastic Relaxation, Gibbs Distributions and the Bayesian Restoration of Images. IEEE Transactions on Pattern Analysis and Machine Intelligence 6, 721-741.

Geweke, J., 1992. Evaluating the Accuracy of Sampling-Based Approaches to the Calculation of Posterior Moments. Bayesian Statistics 4, 169-193.

Geyer, C. J., 1992. Practical Markov Chain Monte Carlo. Statistical Science 7, 473-511.

Gilks, W. R., 1992. Derivative-free Adaptive Rejection Sampling for Gibbs Sampling. Bayesian Statistics 4, 641-649.

Gilks, W. R., Wild, P., 1992. Adaptive Rejection Sampling for Gibbs Sampling. Applied Statistics 41, 337-348.

Hastings, W. K., 1970. Monte Carlo Sampling Methods Using Markov Chains and Their Applications. Biometrika 57, 97-109.

Heckman, G. , Kunches, J., Allen, J., 1992. Prediction and Evaluation of Solar Particle Events Based on Precursor Information. Advances in Space Research 12, 313-320.

Heidelberger, P., Welch, P., 1983. Simulation Run Length Control in the Presence of an Initial Transient. Operations Research 31, 1109-1144.

Kahler, S. W., 1993. Coronal Mass Ejections and Long Risetimes of Solar Energetic Particle Events. Journal of Geophysical Research 98, 5607-5615.

Kahler, S. W., Sheely, N. R., Howard, R. A., Koomen, M. J., Michels, D. J., McGuire, R. E., von Rosenvinge, T. T., Reames, D. V., 1984. Associations between coronal mass ejections and solar energetic proton events. Journal of Geophysical Research 89, 9683.

Kovtunenko, V. M., Kremnev, R. S., Pichkhadze, K. M., Bogomolov, V. B., Kontor, N. N., Filippichev, S. A., Petrov, V. M., Pissarenko, N. F., 1994. Advances in Space Research 14, (10)77-(10)84.

Lamarche, A.H., Poston, J.W., 1996. Parameterization of Solar Flare Dose. Transactions of the American Nuclear Society 75, 302-303.

Le Cam, L., 1953. On Some Asymptotic Properties of Maximum Likelihood Estimates and Related Bayes Estimates. University of California Publications in Statistics 1 (11), 277-330.

Lindley, D. V., Smith, A. F. M., 1972. Bayes Estimates for the Linear Model. Journal of the Royal Statistical Society B34, 1-41 (with discussion).

Metropolis, N., Rosenbluth, A. W., Rosenbluth, M. N., Teller, A. H., Teller, E., 1953. Equation of State Calculations by Fast Computing Machine. Journal of Chemical Physics 21, 1087-1091.

Muller, P., 1991. Metropolis Based Posterior Integration Schemes. Technical Report, Statistics Department, Purdue University.

Neal, J. S., Townsend, L. W., 2000. Solar Particle Event Dose and Dose Rate Distributions: Parameterization of Dose-Time Profiles Using Bayesian Inference and Markov Chain Monte Carlo Methods. Proceedings of the 2000 American Nuclear Society Radiation Protection and Shielding Division Topical Meeting, 470-477.

Neal, R., 1997. Markov Chain Monte Carlo Methods Based on Slicing the Density Function. Technical Report No. 9722, Department of Statistics, University of Toronto.

Parsons, J. L. and Townsend, L. W., 2000. Interplanetary Crew Dose Rates for the August 1972 Solar Particle Event. Radiation Research, 153, 729-733.

Price, R., 1763. An Essay Towards Solving a Problem in the Doctrine of Chances. Philosophical Transactions of the Royal Society 53, 370.

Raferty, A. E., Lewis, S., 1992. How Many Iterations in the Gibbs Sampler? Bayesian Statistics 4, 763-773.

Reames, D.L., Barbier, L., Ng, C., 1996. The spatial distribution of particles accelerated by coronal mass ejection-driven shocks. Astrophysical Journal 466, 473-486.

Roberts, G.O., 1996. Markov Chain Concepts Related to Sampling Algorithms. In Markov Chain Monte Carlo in Practice, 45-57, Chapman & Hall, London.

Rubin, D. B., 1984. Bayesianly Justifiable and Relevant Frequency Calculations for the Applied Statistician. Annals of Statistics 12, 1151-1172.

Schenk, K., 2001. Personal communications, EIT and LASCO Operations, Goddard Space Flight Center.

Smart, D. F., Shea, M. A., 1997. Solar Radiation. Encyclopedia of Applied Physics. The American Institute of Physics, Volume 18, VCH Publishers Inc., New York.

Smith, A. F. M., 1991. Discussion of the Paper by M. Aitkin. Journal of the Royal Statistical Society B 53, 132-133.

Smith, B. J., 2000. Bayesian Output Analysis Program (BOA), Version 0.5.0. Department of Biostatistics, The University of Iowa, College of Public Health.

Space Environment Services Center products and services user guide, NOAA Space Environment Center, Boulder, CO, 1993.

Spiegelhalter, D. J., Thomas, A., Best, N. G., Gilks, W. R., 1999. BUGS: Bayesian Inference Using Gibbs Sampling, Version 1.1.1. MRC Biostatistics Unit, Cambridge.

Spiegelhalter, D. J., Thomas, A., Best, N. G., 2000. WinBUGS, Version 1.3. MRC Biostatistics Unit, Cambridge.

Stone, M., 1974. Cross-validatory Choice and Assessment of Statistical Predictions. Journal of the Royal Statistical Society B 36, 111-147.

Tehrani, Nazila H., 1998. Predicting Astronaut Radiation Doses from Major Solar Particle Events Using Artificial Intelligence. Doctoral Dissertation, The University of Tennessee, Knoxville.

Townsend, L. W., Cucinotta, F. A., Wilson, J.W., 1992. Interplanetary Crew Exposure Estimates for Galactic Cosmic Rays. Radiation Research, 129, 48-52.

Townsend, L. W., Neal, J. S., Hines, J. W., 2001. Solar Particle Event Doses and Dose Rates for Interplanetary Crews: Predictions Using Artificial Intelligence and Bayesian Inference. Advances in Space Research 2001 in press.

Townsend, L.W., Zapp, E.N., 1999. Dose Uncertainties for Large Solar Particle Events: Input Spectra Variability and Human Geometry Approximations. Radiation Measurements 30, No. 3, 337-343.

Turner, R., 1996. Physics of Solar Particle Events. Part One in a Series of Reports on Risk Management During Solar Particle Events. ANSER Technical Report, Arlington, Virginia.

Turner, R., 1997. Forecasting Solar Particle Events. Part Two in a Series of Reports on Risk Management During Solar Particle Events. ANSER Technical Report, Arlington, Virginia.

Wilkinson, D., Ushomirskiy, G., 1994. GOES Space Environment Monitor CD-ROM. User Documentation. National Oceanic and Atmospheric Administration.

Wilson, J. W., Townsend, L. W., Nealy, J. E., Chun, S. Y., Hong, B. S., Lamkin, S. L., Ganapol, B. D., Khan, F., Cucinotta, F. A., 1989. BRYNTRN: A Baryon Transport Model. NASA Technical Paper 2887.

Wilson, J.W., Townsend, L.W., Schimmerling, W., Khandelwal, G.S., Khan, F., Nealy, J.F., Cucionatta, F.A., Simonsen, L.C., Shinn, J.L., Norbury, J.W., 1991. Transport Methods and Interactions for Space Radiations, NASA Reference Publication no. RP-1257.

Zapp, E. N., Ramsey, C. R., Townsend, L.W., Badhwar, G.D., 1998. Solar Particle Event Dose Distributions: Parameterization of Dose-Time Profiles. Acta Astronautica, 43, 249-259.

Zapp, E. N., Ramsey, C. R., Townsend, L.W., Badhwar, G.D., 1999. Solar Particle Event Dose and Dose-Rate Distributions: Parameterization of Dose-Time

Profiles, with Subsequent Dose-Rate Analysis. Radiation Measurements 30, 393-400.

BIBLIOGRAPHY

Bernardo, J. M., Smith, A. F. M., 1994. Bayesian Theory. John Wiley and Sons, Inc., New York.

Box, G.E.P., Jenkins, G.M., 1976. Time Series Analysis: Forecasting and Control (2nd ed.). Holden-Day, San Francisco.

Brooks, S. P., Gelman, A., 1998. General Methods for Monitoring Convergence of Iterative Simulations. Journal of Computational and Graphical Statistics 7, 434-455.

Brown, R.G., 1959. Statisitical Forecasting for Inventory Control. McGraw-Hill, New York.

Brown, R.G., 1962. Smoothing, Forecasting and Prediction of Discrete Time Series. Prentice-Hall, Englewood Cliffs, NJ.

Carlin, B. P., Louis, T. A., 1998. Bayes and Empirical Bayes Methods for Data Analysis. Chapman and Hall/CRC, New York.

Gamerman, D., 1997. Markov Chain Monte Carlo. Chapman and Hall, Great Britain.

Gelman, A., Carlin, J. B., Stern, H. S., Rubin, D. B., 1995. Bayesian Data Analysis. Chapman and Hall/CRC, New York.

Pole, A., West, M., Harrison, P.J., 1994. Applied Bayesian Forecasting and Time Series Analysis. Chapman and Hall, New York

Ratkowsky, D.A., 1983. Nonlinear Regression Modeling. Marcel Dekker, New York

West, M., Harrison, P.J., 1997. Bayesian Forecasting and Dynamic Models. Springer-Verlag, New York

APPENDICES

Appendix A

Table A.1. Skin and eye dose data for the March 23, 1991 SPE, estimated using the BRYNTRN computer code.

Time (days)	Skin Dose (cGy)	Eye Dose (cGy)
0.0833	0.0026	0.0021
0.1667	0.0044	0.0037
0.25	0.0066	0.0054
0.4167	0.41	0.25
0.5	1.8	1.0
0.5833	5.6	3.2
0.6667	10.7	6.1
0.75	18.8	10.7
0.9167	50.7	29.2
1.0833	98.5	57.2
1.25	134	76.8
1.6667	138	80.1
3	140	81.5
3.333	141	81.8
3.5833	141	82
10	143	82.6

Table A.2. Skin and eye dose data for the June 4, 1991 SPE, estimated using the BRYNTRN computer code.

Time (days)	Skin Dose (cGy)	Eye Dose (cGy)
0.0833	0.02	0.01
0.25	0.05	0.03
0.3333	0.6	0.56
0.5	4.6	3.8
0.5833	6.4	5.2
0.75	9.9	7.8
0.8333	11.8	9.1
0.9167	13.5	10.3
1	14.8	11.3
1.1667	16.8	12.7
1.25	17.6	13.2
1.4167	19.3	14.4
1.5	20.1	15.0
1.667	20.4	15.2
1.75	21.3	15.8
2.0833	21.8	16.2
2.5	22.2	16.4
3.1667	22.5	16.6
5	22.5	16.6
8.0833	22.5	16.7

Table A.3. Skin and eye dose data for August 4, 1972 SPE, estimated using the BRYNTRN computer code.

Time (days)	Skin Dose (cGy)	Eye Dose (cGy)
0.0417	5.8	4.5
0.125	31.2	23.2
0.2083	93.9	72.5
0.25	159	125
0.2917	226	179
0.3333	297	235
0.375	350	275
0.4167	402	316
0.4583	462	360
0.5	522	404
0.5417	606	461
0.5833	656	495
0.6667	666	502
0.75	671	505
0.8333	695	522
1.0417	705	528
1.625	724	541

Table A.4. Percentage of observations that fall within 50% and 95% predictive intervals of skin and eye dose-time profile fits.

SPE	Model	50% Interval	95% Interval
March 23, 1991 skin	Weibull	69	100
March 23, 1991 skin	Gompertz	50	94
March 23, 1991 skin	Logistic	69	100
June 4, 1991 skin	Weibull	90	100
June 4, 1991 skin	Gompertz	30	95
June 4, 1991 skin	Logistic	35	100
August 4, 1972 skin	Weibull	53	100
August 4, 1972 skin	Gompertz	76	94
August 4, 1972 skin	Logistic	29	100
March 23, 1991 eye	Weibull	69	94
March 23, 1991 eye	Gompertz	75	94
March 23, 1991 eye	Logistic	69	100
June 4, 1991 eye	Weibull	75	95
June 4, 1991 eye	Gompertz	75	100
June 4, 1991 eye	Logistic	45	100
August 4, 1972 eye	Weibull	47	100
August 4, 1972 eye	Gompertz	76	94
August 4, 1972 eye	Logistic	35	100

Appendix B

Table B.1. Water dose data for the May 6, 1989 SPE, estimated using the BRYNTRN computer code.

Time (hours)	Dose (cGy)	Time (hours)	Dose (cGy)
0.5	0.0023	15.5	0.033
1	0.0029	16	0.034
1.5	0.0037	16.5	0.036
2	0.0041	17	0.037
2.5	0.0046	17.5	0.038
3	0.0054	18	0.039
3.5	0.0065	18.5	0.040
4	0.0072	19	0.042
4.5	0.0077	19.5	0.043
5	0.0084	20	0.044
5.5	0.0092	20.5	0.045
6	0.0097	21	0.046
6.5	0.011	21.5	0.047
7	0.012	22	0.047
7.5	0.013	22.5	0.048
8	0.014	23	0.049
8.5	0.015	23.5	0.050
9	0.016	24	0.050
9.5	0.018	28	0.055
10	0.02	32	0.061
10.5	0.021	36	0.065
11	0.022	40	0.07
11.5	0.024	44	0.074
12	0.025	48	0.077
12.5	0.026	60	0.087
13	0.028	72	0.094
13.5	0.028	84	0.10
14	0.029	96	0.10
14.5	0.031	108	0.11
15	0.032	-	-

Table B.2. Water dose data for the January 31, 1991 SPE, estimated using the BRYNTRN computer code.

Time (hours)	Dose (cGy)
0	0.018
4	0.11
8	0.24
12	0.29
16	0.30
20	0.31
24	0.32
28	0.33
32	0.33
36	0.33
40	0.33
44	0.34
48	0.34
60	0.34
72	0.34
96	0.34

Table B.3. Water dose data for the March 23, 1991 SPE, estimated using the BRYNTRN computer code.

Time (hours)	Dose (cGy)	Time (hours)	Dose (cGy)
0.25	0.029	7.25	22.3
0.5	0.040	7.5	25.4
0.75	0.053	7.75	28.6
1	0.072	8	31.8
1.25	0.094	8.25	35.3
1.5	0.12	8.5	38.7
1.75	0.17	8.75	42.2
2	0.23	9	46.0
2.25	0.31	10	62.2
2.5	0.43	11	81.4
2.75	0.58	12	106
3	0.78	13	143
3.25	1.0	14	184
3.5	1.3	15	228
3.75	1.7	16	275
4	2.1	17	324
4.25	2.6	18	376
4.5	3.2	19	449
4.75	4.0	20	579
5	5.0	25	754
5.25	6.0	30	774
5.5	7.0	35	781
5.75	8.1	48	796
6	9.7	60	800
6.25	11.6	72	805
6.5	14.0	96	811
6.75	16.8	120	814
7	19.5	-	-

Table B.4. Water dose data for the June 4, 1991, SPE, estimated using the BRYNTRN computer code.

Time (hours)	Dose (cGy)
0	0.10
4	0.19
8	0.28
12	0.42
16	0.77
20	1.3
24	1.9
28	2.3
32	2.7
36	3.3
40	4.1
44	5.1
48	6.2
60	10.9
72	18.5
96	33.9
120	48.2
144	52.8
156	54.5

Table B.5. Water dose data for the August 26, 1991 SPE, estimated using the BRYNTRN computer code.

Time (hours)	Dose (cGy)
0	0.067
4	0.092
8	0.13
12	0.17
16	0.21
20	0.24
24	0.34
28	0.60
32	0.70
36	0.74
40	0.77
44	0.79
48	0.80
60	0.84
72	0.86
96	0.90
120	0.91

Appendix C

Table C.1. Water dose data for the November 08, 2000 SPE, estimated using the BRYNTRN computer code.

Time (hours)	Dose (cGy)
0	.083
1	10.8
2	39.2
3	77.9
4	126
5	178
6	233
7	291
8	347
9	402
10	461
11	523
12	580
13	637
14	692
15	741
16	793
17	832
18	867
19	899
20	928
24	1011
28	1049
32	1071
36	1079
40	1088
44	1094
48	1098
60	1105
72	1106

Table C.2. Water dose data for the September 29, 1989 SPE, estimated using the BRYNTRN computer code.

Time (hours)	Dose (cGy)	Time (hours)	Dose (cGy)	Time (hours)	Dose (cGy)
-	-	5	31.4	13	149
0.25	0.078	5.25	34.5	14	163
0.5	0.15	5.5	37.6	15	179
0.75	0.29	5.75	40.7	16	193
1	0.52	6	43.7	17	207
1.25	0.93	6.25	46.9	19	220
1.5	1.5	6.5	50.6	20	235
1.75	2.4	6.75	54.2	21	250
2	3.4	7	57.4	22	266
2.25	4.6	7.25	60.7	23	280
2.5	6.1	7.5	64.3	24	293
2.75	7.6	7.75	68.3	25	304
3	9.2	8	72.2	26	315
3.25	11.2	8.25	76.6	27	324
3.5	13.9	8.5	81.3	30	349
3.75	16.8	8.75	83.7	48	419
4	19.8	9	87.5	60	426
4.25	22.8	10	103	72	429
4.5	25.7	11	119	96	432
4.75	28.5	12	134	120	432

Table C.3. Percentage of observations that fall within 50% and 95% predictive intervals for the November 8, 2000 SPE.

Model	Hours into event	50% Interval	95% Interval
Weibull	5	50	100
Gompertz	2	67	100
Gompertz	3	75	100
Gompertz	4	40	100
Gompertz	5	33	100
Logistic	2	67	100
Logistic	3	50	100
Logistic	4	60	100
Logistic	5	33	100

Table C.4. Percentage of observations that fall within 50% and 95% predictive intervals for the September 29, 1989 SPE.

Model	Hours into event	50% Interval	95% Interval
Weibull	9	35	97
Weibull	19	60	100
Weibull	27	45	100
Gompertz	4.25	47	100
Gompertz	6	54	96
Gompertz	9	33	100
Gompertz	19	33	98
Gompertz	27	43	98
Logistic	4.25	35	100
Logistic	6	46	100
Logistic	9	33	100
Logistic	19	33	100
Logistic	27	42	91

Appendix D

Table D.1. Water dose data for the July 14, 2000 SPE, estimated using the BRYNTRN computer code.

Time (hours)	Dose (cGy)
0	0.03
1	.15
2	3.0
3	11.0
4	25.6
5	42.5
6	63.9
7	103
8	142
9	186
10	226
11	266
12	308
13	351
14	391
15	434
16	477
17	525
18	584
19	654
20	718
24	989
28	1305
32	1469
36	1502
40	1509
44	1513
48	1517
60	1525
72	1530

Table D.2. Water dose data for the March 23, 1991 SPE, estimated using the BRYNTRN computer code.

Time (hours)	Dose (cGy)
0	0.02
1	0.07
2	0.23
3	0.78
4	2.1
5	5.0
6	9.7
7	19.5
8	31.8
9	46.0
10	62.2
11	81.4
12	106
13	143
14	184
15	228
16	275
17	324
18	376
19	449
20	579
24	734
28	772
32	777
36	781
40	789
44	793
48	796
60	800
72	805
96	811
120	814

Table D.3. Water dose data for the October 19, 1989 SPE, estimated using the BRYNTRN computer code.

Time (hours)	Dose (cGy)
0	0.005
1	0.26
2	1.0
3	2.7
4	4.9
5	8.6
6	13.2
7	19.2
8	25.9
9	33.1
10	40.6
11	48.9
12	58.2
13	67.9
14	78.4
15	88.6
16	98.5
17	108
18	117
19	125
20	132
24	167

Table D.4. Water dose data for the September 29, 1989 SPE, estimated using the BRYNTRN computer code.

Time (hours)	Dose (cGy)
0	0.03
1	0.52
2	3.4
3	9.2
4	19.8
5	31.4
6	43.7
7	57.4
8	72.2
9	87.5
10	103
11	119
12	135
13	149
14	163
15	179
16	194
17	207
19	220
20	235
24	293
28	333
32	366
36	389
40	409
44	414
48	419
60	426
72	429
96	432
120	432

Table D.5. Water dose data for the June 4, 1991 SPE, estimated using the BRYNTRN computer code.

Time (hours)	Dose (cGy)
0	0.10
4	0.19
8	0.28
12	0.42
16	0.77
20	1.3
24	1.9
28	2.3
32	2.7
36	3.3
40	4.1
44	5.0
48	6.2
60	10.9
72	18.5
96	33.3
120	48.2

Table D.6. Water dose data for the March 19, 1990 SPE, estimated using the BRYNTRN computer code.

Time (hours)	Dose (cGy)
0	.015
4	0.29
8	1.1
12	3.0
16	4.8
20	6.1
24	6.7
28	6.9
32	7.1
36	7.1
40	7.1
44	7.1
48	7.1
60	7.0
72	18.455
96	33.28
120	48.166

Table D.7. Water dose data for the November 30, 1989 SPE, estimated using the BRYNTRN computer code.

Time (hours)	Dose (cGy)
0	0.01
4	0.05
8	0.74
12	4.0
16	10.2
20	21.9
24	35.9
28	47.8
32	53.8
36	56.6
40	57.9
44	58.7
48	59.1

Table D.8. Water dose data for the August 26, 1991 SPE, estimated using the BRYNTRN computer code.

Time (hours)	Dose (cGy)
0	0.067
1	0.072
2	0.080
3	0.086
4	0.092
5	0.10
6	0.11
7	0.12
8	0.13
9	0.14
10	0.15
11	0.16
12	0.17
13	0.18
14	0.19
15	0.20
16	0.21
17	0.21
18	0.22
19	0.23
20	0.24
24	0.34
28	0.60
32	0.70
36	0.74
40	0.77
44	0.79
48	0.80
60	0.84
72	0.86
96	0.90
120	0.91

Table D.9. Water dose data for the January 31, 1991 SPE, estimated using the BRYNTRN computer code.

Time (hours)	Dose (cGy)
0	0.018
1	0.022
2	0.032
3	0.057
4	0.11
5	0.16
6	0.20
7	0.22
8	0.24
9	0.26
10	0.27
11	0.28
12	0.29
13	0.29
14	0.30
15	0.30
16	0.30
17	0.30
18	0.31
19	0.31
20	0.31
24	0.32
28	0.33
32	0.33
36	0.33
40	0.33
44	0.34
48	0.34
60	0.34
72	0.34
96	0.34

Table D.10. Water dose data for the November 8, 1987 SPE, estimated using the BRYNTRN computer code.

Time (hours)	Dose (cGy)
0	0.005
1	0.010
2	0.017
3	0.030
4	0.042
5	0.051
6	0.070
7	0.091
8	0.13
9	0.16
10	0.18
11	0.19
12	0.21
13	0.22
14	0.23
15	0.23
16	0.24
17	0.24
18	0.25
19	0.25
20	0.25
24	0.26
28	0.26
32	0.27
36	0.27
40	0.28
44	0.28
48	0.28
60	0.29

Table D.11. Water dose data for the November 8, 2000 SPE, estimated using the BRYNTRN computer code.

Time (hours)	Dose (cGy)
0	0.083
1	10.8
2	39.2
3	77.9
4	126
5	178
6	233
7	291
8	347
9	402
10	461
11	523
12	580
13	637
14	692
15	741
16	793
17	832
18	867
19	899
20	928
24	1011
28	1049
32	1071
36	1079
40	1088
44	1094
48	1098
60	1105
72	1106

Table D.12. Water dose rate data for the November 8, 2000 SPE, estimated using the BRYNTRN computer code.

Time (hours)	Dose Rate (cGy/hr)
0	0.99
1	2.0
2	34.6
3	45.0
4	51.4
5	54.6
6	54.5
7	58.8
8	51.8
9	54.3
10	58.4
11	58.8
12	57.0
13	54.5
14	51.7
15	48.3
16	47.4
17	30.9
18	28.5
19	25.0
20	24.2
24	12.8
28	6.4
32	2.4
36	2.2

Table D.13. Percentage of observations that fall within 50% and 95% predictive intervals for the November 8, 2000 SPE using hierarchical models and Weibull growth curves.

Hours into event	50% Interval	95% Interval
2	55	97
3	58	97
4	58	97
5	60	97
6	59	97

Table D.14. Percentage of observations that fall within 50% and 95% predictive intervals for the November 8, 2000 SPE using hierarchical models and Gompertz growth curves.

Hours into event	50% Interval	95% Interval
2	55	97
3	58	95
4	60	96
5	60	96
6	59	96

Table D.15. Percentage of observations that fall within 50% and 95% predictive intervals for the November 8, 2000 SPE using hierarchical models and logistic growth curves.

Hours into event	50% Interval	95% Interval
2	63	97
3	64	98
4	63	97
5	63	97
6	62	97

Table D.16. Water dose data for the August 12, 1989 SPE, estimated using the BRYNTRN computer code.

Time (hours)	Dose (cGy)
0	0.024
1	0.074
2	0.31
3	1.3
4	3.7
5	7.1
6	11.3
7	15.9
8	21.1
9	33.5
10	45.0
11	64.0
12	89.9
13	122
14	154
15	188
16	222
17	251
18	277
19	300
20	321
24	374
28	418
32	446
36	463
40	470
44	476
48	480
60	483
72	485

Table D.17. Water dose rate data for the August 12, 1989 SPE, estimated using the BRYNTRN computer code.

Time (hours)	Dose Rate (cGy/hr)
0	0.046
1	0.076
2	0.51
3	1.8
4	2.6
5	4.1
6	4.7
7	4.3
8	8.0
9	14.9
10	13.0
11	21.0
12	29.1
13	33.4
14	32.4
15	35.3
16	33.3
17	28.7
18	24.9
19	22.8
20	21.8
24	10.2
28	9.9
32	5.5

Table D.18. Percentage of observations that fall within 50% and 95% predictive intervals for the August 12, 1989 SPE using hierarchical models and Weibull growth curves.

Hours into event	50% Interval	95% Interval
5	68	97
6	63	95
7	66	97
8	69	95
9	65	97
10	67	97
11	68	97

Table D.19. Percentage of observations that fall within 50% and 95% predictive intervals for the August 12, 1989 SPE using hierarchical models and Gompertz growth curves.

Hours into event	50% Interval	95% Interval
5	61	98
6	59	98
7	63	98
8	58	98
9	63	98
10	62	98
11	60	98

Table D.20. Percentage of observations that fall within 50% and 95% predictive intervals for the August 12, 1989 SPE using hierarchical models and logistic growth curves.

Hours into event	50% Interval	95% Interval
5	54	100
6	53	100
7	54	100
8	53	97
9	54	98
10	52	97

VITA

John Neal was born in Charles Town, West Virginia on September 28, 1964. He graduated from Jefferson High School in June 1982. He entered the United States Naval Academy in July 1982 and graduated with distinction in May 1986. Upon commissioning as an Ensign in the United States Navy, he entered the Navy's Nuclear Power Propulsion Program. While on active duty, he completed a Masters of Science degree in physics at the University of Wisconsin-Madison in December 1992. After resigning from the Navy in May 1995, he entered the doctoral program in Nuclear Engineering at The University of Tennessee in August 1995. The Doctor of Philosophy degree was received in May 2001.